Attitude determination using a GPS multi antenna array

Master Thesis

by

Katrin LANDFAHRER

Supervisor:
Ao.Univ.-Prof. Dipl.-Ing. Dr.techn. Norbert KÜHTREIBER

Institute of Navigation and Satellite Geodesy
Graz University of Technology

Graz, December 2009

Acknowledgments

I would like to thank my supervisor Ao.Univ.-Prof. Dipl.-Ing. Dr.techn. Norbert Kühtreiber for his supervision and help during developing this work. He supported me by valuable references and suggestions.

Moreover I have to thank all my colleagues of the institute for their help and inspired discussions, especially to Daniel for proofreading my thesis.

Additionally I want to thank my friends Elise and Petra for their assistance during the whole degree. We always helped each other to successful cope the Bachelor and Master studies. I hope we still keep friends for a long time.

I also want to thank my good friend Barbara for her motivation and discussions beside my studies.

Further I would like to thank my boyfriend Philipp for his patience during the last years. He always supports and helps me to improve my understandings of miscellaneous topics and for his assistance by solving problems concerning GNSS.

Last but not least, I would like to thank my family for giving me the opportunity to complete my academic studies and for their great support over all the past years.

Abstract

Katrin Landfahrer (2009): Attitude determination using a GPS multi antenna array

Attitude parameters enable the determination of an object's alignment with respect to the coordinate frame. The common attitude determination systems are based on INS (Inertial Navigation System) measurements. Since INS systems are still very expensive, the number of users are limited. Therefore another opportunity for the attitude determination is the use of GNSS measurements. The attitude determination with GNSS (Global Navigation Satellite System) can be applied in different operational areas, like ships, planes, cars or unmanned vehicles.

This master thesis is based on the project GRAVIS, realized by the Institute of Navigation and Satellite Geodesy at Graz University of Technology. The aim of the project is the gravity determination using INS and GNSS measurements. For this application the attitude and acceleration parameters based on GNSS data are used to support the strapdown procedure. The attitude can be derived on the one hand by using a GNSS antenna array and on the other hand by using an INS. Both systems are mounted on a platform, which can be used for different applications. My thesis deals with the attitude determination based on GNSS measurements. In this case four antennas are used to define a multi antenna array. An attitude computation can be performed with three antennas.

After presenting the principles of GNSS positioning methods, this thesis focuses on the attitude determination using GNSS measurements. In a first step the mathematical background is discussed. Afterwards an error propagation of the GNSS attitude determination and the calibration procedure of the platform is presented. Within several practical tests, beside the actual attitude determination, also analysis regarding proper update rates are discussed. The results of the field tests are evaluated and compared to actual INS measurements. The attitude computation algorithm and further the solution of the attitude computation based on GNSS data represent the main content of this master thesis.

Key words: GNSS, attitude, IMU, terrestrial platform

Zusammenfassung

Katrin Landfahrer (2009): Attitude determination using a GPS multi antenna array

Die Attitudeparameter beschreiben die Ausrichtung eines Objektes in Bezug auf ein Koordinatensystem. Die Attitudewinkel - Roll, Pitch und Yaw, werden herkömmlicherweise mittels inertialer Messsysteme (INS) bestimmt. Derzeitige präzise INS Systeme haben den Nachteil, dass sie teuer sind und somit für einen breiten Nutzerkreis nicht eingesetzt werden können. Zusätzlich gibt es auch die Möglichkeit die Attitudeparameter mit GNSS (Global Navigation Satellite System) Messungen herzuleiten. Die Attitudebestimmung mittels GNSS ermöglicht eine Vielzahl von Anwendungen.
Der Themenschwerpunkt dieser Diplomarbeit definiert sich durch die Aufgabenstellung im Projekt GRAVIS, welches am Institut für Navigation und Satellitengeodäsie der Technischen Universität Graz realisiert wird. Ziel dieses Projektes ist die Schwerebestimmung mit der Hilfe von IMU und GNSS Daten. Hierbei unterstützen die aus GNSS Daten hergeleiteten Attitude- und Beschleunigungsparameter das inertiale Strapdown-Verfahren. Teil meiner Masterarbeit war die Attitudebestimmung basierend auf GNSS-Messungen. Hierzu sind eine IMU und vier GNSS-Antennen auf einer Messplattform befestigt. Die Attitudeberechnung erfolgt zunächst ohne Berücksichtigung der Überbestimmung, durch Verwendung der Messergebnisse von drei Antennen.
In der Masterarbeit werden in einem ersten Schritt, die Positionierungsmethoden mittels GNSS ausführlich erläutert. Das mathematische Konzept der Attitudeberechnung, sowie eine Varianzfortpflanzung der Attitudeparameter und der Kalibrierungsprozess der Messplatform werden in dieser Arbeit näher gebracht. Neben einigen praktischen Tests zur Attitudeberechnung, erfolgte auch eine Untersuchung bezüglich der optimalen Messintervalle. Die Ergebnisse der Attitudeberechnung werden mit den Ergebnissen der IMU verglichen und interpretiert. Der Inhalt dieser Diplomarbeit beschäftigt sich primär mit dem Attitude-Berechnungsalgorithmus und den resultierenden Attitudeparametern aus GNSS-Daten.

Stichwörter: GNSS, Attitude, IMU, terrestrische Plattform

Contents

Abbreviations

APOS	Austrian Positioning Service
ASAP	Austrian Space Application Program
AVL	Anstalt für Verbrennungskraftmaschinen
BEV	Bundesamt für Eich- und Vermessungswesen
C/A	Coarse/Acquisition
CDMA	Code Devision Multiple Access
CS	Control Segment
DGPS	Differential GPS
DOP	Dilution Of Precision
ECEF	Earth-Centered-Earth-Fixed
EGNOS	European Geostationary Navigation Overlay Service
ERNP	European Radio Navigation Plan
ESA	European Space Agency
EU	European Union
FDMA	Frequency Division Multiple Access
GCC	Galileo Control Center
GK	Gauß Krüger
GLONASS	Global Navigation Satellite System
GNSS	Global Navigation Satellite System
GOCE	Gravity Field and Steady-State Ocean Circulation Explorer
GPS	Global Positioning System
GRAVIS	Terrestrial Moving-Base Gravimetry Using a GNSS/SINS Platform
iMAR	Internationale Meß-, Automatisierungs- und Regelsysteme
IMU	Inertial Measurement Unit
INS	Inertial Navigation System
IPF	Integrity Processing Facility
KAR	Kinematic Ambiguity resolution

MCF	Mission Control Facility
MEMS	Micro-Electro-Mechanical Systems
MSAS	Multi-functional Satellite Augmentation System
OEAMTC	Österreichische Automobil-, Motorrad- und Touring Club
OEM	Original Equipment Manufacturer
OSPF	Orbit and Synchronization Processing Facility
OTF	On-The-Fly
PDOP	Position Dilution of Precision
PPS	Precise Positioning Service
PRC	Pseudorange Correction
PRN	Pseudorandom Noise
PTF	Precision Timing Facility
RAIM	Receiver Autonomous Integrity Monitoring
RMS	Root Mean Square
RNSS	Radio Navigation Satellite System
RRC	Range Rate Correction
RTK	Real Time Kinematic
SA	Selective Availability
SAR	Search and Rescue
SCF	Satellite Control Facility
SINS	Strapdown Inertial Measuring System
SPF	Sub-Processing Facility
SVN	Space Vehicle Number
WAAS	Wide Area Augmentation System
WGS	World Geodetic System

1 Introduction

The content of this master thesis is based on the Project GRAVIS, which deals with Terrestrial Moving-Base Gravimetry Using a GNSS/SINS Platform. GRAVIS is realized by the Institute of Navigation and Satellite Geodesy at Graz University of Technology and is funded within the 5^{th} call of the Austrian Space Application Program (ASAP). A large output of this master thesis was gained during the activities as a project collaborator within the project GRAVIS. The following sections give a synopsis about the motivation of the project and furthermore of this master thesis. An illustration of the concept of this master thesis, with the implementation and the outcome, is briefly shown in section 1.2.

1.1 Motivation

The project GRAVIS constitutes the foundation of this thesis. GRAVIS stands for Terrestrial Moving-Base Gravimetry, using a GNSS/INS (Global Navigation Satellite System/ Inertial Navigation System) platform. The object of this project is the determination of the Earth's gravity field, by using a GNSS/INS platform mounted on a car (cf. Kuehtreiber et al. (2007)). The knowledge of the gravity field is essential for many scientific disciplines, like the determination of heights, the mass distributions and also for the exploration of the climate change. Depending on the required spatial and spectral resolution, terrestrial or global techniques are used to measure first or second order derivatives of the Earth's gravity potential. While satellite missions - such as the GOCE mission - can be used to determine the long wavelength characteristics of the Earth's gravity field, terrestrial measurements provide the high frequency part - the local and regional structure. The usual methods of gravity determination are based on the measurements of the deflections of the vertical or on absolute and relative gravimetry measurements.

Another method of determining the regional gravity field, is the use of airborne gravity mapping systems based on GNSS/INS measurements. This system can also be adapted for terrestrial use, where the platform is mounted on a vehicle moving on the Earth's surface (cf. Figure 1.1). The measured gravity vector g^l consists of the normal gravity vector γ^l of

the gravity ellipsoid and the gravity anomaly δg^l which can be described as the difference vector between the normal and measured gravity vectors. Gravity measurements observed by a moving car, are a fast and cheap alternative to airborne and terrestrial gravimetry (cf. Bruton et al. (2000)). The method can especially be applied for the densification of gravity measurements in difficult regions with sparse gravity distribution. As a result, line-based measurements can be gained.

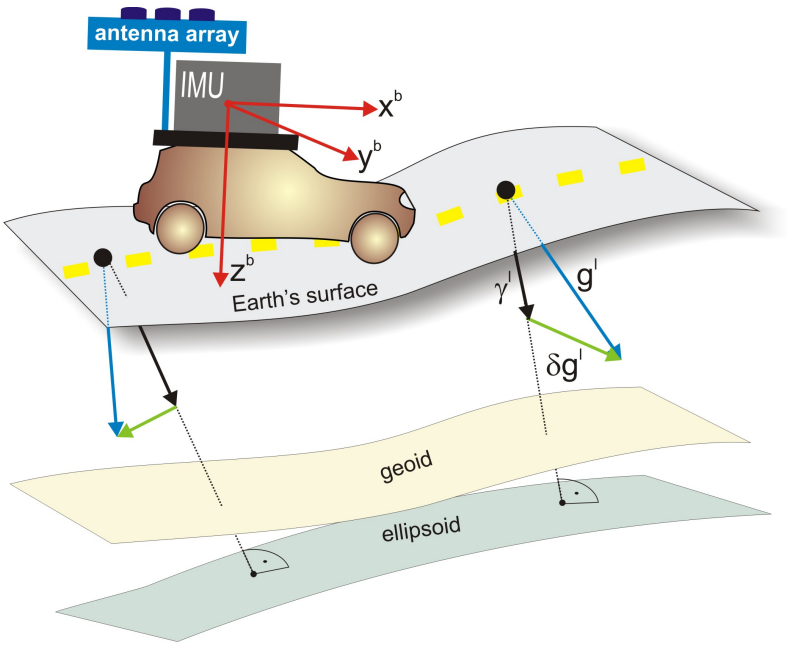

Figure 1.1: Principles of mobile gravity measurements

The project GRAVIS will start with state-of-the-art analysis, concerning GPS and INS as well as the sensor integration. Special emphasis is put on the error analysis and the accuracy estimation. The output of these tasks will define the requirements, needed for a successful implementation of this concept. In principle the error of the gravity vector for the strapdown inertial gravimetry is mainly a function of attitude errors due to the initial misalignment, the noise of the gyro measurements, the noise of the accelerometer measurements, errors of the determination of the vehicle's acceleration determined by GNSS, and a synchronization error between the INS and GNSS system. Furthermore it is important to develop a concept for a stable determination of accelerations from GNSS position measurements. Due to the unfavorable local conditions cycle slips, multipath and shadowing effects may be deteriorate the GNSS observations and should therefore be avoided.

In a second phase of the project a design for the system architecture will be proposed. This includes the consideration of the required soft- and hardware together with their interfaces. One important task herein is the investigation of the usability of antenna arrays for the attitude determination via GNSS on the vehicle, which will be used to compensate the gyro drift behavior of the IMU. Finally a proof of the concept will done during a test phase.

1.1.1 Objectives

One of the objectives of the proposed project is to perform a feasibility study about the use of GNSS to determine the Earth's gravity field by terrestrial moving-base gravimetry. Following Hofmann-Wellenhof et al. (2006), the principle of strapdown inertial gravimetry is given by

$$\delta g^l = \dot{v}^l - R_b^l \cdot f^b + (2 \cdot \Omega_{ie}^l + \Omega_{el}^l) v^l - \gamma^l. \tag{1.1}$$

The superscript l denotes the local-level frame and b denotes the body frame of the vehicle. δg^l corresponds to the gravity anomaly at the measured position. R_b^l is the rotation matrix for the rotation of vectors from the body frame (subscript b) to the local-level frame (superscript l). The specific force f^b is measured by the accelerometers in the body frame. The terms $\dot{v}^l$ and v^l are the vehicle's acceleration and the vehicle's velocity given in the local-level frame and derived from the GNSS measurements. The matrix Ω_{ie}^l describes the influences due to the earth rotation between the inertial- and the local-level frame. The vehicle motion is described by the matrix Ω_{el}^l. Both matrices are skew-symmetric matrices of the angular velocity vectors ω_{ie}^l and ω_{el}^l.

$$\Omega_{ie}^l = \begin{bmatrix} 0 & -\omega_3 & -\omega_2 \\ \omega_3 & 0 & -\omega_1 \\ -\omega_2 & \omega_1 & 0 \end{bmatrix} \tag{1.2}$$

The elements of ω, of the skew-symmetric matrix Ω_{ie}^l or Ω_{el}^l, can be interpreted as components of the corresponding axial vector ω_{ie}^l or ω_{el}^l. For example, the angular rate Ω_{ie}^l describes the rotations of the e-frame (earth fixed frame) with respect to the i-frame (inertial frame), expressed in the local-level frame. The term $(2 \cdot \Omega_{ie}^l + \Omega_{el}^l)$ is also known as the Coriolis acceleration. The term γ^l is the normal gravity vector, which can be obtained from gravity models.

In principle GNSS is used for the determination of the vehicle's accelerations, as well as the vehicle's velocities and positions. The block diagram in Figure 1.2 shows the operation process of the strapdown inertial scalar gravimetry.

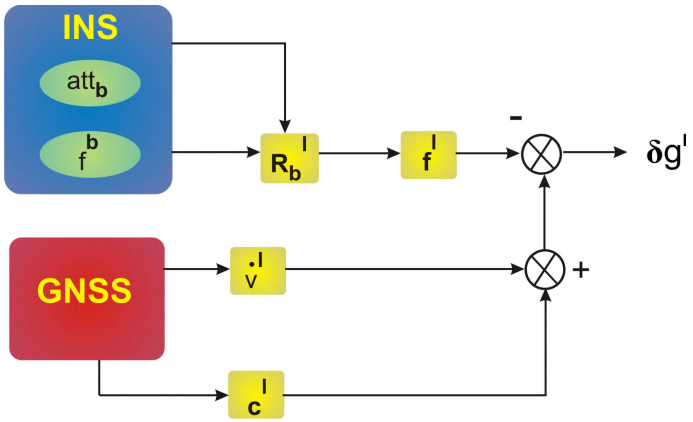

Figure 1.2: Procedure of the strapdown process for gravity anomaly determination

The measured angular rates of the INS gyros are integrated to obtain the attitude att_b in the local-level frame. Thus the transformation of the specific force (f^b) from the body to the local-level frame can be done. The vehicle's acceleration $\dot{v}^l$, as well as Coriolis acceleration or Eötvös correction and normal gravity, combined together under the symbolic notation c^l (cf. Legat et al. (2007)) are derived from GNSS and INS measurements. The term f^l describes the specific force in the local-level frame. A combination of the $\dot{v}^l$-, c^l- and f^l-term results in the gravity anomaly δg^l. Thus all parts on the right hand side of the gravity anomaly equation, except the second term $R_b^l \cdot f^b$, are derived from GNSS measurements.
Beside the above presented application, many other application scenarios exist, where GNSS measurements can be used for attitude determination. Especially when a low-cost solution is needed the case of GNSS receivers might be appropriate. Possible fields of applications are:

- automobile sector
- areosphere
- helicopter
- vessel
- unmanned vehicle, like robots and drones

There already exist professional solutions for GNSS attitude determination on the market, as for instance:

- Javad
- Hemisphere
- iMAR

The advantage of using GNSS systems for the attitude determination is, that a GNSS receiver is cheaper compared to the currently available IMU systems. It has therefore more potential to have a bigger user community. Furthermore the measurements are not influenced by drift effects, which appear in IMU measurements over a longer time period. The GNSS receivers do not consist of moving parts, like the rotated gyros and accelerometers in the IMU. Furthermore the GNSS system is able to determine the absolute attitude values for each measurement epoch. However the disadvantage of using GNSS is the low update rate of maximum 100 Hz and the medium accuracy of about 0.1° - 1° root mean square (RMS). moreover for each measurement epoch a direct view of up to four or more satellites is necessary.

Beside GNSS also other sensors can be used for attitude determination:

- Gyroscopes
- Rate gyros
- Star trackers
- Sun sensors
- Magnetometers

1.2 Structure of this master thesis

The purpose of this master thesis is the investigation of the attitude computation by using four GNSS antennas. Figure 1.3 gives a short overview about the structure of this work.

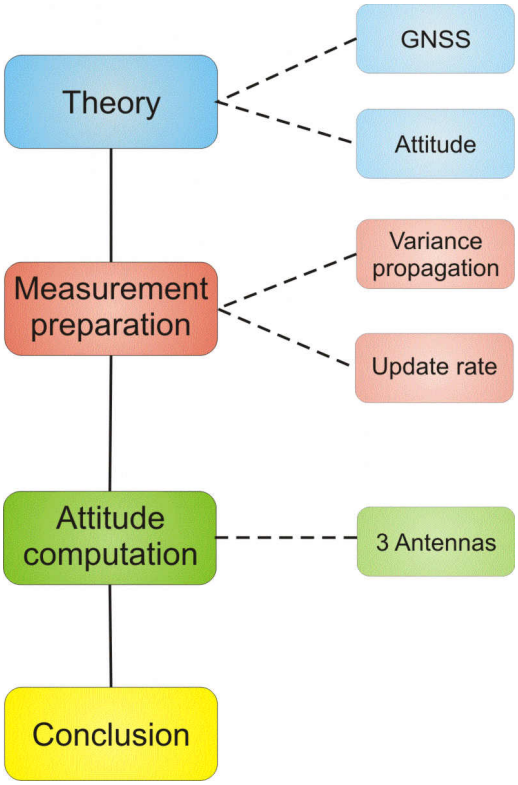

Figure 1.3: Structure of this master thesis

The first part of this master thesis deals with the theoretical aspects of GNSS and the attitude determination. An introduction of existing GNSS systems at the present time is given. The satellite constellations, the orbits as well as the signal structures of GPS, Galileo and GLONASS are briefly explained. Furthermore the different positioning methods like single point positioning, differential positioning (DGPS) and relative positioning are stated in more detail. The second part of the thesis deals with the attitude determination. This section gives information about the definition of the attitude parameters roll, pitch and yaw. The local-level frame and the body frame are explained and the transformation between both frames is derived. Furthermore an overdetermined attitude computation algorithm is explained.

The next part deals with preparatory measurements for the test drive and the attitude computation. First of all a variance propagation of the computed attitude parameters is performed in order to account for the GNSS errors in the positioning process. The resulting necessary GNSS positioning accuracy influences the requirements of the proof-of-concept setup. To enable an optimal sampling of the trajectory, different measurement update rates are tested and compared.

The third part of this thesis shows the solutions of the attitude determination of the kinematic test drives. Therefore two test drives were performed. The trajectories show complete different conditions, concerning shading and multipath effects. The attitude determination of both trips is mathematically described and furthermore the solutions are visualized and interpreted. Also a comparison with the attitude solution derived from IMU data is shown and interpreted.
A conclusion of the attitude determination solutions with a GNSS antenna array and some ideas for further investigations completes this master thesis.

2 Principles of GNSS

Position, velocity, acceleration and time determination is offered by the satellite based Global Navigation Satellite Systems (GNSS). The first implementation of GNSS1 consists of the American Global Satellite Positioning System (GPS), the Russian Global Satellite Navigation System (GLONASS) and finally of some augmentation systems, comprising of geostationary satellites. The geostationary satellites improve accuracy, integrity and additional ranging of the satellite positioning systems (cf. Hoffmann-Wellenhof et al. (2001)). Three augmentation systems are currently operating:

WAAS Wide Area Augmentation System (American System)

MSAS Multi-functional Satellite Augmentation System (Japanese System)

EGNOS European Geostationary Navigation Overlay Service

At the moment an upgrading of GNSS1 is realized - called GNSS2. It is considered as the transition from military systems to a system under complete civil control. Beside GPS and GLONASS, the new European satellite system Galileo will complete GNSS2. Furthermore the GPS system will be modernized and two new civil signals L2C and L5 will be provided. Another major component of the modernization process is the new military signal called M-code. During the GNSS1 phase the GLONASS system has fallen into disrepair, leading to gaps in coverage and only partial availability. However till 2010 the Russian Federation has promised to restore it to full global availability and new civil signals will be available.

2.1 GPS

GPS is an all-weather, worldwide, continuous coverage, satellite-based radio navigation system. GPS receivers measure phase and code pseudoranges and decode messages from in-view satellites to determine the information necessary to complete position and time calculations (cf. Hoffmann-Wellenhof et al. (2001)). The system consists of three major segments, the space, the control and the user segment. In the following the three segments are described briefly.

2.1.1 Segments of GPS

Space Segment

The space segment is composed of nominal 24 satellites. The satellites are separated upon six orbital planes, therefore four satellites are on each orbit. The orbits are nearly circular (eccentricity of 0.1) with an inclination of 55°. The inclination of orbits of artificial satellites is measured relative to the equatorial plane of the body they orbit. The orbital planes are equal spaced around the equator, resulting in 60° separation (cf. Figure 2.1). The altitude of GPS satellites is approximately 20200 km. This constellation ensures that a user, located anywhere on the Earth, has a direct line of sight to at least four satellites at any time. Since the satellites are not in geosynchronous orbits, the geometric relation (constellation) between the satellites is always changing. This changing geometry leads to a changing but predictable position accuracy estimation, the so called DOP (Dilution Of Precision) values (cf. Farrell et al. (1998)). The orbiting time is one sidereal day ($\sim$ 12 hours).

Control Segment

The control segment (CS) supervises the space segment. The CS consists of six monitor stations, four ground control stations and one master station worldwide. The ground monitor stations are monitoring all signals of all satellites and transfer the data to the master control station. The master control station determines the orbital model of the satellites, the clock correction parameters and the ionospheric correction parameters. These parameters are then transferred back to the ground antennas for uploading the broadcast navigation message to the satellites (cf. De Jong et al. (1998)).

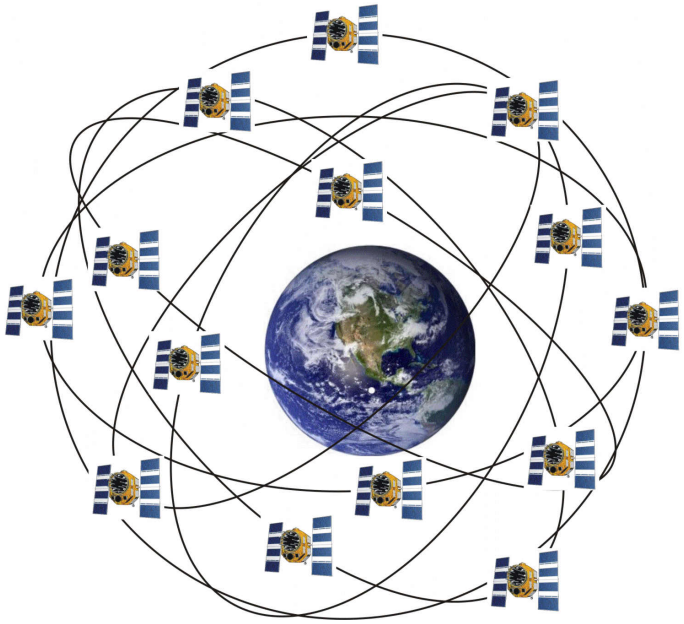

Figure 2.1: GPS constellation

User Segment

The last segment represents the user community, either for civil or for military purposes. The key element of this segment are the receivers, which transform the signal in space into services for the users. The receivers consist of antennas and receiver hardware and software. The receiver acquires the satellite signal, measures either the pseudorange or phase, decodes the navigation message and finally calculates the position of the antenna in a global reference frame. Position, velocity and precise time information is provided to the user. The GPS space segment is working for an unlimited number of users. For GPS measurements it is essential to have a free sight between the receiver and the satellites. GPS is a line of sight system, therefore the path between receiver and a satellite should not be obstructed to receive the satellite signal.

2.1.2 Signal

Each GPS satellite transmits ranging codes and navigation data by using code division multiple access (CDMA) on the two carrier frequencies L1 (1575.42 MHz) and L2 (1227.60 MHz). The fundamental frequency f_0 of GPS is 10.23 MHz. The two carrier phase frequencies in the L-band (L1, L2) are generated by an integer multiplication of f_0 ($f_1 = 154 \cdot f_0$, $f_2 = 120 \cdot f_0$). Two codes are used for the satellite clock readings, both characterized by a pseudorandom noise (PRN) sequence. The C/A-code (Coarse/Acquisition-Code) modulates the L1 carrier phase and recently the L2 carrier phase. The frequency of the C/A-code signal is $f_0/10$. Each satellite broadcasts a different C/A-code. The receivers internally generate a C/A-code for each satellite and correlate the signals with the received code signal of the satellite. Therefore a correlation peak appears, if the received and the internally generated signal coincide with each other. This procedure allows an unambiguous detection of the received satellite. The precise (P-) code is modulated onto the L1 and L2 phase and has the frequency f_0. The P-code is encrypted by using a W-code. The encrypted P-code is then called Y-code. This is also known as the antispoofing (AS) mode. AS is a method implemented in the GPS technology to prevent non-U.S. military users to use the signal and thus the accuracy of the P-code. Furthermore a navigation message is modulated upon the L1 and L2 code signals. The corresponding signal frequency is 50 Hz. The message includes information about the GPS time and date, the satellite status and an indication of it's health. In addition ephemeris data of the received satellite and almanac parameters of all satellites are included. This information is further used for the determination of the satellite position, the satellite clock error and for the atmospheric correction at a given time (cf. Farrell et al. (1998)). An overview of the different GPS signals can be seen in Figure 2.2.

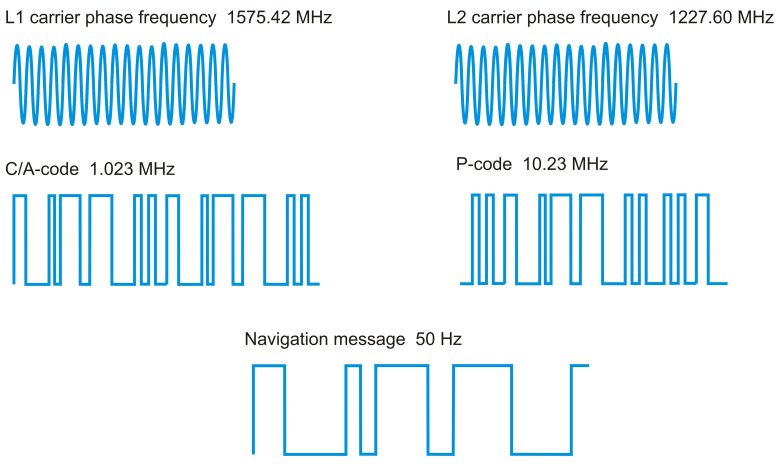

Figure 2.2: GPS signal components

2.2 GLONASS

The GLobal'naya NAvigatsionnaya Sputnikovaya Sistema [engl. GLObal NAvigation Satellite System] (GLONASS) is the Russian counterpart to the United States' GPS system (cf. Hoffmann-Wellenhof et al. (2001)). It is operated for the Russian government by the Russian Space Forces. Like GPS, the nominal GLONASS constellation consists of 24 satellites, 21 operating in three orbital planes which are equally distributed. Each orbital plane contains eight satellites with an inclination of 64.8° and an altitude of 19100 km. Each satellite completes an orbit approximately in 11 hours 15 minutes. The main difference between GPS and GLONASS arises from the method of the satellite signal division. While GPS uses code division multiple access (CDMA) (cf. section 2.1.2), GLONASS uses frequency division multiple access (FDMA). Therefore two individual frequencies are assigned to each satellite. The PRN codes are the same for each satellite. Due to the economic situation in Russia only eight satellites were in a healthy status in April 2002, making it almost useless as a navigation system. The rebuilding of GLONASS has already started and today (December 2009) 19 active satellites set up the GLONASS system. Additionally, an advanced GLONASS satellite, the GLONASS-M has been developed. The new GLONASS-M satellites have better signal characteristics, as well as a longer design life (seven to eight years instead of the current three years). The GLONASS-M generation has a new civil signal on the L2 frequency band for higher accuracy. Two satellites of this new version were launched till December 2004. A new satellite generation - the GLONASS-K - will be developed until 2010. The GLONASS-K satellites will have a third civil signal at the L3 frequency for higher reliability and accuracy, especially designed for safety of life applications. There also will be a GNSS integrity information on the L3 frequency. It is proposed that GLONASS will be fully operational again by 2011 with 21 satellites.

2.3 Galileo

The European contribution to GNSS-2 is Galileo (cf. Farrell et al. (1998)). Galileo is a satellite navigation system for a wide field of different user requirements. This system development is a joint by the EU (European Union) and the ESA (European Space Agency). The aim is to establish an independent navigation system besides the GPS system of the United States and the Russian GLONASS system, which are both designed for military purposes and made available for civil users. Today satellite navigation is becoming more important and more widespread across many different market sectors. Therefore Galileo will strengthen up the European economic market. The full deployment to reach the 30-satellite Galileo constellation shall be performed at the end of 2013 (cf. Marco et al. (2009)). The space segment comprises the following specifications:

- 27 satellites + 3 spare satellites
- Altitude of 23222 km
- Orbital inclination of 56°
- Three equally spaced orbital planes
- Period of 14 hours and 4 minutes.

The chosen satellite constellation shall provide the best solution in terms of robustness, performance and homogeneity including northern latitudes. The orbital and constellation parameters of Galileo and GPS will be different. At any time, and at any location on Earth, the maximum number of visible satellites is shown within Table 2.1 (cf. Basker et al. (2004)).

Receiver elevation masking angle	Number of visible Galileo satellites	Number of visible GPS satellites	Total (Galileo+GPS)
5°	13	12	25
10°	11	10	21
15°	9	8	17

Table 2.1: Benefit of combining GPS and Galileo

The Galileo satellites will transmit in total ten navigation signals and one Search and Rescue (SAR) signal. The navigation signals will be emitted in the Radio Navigation Satellite Service (RNSS) allocated bands and the SAR signal will be broadcasted in one of the frequency bands reserved for the emergency services (1544 - 1545 MHz). The following Galileo navigation signals will be emitted by the satellites:

- 4 signals in the frequency range 1164 - 1215 MHz (E5a - E5b)
- 4 signals in the frequency range 1260 - 1300 MHz (E6)
- 3 signals in the frequency range 1559 - 1591 MHz (L1).

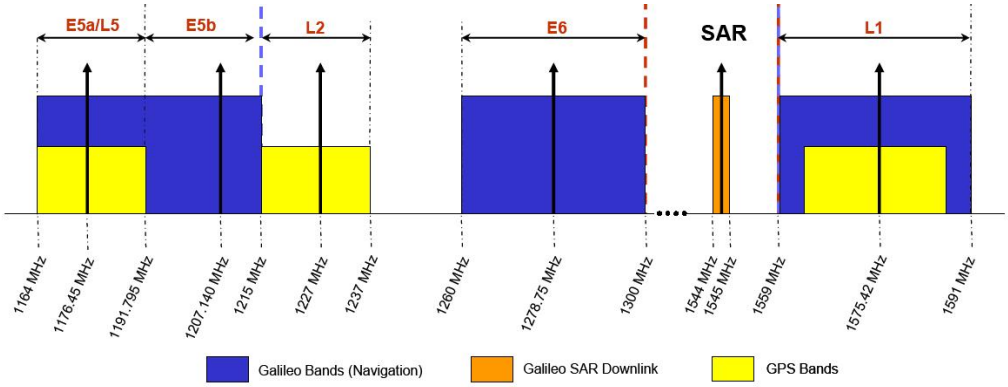

Figure 2.3: Signal bands of the Galileo and GPS system

Figure 2.3 shows the arrangement of the used GPS and Galileo signal bands. The interoperability of GPS and Galileo is possible by using the L1 and the L5/E5a band.

2.3.1 Ground segment

The control of the satellite constellation, the synchronization of the satellite atomic clocks, the processing of the integrity signal, and the data handling of all internal and external elements will be performed by two redundant Galileo Control Centers (GCC), which will be located in Europe. The first one was opened in 2008 in Oberpfaffenhofen in Germany.

These GCC's will contain:

- Orbit Synchronization and Processing Facilities (OSPF)
- Precision Timing Facilities (PTF)
- Integrity Processing Facilities (IPF)
- Mission Control Facility (MCF)
- Satellite Control Facility (SCF) - including uplink to the Galileo satellites
- Services Product Facility (SPF)

2.3.2 Galileo services

Galileo supports positioning and navigation by different services with varying positioning accuracy and cost factors (cf. Hoffmann-Wellenhof et al. (2008)). A short overview of the defined services should be given in a short synopsis:

Open service, provides positioning, velocity and timing information for each user

Safety of life services, for safety critical users

Commercial services, can be offered for commercial services

Public Regulated Services, for sovereign services like police and secret services

Search and rescue services, effort on humanitarian Search and Rescue activities

In the following a short explanation of the GNSS observations and the possible positioning methods is given. All positioning methods work consistently for GPS, Galileo and GLONASS. Therefore the following description of the positioning determination is based on the GPS system.

2.4 Observations

GPS observables are ranges which are derived from measured time or phase differences based on a comparison between received signals and a generated signal in the receiver. For the GPS concept two clocks, one satellite clock and one receiver clock, are used. The GPS receiver determines the time required for the signal to propagate from the satellite to the receiver. The measured satellite-to-receiver range defines a sphere of possible receiver locations (cf. Figure 2.4).

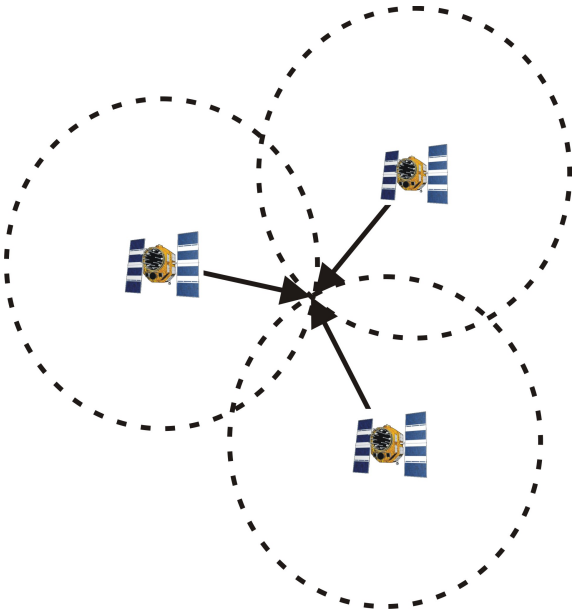

Figure 2.4: Range measurements of three satellites

The intersection of three spheres is sufficient to determine the position of the user if the clocks in the satellite and the receiver were perfectly synchronized (cf. Bauer et al. (2003)). Because the clock behavior shows some instabilities, clock errors in the satellite and the receiver appear. Therefore a fourth satellite is needed to determine the user position as well as clock bias. The satellite clock error can be modeled by a polynomial which is transmitted via the navigation message. The measured ranges are biased by the satellite and receiver clock errors and are denoted as pseudoranges.

The code pseudorange is deduced by the measured time and is affected by the clock biases and other error sources. Within the code pseudorange method the position of the user can be determined with an accuracy of $\pm 10\ m$ (cf. U.S Coast Guard Navigation Center-NAVCEN).

The pseudorange R can be represented by

$$R = c \cdot \Delta t, \tag{2.1}$$

where the time difference Δt can be expressed by

$$\Delta t = t_R - t^S = [t_R(GPS) + \delta_R] - [t^S(GPS) + \delta^S]. \tag{2.2}$$

The pseudorange R can be calculated by multiplication of the speed of light c with the time difference Δt. The time shift can be calculated by differencing the time of the receiver clock t_R with the time of the satellite clock t^S, which are influenced by the errors of the receiver clock δ_R and the satellite clock δ^S, respectively.

In addition to the code pseudorange the user position can also determined by the measurement of phase pseudoranges (denoted as Φ). In this method, only the fractional beat phase of the carrier frequency signal is measured. The initial integer number of cycles between the satellite and receiver is unknown. These unknown cycles are called ambiguities. For each received satellite signal the ambiguity has to be determined. The ambiguity remains unchanged during the whole measurement as long as no interruption of the signal appears. Every change of the distance between receiver and satellite changes the fractional beat phase. The model of the phase pseudorange measurement can be expressed by

$$\Phi = \frac{1}{\lambda} \cdot \rho + \frac{c}{\lambda} \cdot \Delta\delta + N, \tag{2.3}$$

where ρ is the geometrical distance between the satellite and the GPS receiver and is given by

$$\rho = \sqrt{(X^S - X_R)^2 + (Y^S - Y_R)^2 + (Z^S - Z_R)^2}. \tag{2.4}$$

The phase pseudorange can be computed with the wavelength λ of the signal, the difference of the clock errors of the receiver and the satellite $\Delta\delta$ and the ambiguity N. The coordinate triples of the satellite (X^S, Y^S, Z^S) and the receiver position (X_R, Y_R, Z_R) allow the determination of the range ρ between the satellite and the receiver.

The time derivation of the geometrical distance (ρ), which is denoted as ($\dot{\rho}$), can be obtained by the Doppler observables. The Doppler shift is linearly dependent on the radial velocity and, thus, allowing velocity determination in real time which is important for navigation. The equation of the observed Doppler rate is given by

$$D = \lambda \cdot \dot{\Phi} = \dot{\rho} + c \cdot \Delta\dot{\delta}. \tag{2.5}$$

The Doppler rate D is a function of the time derivation of the range $\dot{\rho}$, the fractional phase $\dot{\Phi}$ and the clock error $\Delta\dot{\delta}$. The raw Doppler shift is also applied to determine integer ambiguities in kinematic surveying or is used as an additional independent observable for point positioning (cf. Hofmann-Wellenhof et al. (2001)).

The position determination is always influenced by errors which are caused within the signal transmission, the signal reception and during the signal propagation. Table 2.2 shows the arising biases during GPS measurements.

Signal transmission	Signal propagation	Signal reception
-Satellite clock bias	-Ionospheric refraction	-Receiver clock bias
-Orbital errors	-Tropospheric refraction	-Variations of the antenna phase center
		-Multipath propagation

Table 2.2: Errors affecting GPS measurements

2.4.1 Positioning methods

Point positioning

Point positioning can be implemented with using code ranges and carrier phases (cf. Farrell et al. (1998)). A simplified representation of this positioning method is shown in Figure 2.5.

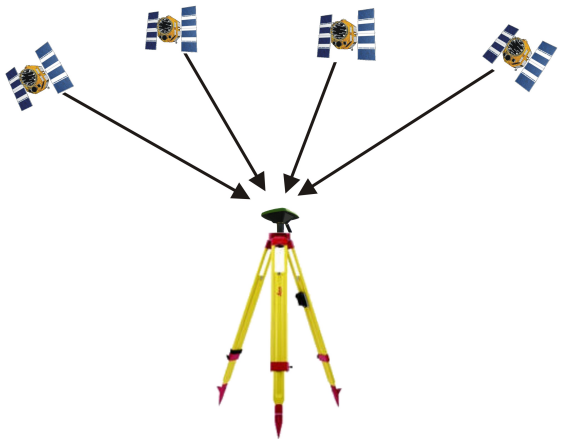

Figure 2.5: Single point positioning method

The principle of point positioning will be explained for the case of code ranges.
The code pseudorange at an epoch t can be written by

$$R_i^j(t) = \rho_i^j(t) + c \cdot [\delta^j(t) - \delta_i(t)] \tag{2.6}$$

(cf. Hoffmann-Wellenhof et al. (2001)). $R_i^j(t)$ is the measured code pseudorange between the receiver (i) and the satellite (j) at an epoch t. The code pseudorange is composed of the geometric distance ρ_i^j, the speed of light c and the satellite clock error $\delta^j(t)$ and the receiver clock error $\delta_i(t)$. Each satellite has one unknown clock bias. The three unknown user coordinates together with the combined clock bias of each satellite are the unknown parameters. Thus, there would always be more unknowns than measurements. To handle this problem the satellite clock information is transmitted via the broadcast navigation message in the form of three polynomial coefficients at a reference epoch. Therefore the calculation of the satellite clock error is possible and the number of unknown parameters is limited in the standard case to four. The number of observations $(n_j \cdot n_t)$ for static point positioning is defined by

$$n_j \cdot n_t \geq 3 + n_t. \tag{2.7}$$

The term n_j denotes the number of satellites and n_t the number of epochs. This means if four satellite signals $(n_j = 4)$ can be received, one measurement epoch $(n_t = 1)$ enables the position determination. The static point positioning will also work if two satellites

($n_j = 2$) are simultaneous observed over three epochs ($n_t \geq 3$). For kinematic point positioning the total number of unknowns amounts to $4 \cdot n_t$.

So the basic configuration is defined by:

$$n_j \cdot n_t \geq 4 \cdot n_t. \tag{2.8}$$

This means, that at least four satellite ($n_j = 4$) are necessary for the kinematic point positioning, because the number of observations must be equal to or greater than the number of unknowns.

Differential positioning

The differential GPS (DGPS) is a real time positioning technique with two or more receivers. One receiver at rest is used as a reference station with known coordinates. The second receiver is the remote station and is denoted as rover. The coordinates of the remote station should be determined. The base station calculates pseudorange corrections (PRC) and range rate corrections (RRC) for each visible satellite. They are then transmitted to the remote station in real time (cf. Figure 2.6).

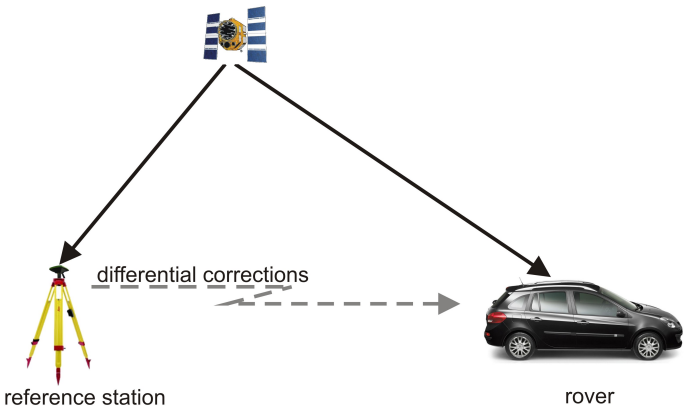

Figure 2.6: Differential positioning method

The rover applies the corrections to the measured pseudoranges to get a better positioning solution. In the following, the principles of the DGPS process are illustrated for the case of code measurements. It should be mentioned that phase measurements can also be used for DGPS (cf. Hofmann-Wellenhof et al. (2001)).

The code range at the reference station is modeled by

$$R_A^j(t_0) = \rho_A^j(t_0) + \Delta\rho_A^j(t_0) + \Delta\rho^j(t_0) + \Delta\rho_A(t_0). \tag{2.9}$$

The pseudorange $R_A^j(t_0)$ includes the geometric range $\rho_A^j(t_0)$, and the range biases, which are depending on the signal propagation $\Delta\rho_A^j(t_0)$, the receiver dependent biases $\Delta\rho_A(t_0)$ and the satellite dependent biases $\Delta\rho^j(t_0)$ (cf Table 2.2). The pseudorange correction for satellite j at reference epoch t_0 is defined by the relation

$$PRC^j(t_0) = \rho_A^j(t_0) - R_A^j(t_0). \tag{2.10}$$

The pseudorange correction at the reference epoch t_0 can be computed since the geometric range is known because of the known reference position and the broadcast ephemerides of the satellite. The time derivative of the PRC or range rate correction (RRC) allows the computation of the PRC for an epoch t:

$$PRC^j(t) = PRC^j(t_0) + RRC_j(t_0) \cdot (t - t_0). \tag{2.11}$$

The term $(t - t_0)$ is denoted as latency. The corrected code pseudorange at the remote receiver yields

$$R_B^j(t)_{corr} = R_B^j(t) + PRC^j(t), \tag{2.12}$$

$$R_B^j(t)_{corr} = \rho_B^j(t) + [\Delta\rho_B^j(t) - \Delta\rho_A^j(t)] + [\Delta\rho_B(t) - \Delta\rho_A(t)]. \tag{2.13}$$

For small distances ($\leq 100\ km$) between the reference and the remote receiver the biases of each receiver are strongly correlated. This leads to a simplified pseudorange model

$$R_B^j(t) = \rho_B^j(t) + \Delta\rho_{AB}(t). \tag{2.14}$$

The bias term $\Delta\rho_{AB}(t)$ includes the multipath effect as well as the combined receiver clock bias. The positioning with the corrected pseudorange at the rover site B leads to an improved accuracy ($< \pm 1\ m$).

Relative positioning

The objective of relative positioning is to define coordinates of an unknown point (B) with respect to a known reference point (A). The baseline vector between these two points is determined. For most applications, relative positioning is performed stationary (cf. Hofmann-Wellenhof et al. (2001)). The position determination of the receiver B is defined by the relation

$$X_B = X_A + b_{AB}. \tag{2.15}$$

The baseline vector b_{AB} is defined by

$$b_{AB} = \begin{bmatrix} X_B - X_A \\ Y_B - Y_A \\ Z_B - Z_A \end{bmatrix}. \tag{2.16}$$

For relative positioning, simultaneous observations to identical satellites at the two points (A) and (B) of the vector are essential. Assuming simultaneous observations to the satellites j and k, linear combinations can be formed, leading to single-differences, double differences and triple-differences (cf. Figure 2.7, 2.8, and 2.9). Their basic mathematical modeling is shown in the following paragraph. It must be noted, that in sequel only phase ranges are considered explicitly.

Single differences The principle of single differences assumes two ground stations A and B which track one single satellite j (cf. Figure 2.7).

The phase equation for the ground station A is

$$\Phi_A^j(t) = \frac{1}{\lambda} \cdot \rho_A^j(t) + N_A^j + \frac{c}{\lambda} \cdot (\delta^j(t) - \delta_A(t)), \tag{2.17}$$

where $\Phi_A^j(t)$ is the measured carrier phase expressed in cycles, λ is the wavelength, and ρ_A^j is the distance between the receiver A and the satellite j. The time independent phase

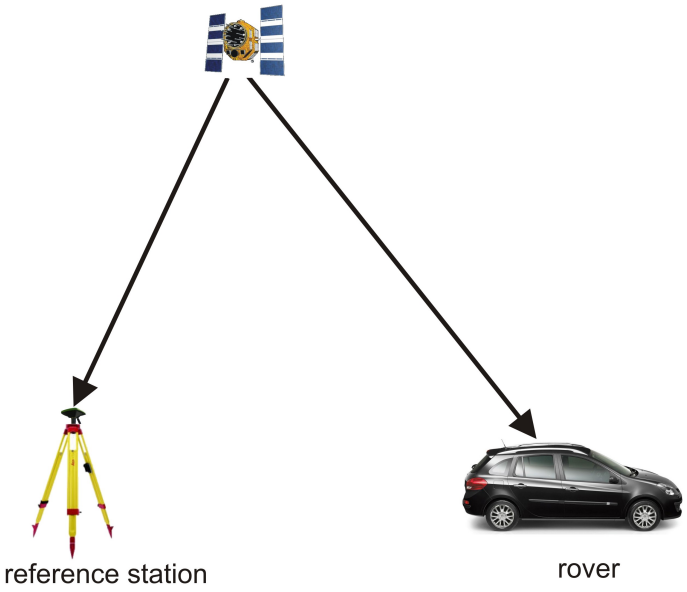

Figure 2.7: Single difference method

ambiguity is expressed by the term N_A^j. The term $\frac{c}{\lambda}$ denotes the frequency of the satellite signal, and $\delta^j(t) - \delta_A(t)$ corresponds to the difference between the satellite clock error $\delta^j(t)$ and the receiver clock error $\delta_A(t)$. The phase equations and the resulting difference between the two points A and B is

$$\begin{aligned} \Phi_A^j(t) &= \frac{1}{\lambda} \cdot \rho_A^j(t) + N_A^j + \frac{c}{\lambda} \cdot (\delta^j(t) - \delta_A(t)) \\ \Phi_B^j(t) &= \frac{1}{\lambda} \cdot \rho_B^j(t) + N_B^j + \frac{c}{\lambda} \cdot (\delta^j(t) - \delta_B(t)) \\ \Phi_B^j(t) - \Phi_A^j(t) &= \frac{1}{\lambda} \cdot [\rho_B^j(t) - \rho_A^j(t)] + N_B^j - N_A^j + \frac{c}{\lambda} \cdot [\delta_B^j(t) - \delta_A^j(t)]. \end{aligned} \tag{2.18}$$

A simplified representation can be given by

$$\Phi_{AB}^j(t) = \frac{1}{\lambda} \cdot \rho_{AB}^j(t) + N_{AB}^j + \frac{c}{\lambda} \cdot \delta_{AB}^j(t). \tag{2.19}$$

The benefit of a single difference is the elimination of the satellite clock error $\delta^j(t)$.

Double differences By combining two single differences an additional simplification of the phase equations, the so called double differences can be formed. For this purpose two ground stations A and B and two satellites j and k, which are tracked by both stations, are required (cf. Figure 2.8).

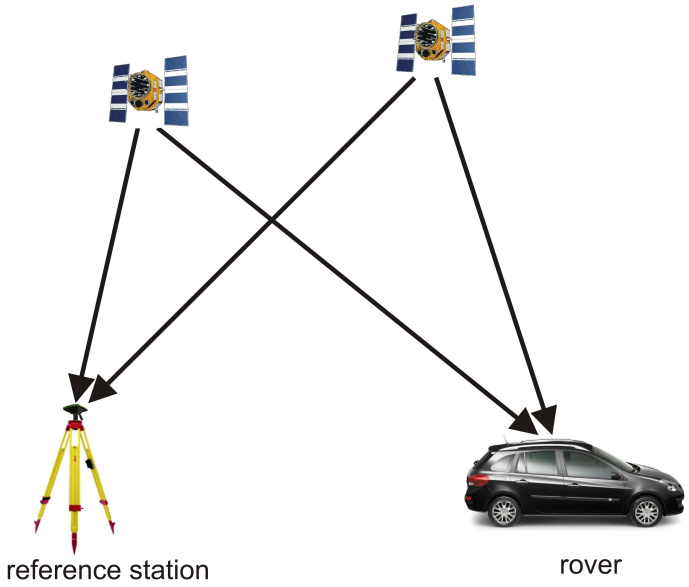

Figure 2.8: Double difference method

Based on single differences, which can be formed for each satellite j and k, further differences of the two single differences can be carried out. The double differences can be modeled by

$$\begin{aligned} \Phi^j_{AB}(t) &= \frac{1}{\lambda} \cdot \rho^j_{AB}(t) + N^j_{AB} + \frac{c}{\lambda} \cdot \delta^j_{AB}(t) \\ \Phi^k_{AB}(t) &= \frac{1}{\lambda} \cdot \rho^k_{AB}(t) + N^k_{AB} + \frac{c}{\lambda} \cdot \delta^k_{AB}(t) \\ \Phi^j_{AB}(t) - \Phi^k_{AB}(t) = \Phi^{jk}_{AB}(t) &= \frac{1}{\lambda} \cdot \rho^{jk}_{AB}(t) + N^{jk}_{AB}. \end{aligned} \tag{2.20}$$

Thus the receiver clock error δ_{AB} is canceled by generating double differences.

Triple differences For the calculation of triple differences once more two stations A and B and two satellites j and k are necessary. Furthermore measurements at two epochs t_0 and t_1 are essential (cf. Figure 2.9).

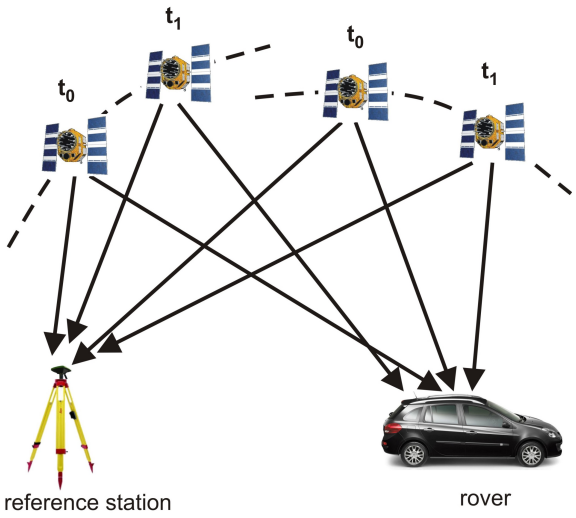

Figure 2.9: Triple difference method

This method is based on differencing double differences between the two epochs. The triple differences are defined by the relation

$$\begin{aligned} \Phi_{AB}^{jk}(t_0) &= \frac{1}{\lambda} \cdot \rho_{AB}^{jk}(t_0) + N_{AB}^{jk} \\ \Phi_{AB}^{jk}(t_1) &= \frac{1}{\lambda} \cdot \rho_{AB}^{jk}(t_1) + N_{AB}^{jk} \\ \Phi_{AB}^{jk}(t_1) - \Phi_{AB}^{jk}(t_0) &= \frac{1}{\lambda} \cdot [\rho_{AB}^{jk}(t_1) - \rho_{AB}^{jk}(t_0)] \end{aligned} \tag{2.21}$$

or

$$\Phi_{AB}^{jk}(t_{01}) = \frac{1}{\lambda} \cdot \rho_{AB}^{jk}(t_{01}). \tag{2.22}$$

Since the ambiguities remain constant over time, the phase ambiguities cancel out by computing the triple differences between two epochs. The only unknown parameter which has to be determined is $\rho_{AB}^{jk}(t_{01})$.

Real time kinematic

The Real Time Kinematic (RTK) positioning method is based on the relative positioning method in real time. Therefore the data of the reference station A have to be transmitted in real time to the rover B and the single-, double- and triple- differences are computed. Some services like the Austrian Positioning Service (*APOS*) of the *BEV* (Bundesministerium für Eich- und Vermessungswesen) offer the opportunity to transmit data of a reference station in real time to the rover station of the user. Therefore the user does not need to define an own reference station, but gets the reference data from the *APOS* service. *APOS* offers also the opportunity to define a virtual reference station, which means that the measurement data of a virtual reference station at a predefined position are derived from the measurement data from the surrounding real reference stations. The advantage of a virtual reference station is the fact that the virtual reference station can be defined anywhere on the Earth surface. The virtual reference station can therefore also be defined, close to the moving rover station B. This leads to a short baseline between both stations and therefore the ionospheric and tropospheric influences are similar and can be eliminated to a high extent.

The positioning method during this master thesis is based on the relative positioning in post processing. The relative positioning method enables to form single, double and triple differences for the elimination of the satellite and receiver clock error, and furthermore of the ambiguities. This forms the basis for the estimation of the ambiguities and therefore for high positioning accuracy.

3 Attitude

In the following the principles of the attitude determination are presented. The common way for precise attitude determination is using INS measurements. The principles of INS attitude determination is shown in Legat (2007). Another way for attitude determination is to use GNSS measurements. This concept will be presented in the following sections. Background knowledge on the GNSS attitude determination can be obtained by the lecture of Gang Lu (1996), (1995) and (1993).

3.1 Definition of attitude

The relative orientation between the local-level frame and the body frame can be defined by the three attitude angles - roll, pitch, and yaw. Due to the area of application in this project, the roll angle measures the rotation around the longitudinal axis of a car. The rotation about the vertical axis is described by the yaw angle, whereas pitch describes the rotation about the transverse axis of the car. Overall the attitude angles rotate around three orthogonal axes. As an example, the definition of the attitude angles of a car are shown in Figure 3.1. The attitude computation can also be done by using quaternions.

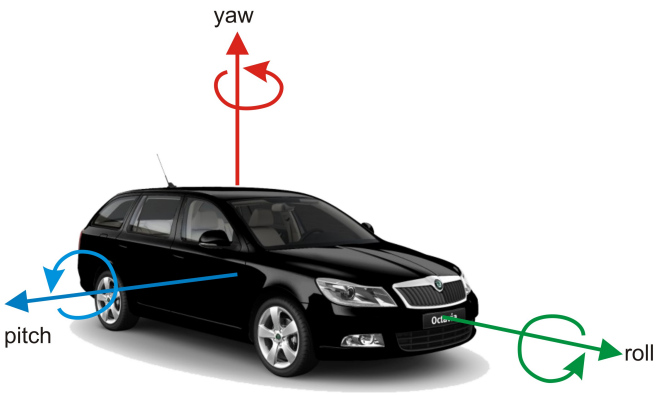

Figure 3.1: Attitude angles for a car

The quaternion attitude determination is a four-parameter representation. It is based on the fact, that the transformation between the collocated frames may be performed by a single rotation around one vector or angle. The attitude parameters roll, pitch and yaw are replaced by four quantities. A detailed description of quaternion computations is given in Legat et al. (2007).
The attitude computation for this master thesis is based on the attitude computation with three rotation angles. To compute the attitude parameters, at least three GNSS antennas are necessary. The concept of the antenna array is explained in chapter 4. The task of the attitude angles is to perform the rotation of the local-level frame into the body frame (cf. Hoffmann-Wellenhof et al. (2001)). Both frame types are briefly explained in the next sections.

3.1.1 Local-level frame

The local-level frame is a coordinate system, which can be defined anywhere on or near the Earth's surface (cf. Hoffmann-Wellenhof et al. (2001)). The origin of the system can be defined arbitrarily. The x-axis of the frame is defined by orientating it to the north direction. The y-axis points towards east and the z-axis to the local zenith (cf. Figure 3.2). Together they form an left handed orthogonal coordinate system with the components north, east and up.

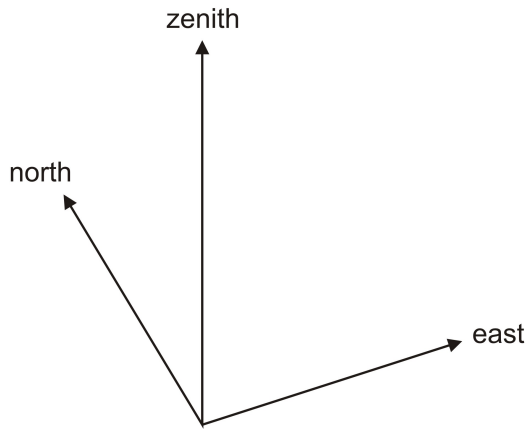

Figure 3.2: Definition of the local-level frame

3.1.2 Body frame

The body frame is defined as a right handed three dimensional Cartesian coordinate frame (cf. Hoffmann-Wellenhof et al. (2001)). The system is connected to an object and is used to determine the relative orientation or attitude of the object with respect to a local-level frame. The origin of the frame is defined by a specific point 'within' the object, mostly the center of mass. The axes coincide with the rotation axes of the object. In this project the object corresponds to a car. The x-axis coincides with the longitudinal axis of the car. The y-axis points towards the transverse axis of the car and the z-axis coincides with the vertical axis of the car. In the case of this study the body frame is defined by a mounting on the roof of the car. For more explanations of this construction see chapter 4.

3.2 Mathematical principles

One aim of this project is the determination of the attitude parameters with a GNSS multi antenna array. Therefore the GPS position data have to be transformed from the terrestrial equatorial frame WGS84 (World Geodetic System 1984) to the local-level frame. Further the transformation matrix which allows the transformation between the local-level and the body frame has to be determined. The elements of the transformation matrix contain the attitude parameters roll, pitch and yaw.

3.2.1 Transformation of the terrestrial equatorial system to the local-level frame

In a first step, the GNSS coordinates, which corresponds to the terrestrial equatorial frame, have to be transformed to the local-level frame (cf. Hoffmann-Wellenhof et al. (2001)). The terrestrial equatorial system is defined as follows. The origin of the frame is the geocenter, which corresponds to the mass center of the Earth. The x-axis points towards the Greenwich meridian, the z-axis corresponds to the mean direction of the rotation axis of the Earth and the y-axis completes the system to a three-dimensional right handed Cartesian system (cf. Figure 3.3).

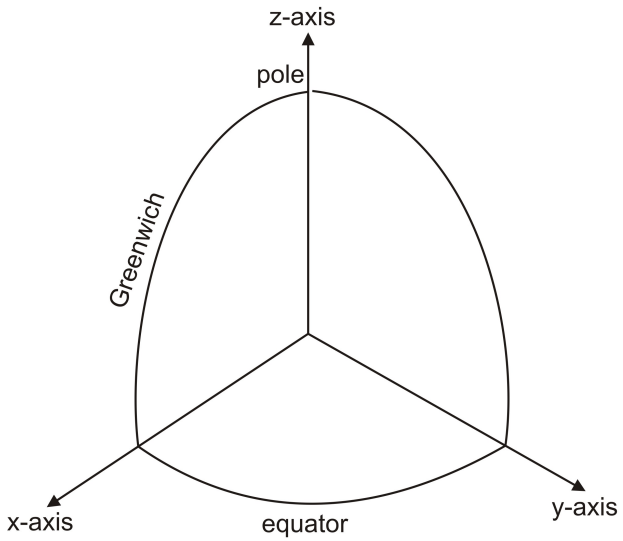

Figure 3.3: Equatorial frame

In the case of GPS this terrestrial equatorial system is realized by the WGS84. At the beginning a transformation of the terrestrial equatorial coordinates from Cartesian (X, Y, Z) to ellipsoidal coordinates (φ, λ, h) is necessary. The longitude λ can be computed directly

$$\tan \lambda = \frac{Y}{X}. \tag{3.1}$$

The height h and the latitude φ have to be computed iteratively, because both equations depend on the parameters φ and h. The algorithm can be founded as

$$p = \sqrt{X^2 + Y^2}, \tag{3.2}$$

$$N = \frac{a^2}{\sqrt{a^2 \cdot \cos^2 \varphi + b^2 \cdot \sin^2 \varphi}}, \tag{3.3}$$

$$h = \frac{p}{\cos \varphi} - N, \tag{3.4}$$

$$\tan \varphi = \frac{Z}{p} \cdot \left(1 - e^2 \cdot \frac{N}{N + h}\right)^{-1}. \tag{3.5}$$

After the transformation of the positions into ellipsoidal coordinates the local-level coordinates (north, east and up) can be computed. For a simplified interpretation the global coordinates are denoted with the subscript i. The quantities of the local-level frame are indicated by the subscript l. The body frame components are characterized by the subscript b. For the transformation from the global frame to the local-level frame vector notation is used. This means, that vectors from the equatorial terrestrial frame can be transformed to local-level vectors with the transformation matrix D. This matrix is defined by the north (n_e), east (e_e) and up (u_e) components

$$D = [n_e, e_e, u_e], \tag{3.6}$$

$$n_e = \begin{bmatrix} -\sin\varphi_e \cdot \cos\lambda_e \\ -\sin\varphi_e \cdot \sin\lambda_e \\ \cos\varphi_e \end{bmatrix}, \qquad e_e = \begin{bmatrix} -\sin\lambda_e \\ \cos\lambda_e \\ 0 \end{bmatrix}, \qquad u_e = \begin{bmatrix} \cos\varphi_e \cdot \cos\lambda_e \\ \cos\varphi_e \cdot \sin\lambda_e \\ \sin\varphi_e \end{bmatrix}. \tag{3.7}$$

The vector transformation from the global Cartesian frame x_e to the local-level frame x_l is denoted by

$$x_l = D^T \cdot x_e \tag{3.8}$$

(cf. Hoffmann-Wellenhof et al. (2001)). The vectors in the local-level frame must be known in the body frame for the computation of the attitude parameters.

3.2.2 Three vector attitude computation

The attitude of the object can be determined. Based on the transformation between vectors of the local-level frame (x_l) and the same vectors in the body frame (x_b). As the attitude angles describe the transformation or rotation from the local-level frame to the body frame, the transformation matrix has to be computed.

The transformation can be expressed by

$$x_b = R_l^b \cdot x_l, \tag{3.9}$$

where R_l^b is the rotation matrix. R_l^b includes the attitude parameters roll, pitch and yaw. Noticeable is, that both frames must have the same center of origin. A vector known in both frames (u_l and u_b) leads to three nonlinear equations with the three unknown attitude parameters. With a single vector, the two frames cannot be defined, since one vector is not sufficient to compute the attitude parameters. A second vector (v_l and v_b) results in an overdetermined system with, six equations for three unknowns. However both vectors u and v have to fulfill some conditions. The length of the vectors u and v has to be the same in the local-level and in the body frame

$$\|u_l\| = \|u_b\|, \qquad \|v_l\| = \|v_b\|. \tag{3.10}$$

Additional the angle between the u vector and the v vector has to be identical in both frames

$$u_l \cdot v_l = u_b \cdot v_b. \tag{3.11}$$

If all conditions are fulfilled, the next step is the computation of a third orthogonal vector w in both systems, based on the u and the v vector

$$w_l = u_l \times v_l, \qquad w_b = u_b \times v_b. \tag{3.12}$$

These three vectors u, v and w are used to define the three-dimensional matrices L and B. The columns of the L matrix contain the u_l, v_l and w_l vectors of the local-level frame. The B matrix consists of the body frame vectors u_b, v_b and w_b. Based on the two matrices the rotation matrix R_l^b, which defines the rotation from the local-level frame to the body frame, can be computed.

In a further step the attitude parameters can be deduced from R_l^b

$$L = [u_l, v_l, w_l], \qquad B = [u_b, v_b, w_b], \tag{3.13}$$

$$B = R_l^b \cdot L, \tag{3.14}$$

$$R_l^b = B \cdot L^{-1}. \tag{3.15}$$

The rotation matrix R_l^b contains the attitude parameters in the form of

$$\begin{aligned}
R_{11} &= \cos r \cdot \cos y - \sin r \cdot \sin p \cdot \sin y, \\
R_{12} &= \cos r \cdot \sin y + \sin r \cdot \sin p \cdot \cos y, \\
R_{13} &= -\sin r \cdot \cos p, \\
R_{21} &= -\cos p \cdot \sin y, \\
R_{22} &= \cos p \cdot \cos y, \\
R_{23} &= \sin p, \\
R_{31} &= -\sin r \cdot \cos y + \cos r \cdot \sin p \cdot \sin y, \\
R_{32} &= \sin r \cdot \sin y - \cos r \cdot \sin p \cdot \cos y, \\
R_{33} &= \cos p \cdot \cos r,
\end{aligned} \tag{3.16}$$

$$R_l^b = \begin{bmatrix} R_{11} R_{12} R_{13} \\ R_{21} R_{22} R_{23} \\ R_{31} R_{32} R_{33} \end{bmatrix}. \tag{3.17}$$

The matrix contains the attitude parameters roll (r), pitch (p) and yaw (y) which can be computed by

$$\tan r = -\frac{R_{13}}{R_{33}}, \tag{3.18}$$

$$\tan p = \frac{R_{23}}{\sqrt{R_{21}^2 + R_{22}^2}}, \tag{3.19}$$

$$\tan y = -\frac{R_{21}}{R_{22}}. \tag{3.20}$$

The attitude parameters can be determined with the components R_{ij} of the rotation matrix R_l^b. The index i of R_{ij} describes the row number of the matrix. The column number of the matrix is defined by the index j.

The aim of this master thesis is the computation of the attitude parameters for each GNSS measurement epoch, to define the orientation of the car along the trajectory.

3.2.3 Overdetermined attitude computation

The disadvantage of the attitude determination using three receivers is, that no redundancy exist. Therefore a lower accuracy due to blunders of the positions can be expected. The use of four antennas enables a redundant attitude determination with higher accuracy. The availability of more than 3 vectors allows a least square solution of the rotation matrix R_l^b.
This procedure described in Hoffmann-Wellenhof et al. (2001) is an adjustment solution for the rotation matrix R_l^b. Therefore all vectors have to be known in the local-level frame and in the body frame. The B matrix of the three vector attitude determination algorithm is denoted as $\bar{B}$ matrix. The columns contains the vectors of the body frame. Whereas the matrix $\bar{L}$ represents all vectors in the local-level frame. Both matrices have three rows and n columns, where n denotes the number of vectors. The number of vectors has to be equal or greater than three to solve the system. Whereas three vectors do not allow a redundant attitude determination. The rotation matrix R_l^b can be computed by introducing the pseudoinverse of the matrix $\bar{L}^+$

$$\bar{L}^+ = \bar{L}^T \cdot (\bar{L} \cdot \bar{L}^T)^{-1}. \tag{3.21}$$

The computation of the rotation matrix R_l^b

$$R_l^b = B \cdot \bar{L}^+, \tag{3.22}$$

and the resulting attitude parameters are described in the section 3.2.1. A simulation of the adjustment of the attitude matrix has been computed to investigate the results with different number of antennas.

Simulation of the attitude algorithm

Before dealing with real measurement data the behavior of the algorithm was investigated by doing simulations. In case of the attitude algorithm the aim of the simulation is the examination of the two presented algorithms regarding robustness. Beside the three vector algorithm also the adjustment procedure is investigated using a closed loop simulation. Therefore five points have been defined in a body frame see Figure 3.4.

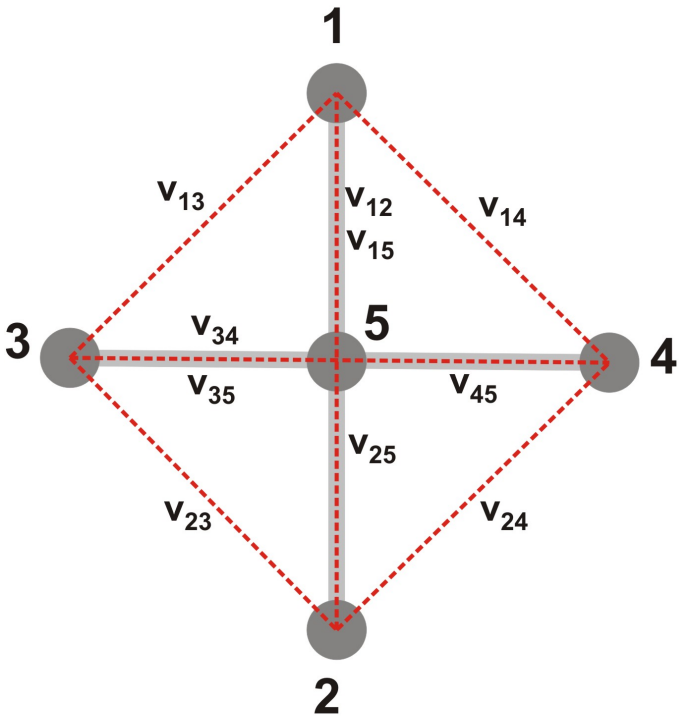

Figure 3.4: Structure of an overdetermined attitude adjustment

Actually the company iMAR offers already a 3D GPS based true heading and positioning system, which works with nine antennas. An attitude adjustment with nine antennas is expected to have a lower standard deviation as one with five antennas like in this simulation. In a next step the transformation of the simulated points into the local-level frame, by using predefined attitude values (cf. Table 3.1), is achieved.

roll [deg]	pitch [deg]	yaw [deg]
5	4	127

Table 3.1: Attitude parameters for the transformation from the body frame into the local-level frame

The LL matrix, which contains the coordinates of the five points in the local-level frame, can be computed by

$$LL = R_l^{bT} \cdot BB. \tag{3.23}$$

The body frame matrix BB consists of the body frame coordinates for each point. The transformation matrix R_l^b contains the defined attitude parameters roll, pitch and yaw.

For considering measurement errors, which can be expected by the GNSS measurements, the local-level coordinates are affected by errors in a range of about -30 cm to 30 cm for each epoch. Afterwards the difference vectors v_{ij}, which represents the antennas, are computed in the local-level frame and in the body frame. The difference vectors are further used to build up the B and the L matrix. The attitude adjustment has been performed three times with three, four and seven difference vectors. The used difference vectors are listed in Table 3.2.

3 antennas	4 antennas	7 antennas
v_{12}	v_{12}	v_{12}
v_{13}	v_{13}	v_{13}
v_{1z}	v_{1z}	v_{1z}
	v_{34}	v_{14}
		v_{23}
		v_{24}
		v_{15}

Table 3.2: Difference vectors used for the attitude adjustment simulation

The vector v_{1z} corresponds to the cross product solution between the vector v_{12} and v_{13}. The differences between the solutions of the attitude adjustment and the input attitude parameters (cf. Table 3.1) are further investigated.

The mean value of the difference between each attitude parameter and the input parameters are listed in Table 3.3.

	roll [deg]	pitch [deg]	yaw [deg]
3 vectors	0.69	-0.87	-0.20
4 vectors	0.64	-0.88	-0.38
7 vectors	0.44	-0.80	-0.27

Table 3.3: Mean values of the differences of the attitude parameter

The mean differences of the roll and yaw angles show larger changes as the mean value of the pitch angle. In case of the adjustment procedure better results can be expected if more vectors are used. This means that also the standard deviation for each attitude solution should be smaller, see Table 3.4.

	roll [deg]	pitch [deg]	yaw [deg]
3 vectors	4.56	7.96	3.76
4 vectors	4.54	7.96	3.73
7 vectors	4.21	6.63	3.59

Table 3.4: Standard deviations of the differences of the attitude parameter

The differences of the standard deviations show a benefit, if more vectors are used. Thus more than three antennas are needed to improve the attitude results to get an overdetermined system of equations. Additionally, more than three antennas enable a blunder detection. Beside the number of used antennas also the baseline length and the actual position accuracies influence the accuracy of the computed attitude parameters. An estimation on these effects is done by calculating a variance propagation before consequently doing field tests.

3.3 Variance propagation

The aim of the variance propagation is the investigation of the effects of erroneous observations on the computed parameters. In this case, the influences of GPS positioning errors on the attitude parameters should be investigated. The variance propagation is computed for the attitude computation algorithm based on three antennas.

3.3.1 Theory of the variance propagation

The variance propagation computation is based on a linear relation between the observations and the unknown parameters. As the equations for the attitude computation are mostly non-linear, a linearization by a Taylor series expansion with regard to the Taylor points (x_0, y_0) has to be done.

$$f(x,y) = f(x_0,y_0) + \frac{\partial f}{\partial x} \mid_{x_0,y_0} \cdot(x - x_0) + \frac{\partial f}{\partial y} \mid_{x_0,y_0} \cdot(y - y_0) + ... \tag{3.24}$$

The Taylor series can be cut off after the linear term as the terms of higher order are already very small. This means that the function $f(x,y)$ should be partial differentiated with respect to the erroneous parameters

$$f(x,y) = f(x_0,y_0) + \frac{\partial f}{\partial x} \cdot (dx) + \frac{\partial f}{\partial y} \cdot (dy). \tag{3.25}$$

To consider the covariances between the parameters the variance propagation is performed in matrix-vector notation. The matrix A contains the partial derivatives of the erroneous parameters

$$A = \left[\frac{\partial f(x,y)}{\partial x} \quad \frac{\partial f(x,y)}{\partial y} \right]. \tag{3.26}$$

The variances of the observations are summarized in the covariance matrix $\Sigma_{observations}$. The covariance matrix Σ comprises the variances σ_{ii}^2 in the main diagonal and in the off-diagonal elements the corresponding covariances σ_{ij}^2.

Σ is a symmetric matrix and is also denoted as correlation matrix

$$\Sigma = \begin{bmatrix} \sigma_{11}^2 & \sigma_{12}^2 & \sigma_{13}^2 \\ \sigma_{21}^2 & \sigma_{22}^2 & \sigma_{23}^2 \\ \sigma_{31}^2 & \sigma_{32}^2 & \sigma_{33}^2 \end{bmatrix}. \tag{3.27}$$

The errors of the computed parameters can be computed by

$$\Sigma_{computed} = A \cdot \Sigma_{observations} \cdot A^T. \tag{3.28}$$

3.3.2 Variance propagation with three antennas

The variance propagation for the attitude parameters is based on the algorithm with three antennas. The computation uses the three points (P1, P2, P3) as shown in Figure 3.5.

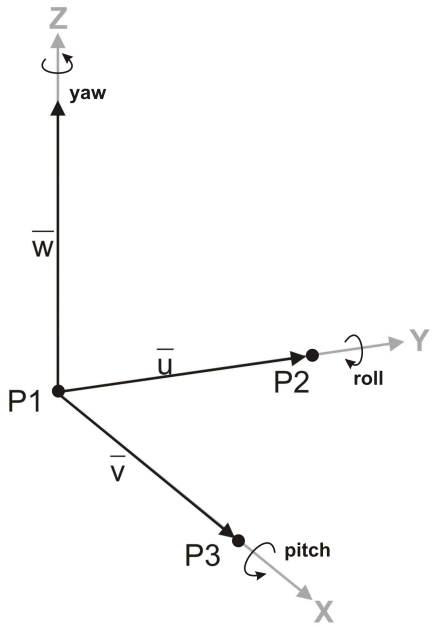

Figure 3.5: Basic setup for the variance propagation

Each coordinate triple is known in the body frame as well as in the local-level frame. The length of the vector u and v corresponds to the baseline length of the roof rack construc-

tion. The length of the baseline is a dominant factor for accuracy of the computation. Longer baselines facilitate a more stable computation of the attitude parameters. As a matter of fact the lengths of the baselines are limited due to the car's size. The covariance matrix of the body frame contains the accuracies of each point which can be obtained by the calibration computation. The errors of the GPS measurements are the fundamentals for the covariance matrix of the local-level frame. The variances of the points in the local-level frame and the body frame influence the whole attitude computation and result in a covariance matrix of the attitude parameters. Therefore the variance propagation has to be computed for each equation which is needed for the attitude computation. The variances of the attitude parameters can be found in the main diagonal of the computed covariance matrix of the last computation step of the attitude computation. The standard deviation can be obtained by calculating the root of the variances.

The variance propagation for the attitude parameters starts with the computation of the variances caused by the transformation of the vector differences from the WGS84 frame to the local-level frame. In a next step the variances of the difference vectors in the body frame have to be computed, followed by the variance computation of the cross product. Afterwards the variances of the L and the B matrices have to be calculated. The last steps enable the variance matrix computation of the transformation matrix R_l^b and further the variances of the attitude parameters.

The covariance propagation of the cross product computation (equation 3.12) is mentioned here for a better understanding. The cross product of two vectors is used for the computation of the orthogonal vector w

$$w = u \times v = \begin{pmatrix} u_y \cdot v_z - u_z \cdot v_y \\ u_z \cdot v_x - u_x \cdot v_z \\ u_x \cdot v_y - u_y \cdot v_x \end{pmatrix}. \tag{3.29}$$

The matrix A, which is required for the variance propagation, contains the partial derivatives of each matrix element

$$A = \begin{bmatrix} \frac{\partial w_x}{\partial u_x} & \frac{\partial w_x}{\partial u_y} & \frac{\partial w_x}{\partial u_z} & \frac{\partial w_x}{\partial v_x} & \frac{\partial w_x}{\partial v_y} & \frac{\partial w_x}{\partial v_z} \\ \frac{\partial w_y}{\partial u_x} & \frac{\partial w_y}{\partial u_y} & \frac{\partial w_y}{\partial u_z} & \frac{\partial w_y}{\partial v_x} & \frac{\partial w_y}{\partial v_y} & \frac{\partial w_y}{\partial v_z} \\ \frac{\partial w_z}{\partial u_x} & \frac{\partial w_z}{\partial u_y} & \frac{\partial w_z}{\partial u_z} & \frac{\partial w_z}{\partial v_x} & \frac{\partial w_z}{\partial v_y} & \frac{\partial w_z}{\partial v_z} \end{bmatrix} \tag{3.30}$$

$$A = \begin{bmatrix} 0 & v_z & -v_y & 0 & -u_z & u_y \\ -v_z & 0 & v_x & u_z & 0 & -u_x \\ v_y & -v_x & 0 & -u_y & u_x & 0 \end{bmatrix}. \tag{3.31}$$

The errors of the u vector and the v vector are collected in the covariance matrix $\Sigma_{observations}$

$$\Sigma_{observations} = \begin{bmatrix} \sigma^2_{u_x u_x} & \sigma^2_{u_x u_y} & \sigma^2_{u_x u_z} & \sigma^2_{u_x v_x} & \sigma^2_{u_x v_y} & \sigma^2_{u_x v_z} \\ \sigma^2_{u_y u_x} & \sigma^2_{u_y u_y} & \sigma^2_{u_y u_z} & \sigma^2_{u_y v_x} & \sigma^2_{u_y v_y} & \sigma^2_{u_y v_z} \\ \sigma^2_{u_z u_x} & \sigma^2_{u_z u_y} & \sigma^2_{u_z u_z} & \sigma^2_{u_z v_x} & \sigma^2_{u_z v_y} & \sigma^2_{u_z v_z} \\ \sigma^2_{v_x u_x} & \sigma^2_{v_x u_y} & \sigma^2_{v_x u_z} & \sigma^2_{v_x v_x} & \sigma^2_{v_x v_y} & \sigma^2_{v_x v_z} \\ \sigma^2_{v_y u_x} & \sigma^2_{v_y u_y} & \sigma^2_{v_y u_z} & \sigma^2_{v_y v_x} & \sigma^2_{v_y v_y} & \sigma^2_{v_y v_z} \\ \sigma^2_{v_z u_x} & \sigma^2_{v_z u_y} & \sigma^2_{v_z u_z} & \sigma^2_{v_z v_x} & \sigma^2_{v_z v_y} & \sigma^2_{v_z v_z} \end{bmatrix}. \tag{3.32}$$

The diagonal elements of the computed covariance matrix of the w-vector corresponds to the variances of each coordinate component (north, east, down). The off-diagonal elements contain the covariances of the w-vector components

$$\Sigma_w = A \cdot \Sigma_{observations} \cdot A^T \tag{3.33}$$

$$\Sigma_{observations} = \begin{bmatrix} \sigma^2_{w_x w_x} & \sigma^2_{w_x w_y} & \sigma^2_{w_x w_z} \\ \sigma^2_{w_y w_x} & \sigma^2_{w_y w_y} & \sigma^2_{w_y w_z} \\ \sigma^2_{w_z w_x} & \sigma^2_{w_z w_y} & \sigma^2_{w_z w_z} \end{bmatrix}. \tag{3.34}$$

For each equation, which is needed for the attitude computation, a variance propagation is computed. The solutions of the variance propagation are shown in the next section, whereas different conditions are considered.

3.3.3 Solutions of the variance propagation

Following the computed standard deviations are investigated for different scenarios, which means that different error results. In a first step the influences of the GNSS positioning

accuracies on the calculated attitude parameters shall be analyzed.
For the computation of the standard deviations the algorithm needs predefined attitude values. Therefore a representative set of attitude parameters was chosen, which can be expected when using a car.

attitude parameter	angle [deg]
roll	2
pitch	6
yaw	12

Table 3.5: Input attitude parameters for the variance propagation

It must be mentioned, that different attitude parameters change the solution of the computed standard deviations. In a first computation step, all points ($P1, P2, P3$) are assumed to be erroneous in each coordinate component (x, y, z). The error varies between 1 mm and 50 cm, which corresponds to the usual positioning accuracy of GNSS using relative or differential positioning techniques. Figure 3.6 shows the results of the variance propagation for roll, pitch and yaw.

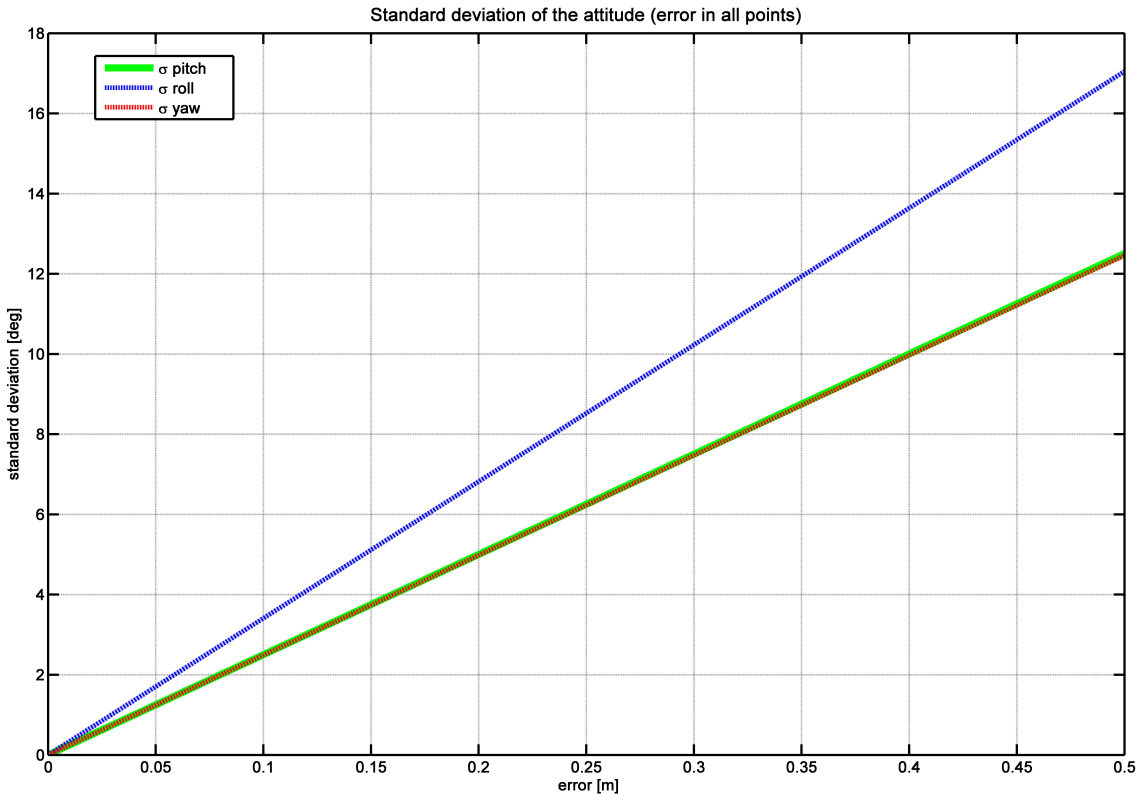

Figure 3.6: Standard deviations of the attitude parameters with different positioning errors

The standard deviations of pitch and yaw are very similar and reach ∼12.5° at a positioning error of 50 cm. The standard deviations of roll are larger and reach ∼17.0° at a 50 cm positioning error. The standard deviations grow continuously with a growing positioning error see Table 3.6.

positioning error	roll [deg]	pitch [deg]	yaw [deg]
1 mm	0.03	0.02	0.02
1 cm	0.34	0.25	0.25
10 cm	3.41	2.50	2.50
50 cm	17.05	12.50	12.50

Table 3.6: Standard deviations of the attitude parameters

In another instance the standard deviation computation investigates following case: Each coordinate of the points shows an error of 10 cm and only the error in one point, in one corresponding coordinate value is assumed to vary between 1 mm and 50 cm. In Figure 3.7, the standard deviations of roll, pitch and yaw are shown for the case of a varying x-component of point $P2$.

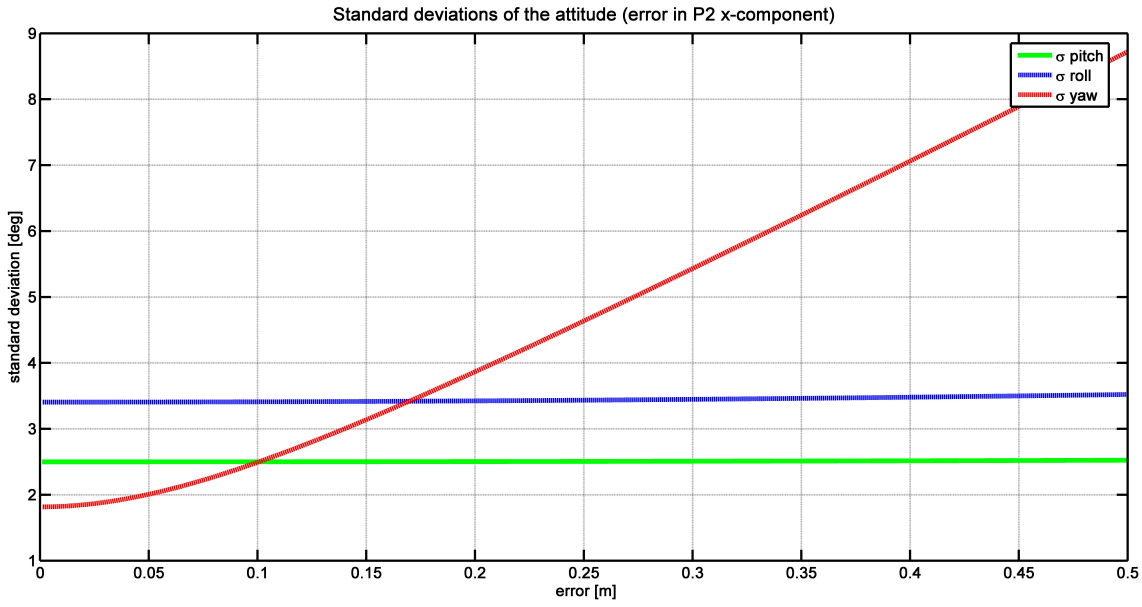

Figure 3.7: Standard deviations of the attitude parameters with a growing error in the x-component of point P2

The standard deviations of pitch and roll seem to be nearly constant with a value of ∼2.5° and ∼3.5°. Only a small increase of the roll standard deviations can be recognized. The standard deviations of the yaw angle show a bigger change with increasing positioning errors at the x-component of P2.

In a second step, the variances of the attitude parameters should be investigated as a function of the baseline length. This computation algorithm is explained by Farrell et al. (1998). The computation algorithm depends on several terms, like the baseline length a and b, the maximum expected positioning error in the north, east and up directions ($\bar{\sigma}$) and the angle Φ. The angle γ describes the angle between the vector $\bar{a}$ and $\bar{b}$ which is expected to be 45° (cf. Figure 3.8). The length of the vector a is 2.16 m, the length of the vector b is 1.57 m.

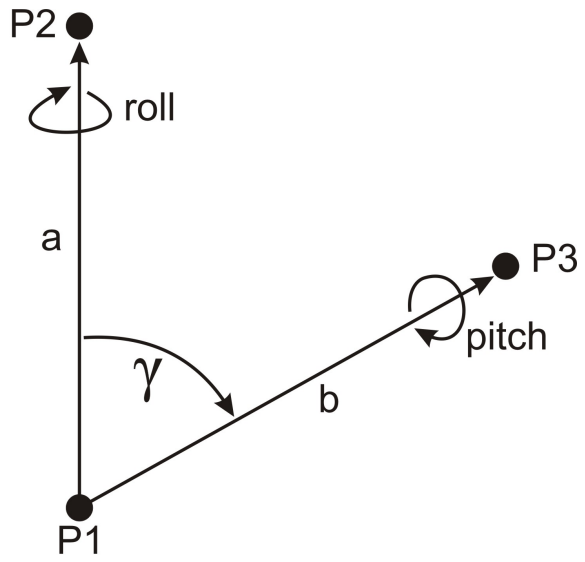

Figure 3.8: GNSS antenna mounted on the body frame

The angle Φ can be computed with the known local-level coordinates north, east and down (n_1, e_1, d_1) of point 1 ($P1$):

$$\Phi = \arctan\left(\frac{-d_1}{\sqrt{e_1^2 + n_1^2}}\right) \tag{3.35}$$

The standard deviations of the attitude parameters can be computed by

$$\begin{aligned} \sigma_{roll} &= \frac{\bar{\sigma}}{\mid b \mid \cdot \cos \gamma}, \\ \sigma_{pitch} &= \frac{\bar{\sigma}}{\alpha}, \\ \sigma_{yaw} &= \frac{\bar{\sigma}}{\mid a \mid \cdot \cos \Phi}. \end{aligned} \tag{3.36}$$

This algorithm enables the determination of the effect of changing the baseline length a (cf. Figure 3.9). The positioning error $\bar{\sigma}$ is expected to be 1 cm. The disadvantage of this computation algorithm is the fact, that the cosines function of the angle γ does not allow an angle of 90°.

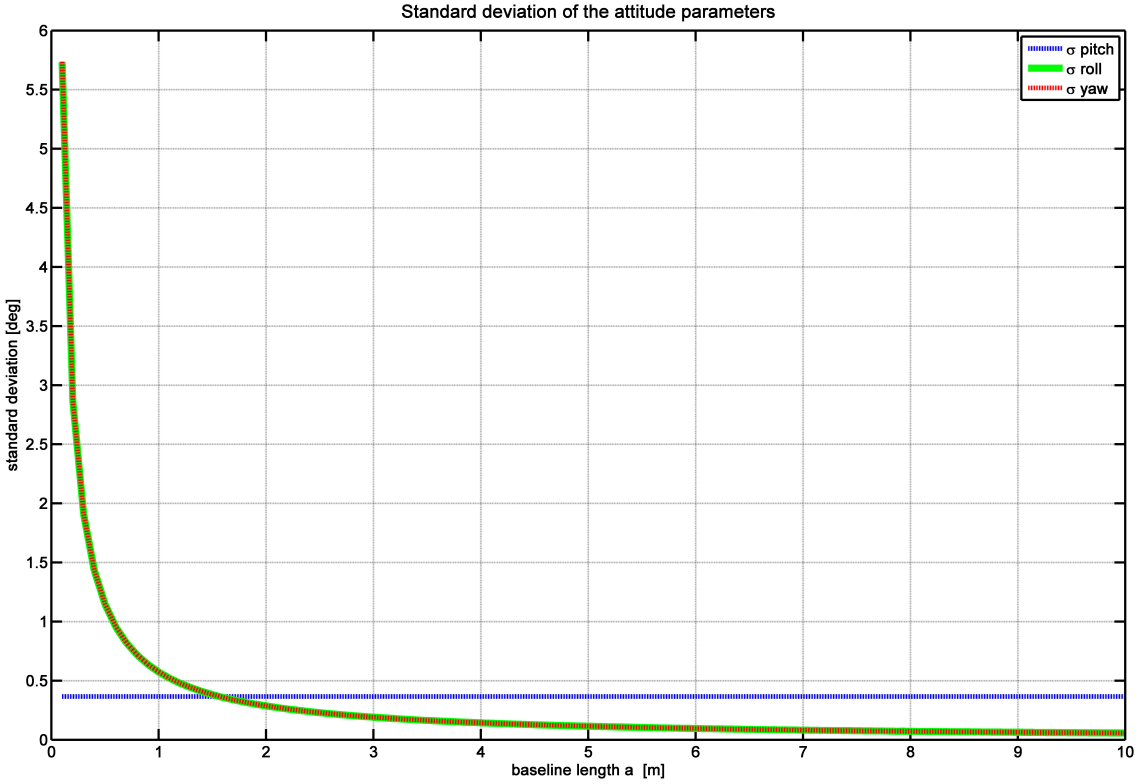

Figure 3.9: Standard deviations of the attitude parameters by changes of the baseline length a

The standard deviations of pitch and yaw show a strong decrease with a growing baseline length a. The standard deviations of pitch and yaw correspond to $\sim$5.7° at a baseline length of 10 cm. However a baseline of 10 m enables standard deviations of $\sim$0.05°. No influences can be seen in the standard deviations of the roll parameter while changing the baseline length a. Only the positioning errors $\bar{\sigma}$ influence the computations in a negative sense. The standard deviations of roll show large changes by varying the baseline length b (cf. Figure 3.10).

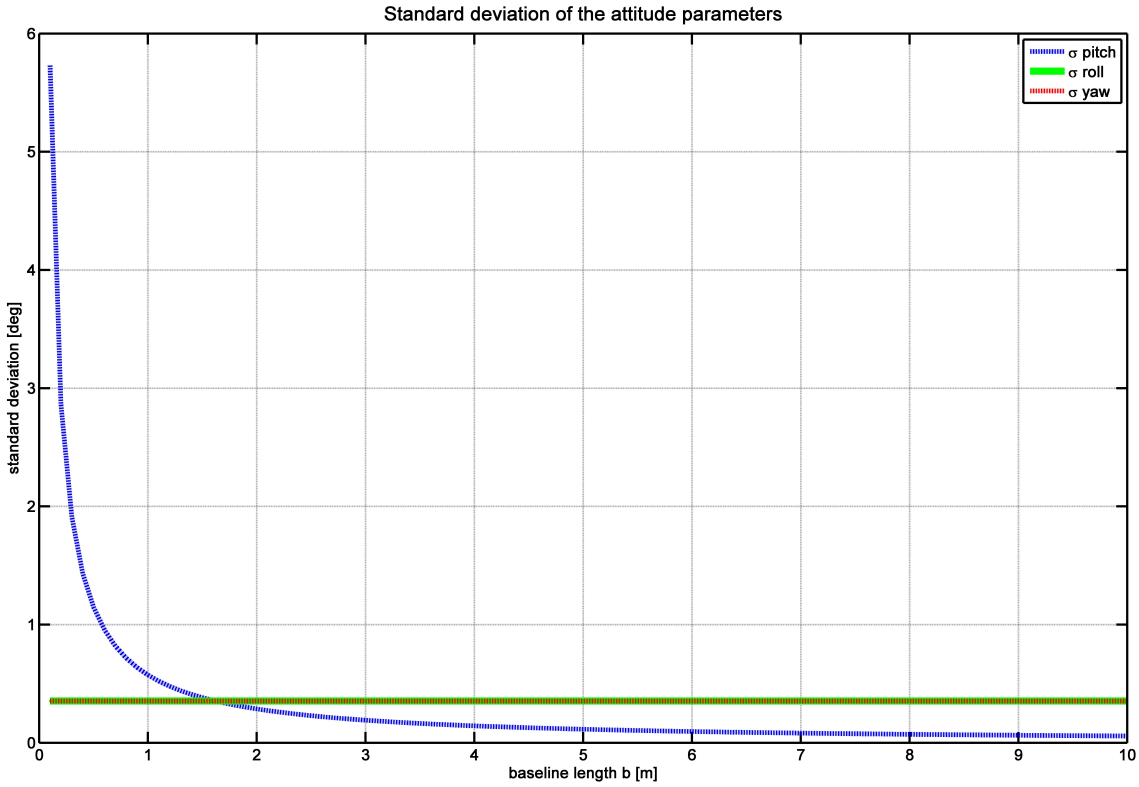

Figure 3.10: Standard deviations of the attitude parameters by changes of the baseline length b

The behavior of roll seems to be very similar, as it occurs by the change of the baseline a to the attitude parameters pitch and yaw (cf. Figure 3.9). The standard deviations of roll varies between $\sim$8.1° at a baseline length b of 10 cm and $\sim$0.08° if b corresponds to 10 m. The attitude errors of yaw and pitch are constant and show no influence by changing the length of baseline b. The solution of the standard deviations with varying baseline length shows a reduction by a factor of 10^{-2} by extending the baseline length by a factor of 10^2.

That means, that all errors are indirect proportional to the baseline length.

Concluding the variance propagation, it can be stated that positioning errors of each point, as well as the baseline lengths and the attitude parameters itself influence the accuracies of the attitude parameters. The attitude errors are getting smaller when the baseline lengths are increasing. Thus longer baselines are focused, since the GNSS errors are hardly to control. Nevertheless the computations of the coordinates of the antenna positions have to be very precise as well.

For this project the baseline lengths were predefined by the construction. Due to the requirements for the gravity estimation, an attitude error of better than $\sim 1^\circ$ is mandatory. Thus the GNSS positioning accuracy must be better than ~ 2 cm. Therefore the relative positioning method has to be used.

4 Construction

As already mentioned, one main goal of the project GRAVIS is the determination of a car's attitude. Therefore the GNSS antennas and the IMU (Inertial Measuring Unit) have to be mounted on a stable construction on the top of the roof of the car. Screw threads fix the position of the antennas on the construction. The IMU is screwed on an iron plate. Hence, for each measurement unit, fixed positions on the construction can be guaranteed. Because of that, a unique calibration of the construction is necessary to compute the relative positions between all GNSS antennas and the IMU. The distances between the GNSS antennas and the IMU are also denoted as lever arms. The knowledge of the lever arms is essential for the combination of the GPS and IMU measurement data. The distances between the antennas are used to set up the body frame, which is needed for the computation of the attitude parameters. Due to the project goal and for an improved accuracy, several requirements regarding the setup arise. The following requisitions are preferable for the construction:

- minimum of two baselines
- shape-retaining
- vibration damper of the construction
- independent concerning temperature changes
- lightweighted construction
- flexible montage

A cooperation with the Joanneum Research in Graz offered the opportunity to lend a suitable construction for the car (cf. Figure 4.1). This construction was used in another project of the Joanneum Research (cf. Abwerzger et al. (2000)).

Figure 4.1: Multi antenna array for the attitude measurements

Four GNSS antennas can be attached in the shape of a cross, where the major axis points along the driving direction of the car. A simplified top view of the construction can be seen in Figure 4.2.

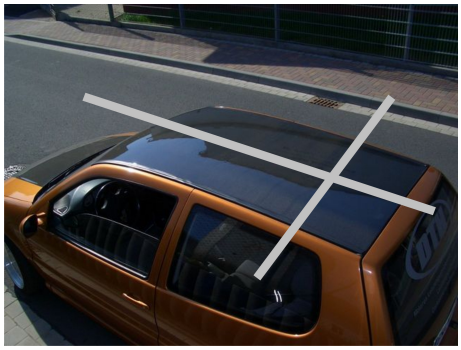

Figure 4.2: Schematic top view of the roof construction

The light gray balks describe the form of the construction and define the baselines between the GNSS antennas, which are mounted at each end of the baselines. An additional iron plate on the bottom of the construction allows a stable mounting of the IMU with respect to the construction. For the computation of the attitude the distances between the antennas and the IMU have to be very precise. Therefore a calibration is essential.

4.1 Calibration

The calibration of the construction has been executed on the roof of the geodesy building at Graz, University of Technology. During the calibration measurements the construction was kept in a solid position, so that an optimum environment for the calibration of the construction was guaranteed. The measurements were done simultaneously by two theodolites from two pillars on the roof of the building (cf. Figure 4.3). The positions of the pillars are precisely known and were controlled by measurements of other known positions in the surrounding area.

Figure 4.3: Calibration setup of the roof construction by terrestrial measurements

Due to the fact, that the antennas are mounted by a screw thread, it's not possible to measure the relative antenna positions on the construction in a direct way. The corresponding measurement centers (phase centers) of the antennas lie inside of the antennas (cf. Figure 4.4) and can therefore not be determined by the calibration only.

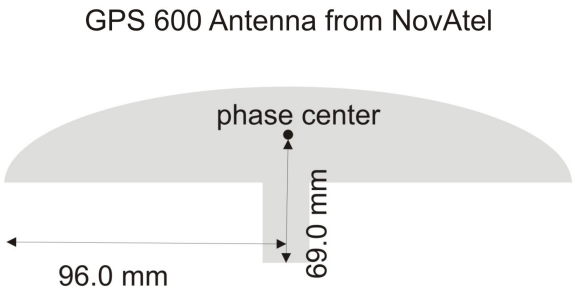

Figure 4.4: Antenna phase center of the GPS 600 antenna from NovAtel

The relative positions of the antennas have to be computed by using the calibration solutions and the corresponding parameters of the antenna phase center, defined in the antenna manuals. For the computations the mathematical methods of plain and line intersection were used.

The evaluation of the measured data was performed with the geodetic evaluation software Geosie 6.0. The used computation method requires measurements from two positions with known coordinates. The pillars on the roof of the geodesy building are selected as suitable measurement points. The measurements were done by two Leica theodolites - TC1800. All measurement points on the construction and the IMU, were marked to allow a consistent measurement of the points from both stations. To reduce the measurement errors, all measurements have been performed simultaneously. All in all, three sets have been measured to get a sufficient redundancy. The theodolites permit the measurement of horizontally directions. An overview about the measurement principle is shown in Figure 4.5.

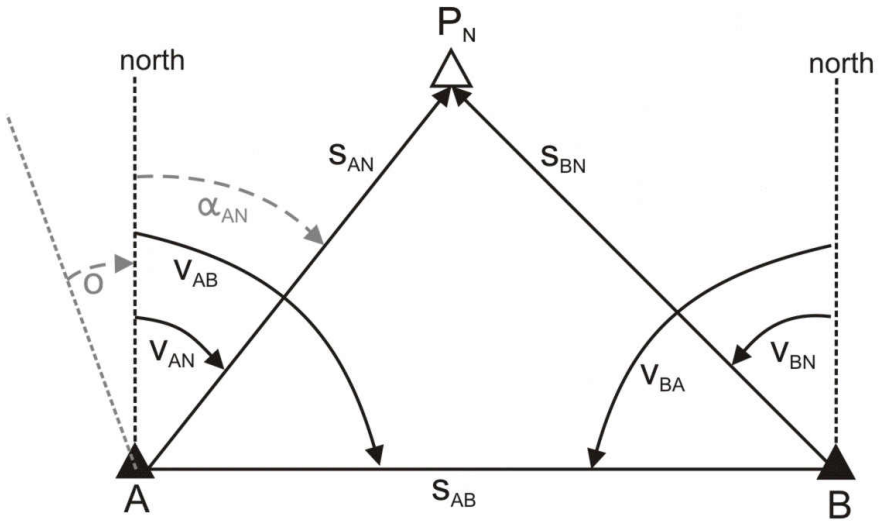

Figure 4.5: Point determination by using measured angles and known coordinates

The points A and B represent the pillar stations where the coordinates are known. The terms s_{AB}, s_{AN} and s_{BN} represent the distances between the points.

The oriented directions are marked by the notation v_{AB}, v_{AN} and v_{BN} and can be computed by addition or subtraction of the measured angles α_{ij} and the orientation angle o

$$v_{ij} = \alpha_{ij} \pm o. \tag{4.1}$$

The coordinates of the two pillars and the measured directions v_{AN} and v_{BN} can be introduced. The distance s_{AB} and the angle v_{AB} between the pillars can be computed by

$$s_{AB} = \sqrt{(x_B - x_A)^2 + (y_B - y_A)^2} \tag{4.2}$$

and

$$\tan v_{AB} = \frac{y_B - y_A}{x_B - x_A}. \tag{4.3}$$

The distance between the pillars and the measured points can be calculated by the formulas

$$s_{AN} = s_{AB} \cdot \frac{\sin(v_{BN} - v_{AB})}{\sin(v_{BN} - v_{AN})} \tag{4.4}$$

and

$$s_{BN} = s_{AB} \cdot \frac{\sin(v_{AN} - v_{AB})}{\sin(v_{BN} - v_{AN})}. \tag{4.5}$$

These parameters allow the determination of the unknown point coordinates $P_N(x_N, y_N)$

$$\begin{aligned} x_N &= x_A + s_{AN} \cdot \cos v_{AN}, \\ y_N &= y_A + s_{AN} \cdot \sin v_{AN}. \end{aligned} \tag{4.6}$$

On the whole, all marked points are measured three times to have a control of each point. The software tool Geosie computes the coordinates of the measured points in the Gauß-Krüger (GK) plane. All computations of Geosie are based on the GK reference system. As mentioned before, the main problem is, that the reference points of the antennas cannot be measured in a direct way. Therefore the reference points are computed by intersection of plains and lines. Finally the parameters of the phase centers, which are

known by the production industry, must be added to the computed reference point to get the measurement center of the GPS antennas.

The known centers of the antennas allow the determination of the distance between the antennas and the IMU. Previously a coordinate transformation, of the computed points, from the GK plane to the WGS84 system was performed (cf. Hoffmann-Wellenhof et al. (2001)). As the GNSS measurements are related to the WGS84 system, it is necessary to transform the computed points of the calibration from the two-dimensional GK system to the three-dimensional WGS84 system to avoid distortions of the lengths between the calculated points. The transformation between the Gauss-Krüger and the WGS84 system can be computed by series expansions

$$\begin{aligned}\phi = \phi_f &+ \frac{t_f}{2 \cdot N_f^2} \cdot (-1 - \eta_f^2) x^2 \\ &+ \frac{t_f}{24 \cdot N_f^4} \cdot (5 + 3t_f^2 + 6\eta_f^2 - 6t_f^2\eta_f^2 - 3\eta_f^4 - 9t_f^2\eta_f^4) x^4 \\ &+ \frac{t_f}{720 \cdot N_f^6} \cdot (-61 - 90t_f^2 - 45t_f^4 - 107\eta_f^2 + 162t_f^2\eta_f^2 + 45t_f^4\eta_f^2) x^6 \\ &+ \frac{t_f}{40320 \cdot N_f^8} \cdot (1385 + 3633t_f^2 + 4095t_f^4 + 1575t_f^6) x^8 + ... \end{aligned} \quad (4.7)$$

$$\begin{aligned}\lambda = \lambda_0 &+ \frac{1}{N_f \cos\phi_f} \cdot x + \frac{1}{6N_f^3 \cos\phi_f}(-1 - 2t_f^2 - \eta_f^2) x^3 \\ &+ \frac{1}{120N_f^5 \cos\phi_f}(5 + 28t_f^2 + 24t_f^4 + 6\eta_f^2 + 8t_f^2\eta_f^2) x^5 \\ &+ \frac{1}{5040N_f^7 \cos\phi_f}(-61 - 662t_f^2 - 1320t_f^4 - 720t_f^6) x^7 + ..., \end{aligned} \quad (4.8)$$

where the terms with the subscript f must be calculated by

$$\begin{aligned} \bar{y} &= \frac{y}{\bar{\alpha}}, \\ \phi_f &= \bar{y} + \bar{\beta}\sin 2\bar{y} + \bar{\gamma}\sin 4\bar{y} + \bar{\delta}\sin 6\bar{y} + \bar{\varepsilon}\sin 8\bar{y} + ..., \\ e'^2 &= \frac{a^2 - b^2}{b^2}, \\ \eta_f^2 &= e'^2 \cdot \cos\phi_f, \\ N_f &= \frac{a^2}{b \cdot sqrt1 + \eta_f^2}, \\ t_f &= \tan\phi_f. \end{aligned} \quad (4.9)$$

The parameters a and b correspond to the semimajor and semiminor axis of the WGS84 ellipsoid. The GK coordinates x and y are essential for the transformation to the WGS84 system. The parameter λ_0 belongs to the reference meridian M34. The footpoint latitude ϕ_f comprises some coefficients of the WGS84 ellipsoid, which are listed in Table 4.1 (Hoffmann-Wellenhof et al. (2001)).

coefficients	value [m]
$\bar{\alpha}$	6 367 449.1458
$\bar{\beta}$	$2.51882658 \cdot 10^{-3}$
$\bar{\gamma}$	$3.70095 \cdot 10^{-6}$
$\bar{\delta}$	$7.45 \cdot 10^{-9}$
$\bar{\varepsilon}$	$17 \cdot 10^{-12}$

Table 4.1: Transformation coefficients for the WGS84

The transformation of the calibration points from the two-dimensional GK system to the three-dimensional WGS84 system is primarily necessary to avoid distortions of the lengths between the calculated points. The distances between the points are mandatory for the definition of the body frame and also for the evaluation with the software module GrafMov (see chapter 5). The length of the baseline in driving direction is 2.669 m and the orthogonal baseline length (cross axis of the car) comes up to 1.565 m in the WGS84 reference system.

4.2 Multi antenna array

Within this project four GNSS antennas are used to constitute a multi antenna array. The measured positions and the calibration parameters manage the computation of the attitude parameters roll, pitch and yaw. The fourth GNSS receiver serves as redundant measurement source, because the principle of attitude determination requires only three receivers. The attitude parameters are used for supporting the IMU data by bounding the long term drift effects experienced by the IMU measurements. The antenna array consists of one Javad and three NovAtel antennas and their corresponding receivers. All receivers are configured for kinematic applications.

The Sigma receiver from Javad, has the capability to measure with an update rate up to 100 Hz. An update rate larger 20 Hz enables only measurements on the L1 frequency band, whereas 20 Hz measurements are available on the L1 and L2 frequency band. In the following, all measurements are made with an update rate of 20 Hz, to use the precise accuracy of two frequency positioning solutions. Furthermore the receiver has the ability to measure GPS, GLONASS and in future also Galileo signals. The receiver is also capable to send at each second a timing strobe (PPS). This skill enables the simultaneous measurements of several measuring instruments with a synchronized time signal. In this project the timing strobe is used to establish a relationship between the receiver's GPS-time and the internal time of the inertial measurement unit. The other three receivers are from NovAtel. The NovAtel DLV3 is a GNSS receiver, capable to measure code and phase data of GPS and GLONASS. Both signal types are used for the evaluation in post processing mode. The maximum update rate of this receiver is 20 Hz. Furthermore two NovAtel FlexPak receivers were used. The FlexPak receivers have the same performance as the DLV3 receiver. All of the four receivers have the opportunity to receive the new L5 signal of the modernized GPS as soon as it is available. Currently only one satellite (SVN 49) transmits the L5 signal. Unfortunately this signal is distorted and cannot be used for the position computations. Table 4.2 sums up the receiver specifications.

Javad - Sigma	Novatel - DLV3	Novatel - FlexPak
- GPS L1/L2/L2C/L5	- GPS L1/L2/L2C	- GPSL1/L2/L2C
- GLONASS L1/L2	- GLONASS L1/L2	- GLONASS L1/L2
- Galileo E1/E5A	- Update rate up to 20 Hz	- Update rate up to 20 Hz
- Update rate up to 100 Hz		
- RAIM		
- 1 PPS timing strobe		

Table 4.2: GNSS receivers

Figure 4.6: Javad

Figure 4.7: DLV3

Figure 4.8: FlexPak

4.3 Body frame - determination

The calibration of the construction allows the determination of the body frame. The computed GK coordinates, which were determined by the calibration, are transformed to the WGS84 reference system. Consequently the calibration solutions as well as the GNSS measurements correspond to the same reference system WGS84. Therefore the distortions between the points in the GK plane and the WGS84 system can be avoided. The origin of the body frame is defined by an arbitrary antenna on the construction. The other antenna positions allow the determination of a set of vectors with the origin as a starting point. The attitude computation is possible, if at least two vectors are available twice, two in the body and two in the local-level frame. An example of the set up of the body frame can be seen in Figure 4.9.

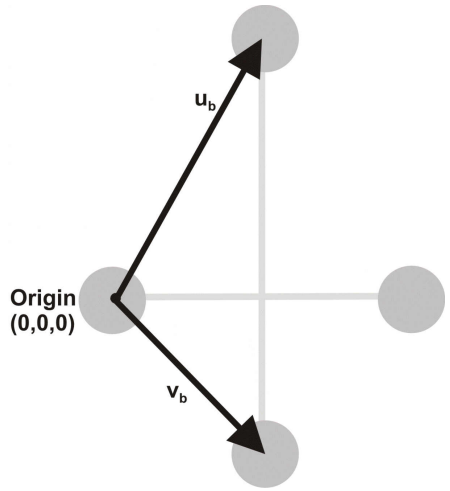

Figure 4.9: Body frame definition of the roof construction

The black vectors u_b and v_b represent the vectors in the body frame, which are also known in the local-level frame by GNSS position measurements. Afterwards the attitude parameters can be computed by the algorithm which is presented in section 3.2.

5 Evaluation Software

All computations concerning the measured GNSS data are done with the GNSS evaluation software of the Waypoint Products Group of NovAtel. The measurements are evaluated in post processing by using the relative positioning method.

5.1 Software packages

The Waypoint software is composed of several software packages. A short report of each package should provide an overview about the capabilities and the performance of the software product, see Waypoint manual (2006).

5.1.1 GrafNet

GrafNet is a static network processing software package. This software provides three types of static baseline processing, the fixed static solution, a float solution and an ionospheric free solution. It is mainly used for GPS network processing and adjustment.

5.1.2 GrafNav

GrafNav is a post-processing software package for kinematic applications. It supports most of the commercial single and dual frequency receivers. GPS and GLONASS data can be processed combined. Also multi-base processing is supported by this package. GrafNav has the opportunity to switch transparently from static to kinematic processing along a trajectory. A static initialization can be used to enable a fixed ambiguity solution for short and medium length baselines. A float solution is available for long and noisy baselines. With Kinematic Ambiguity Resolution (KAR) a fixing of the ambiguities is possible although the user starts in a kinematic mode. For dual frequency users, ionospheric processing can improve the accuracies as well.

5.1.3 GrafNav Lite

GrafNav Lite is a simplified version of GrafNav. It only supports processing intervals of one second or larger. Only the float static initialization is included in this package. The processing mode KAR is not supported within this tool.

5.1.4 GrafNav Batch/GrafNav Lite Batch

This software package facilitates batch processing for static and kinematic baselines. The main use is the evaluation of measurements with one base station and many remote stations. Another possibility is the processing of one kinematic remote station with respect to two or more base stations.

5.1.5 GrafMov

This moving baseline module enables a GPS post-processing of two moving GPS antennas, which have a constant baseline. Using this additional information the accuracy of the relative trajectory can be improved significantly compared to ordinary kinematic processing methods. This is especially true, if the base station distance is much longer than the relative distance between platforms. If the two antennas are fix-mounted, then GrafMov can also compute the heading. GrafMov is an upgrade to GrafNav and GrafNet. GrafMov enables relative processing which includes all advanced features of GrafNav. Furthermore relative vectors as well as local level coordinates, ECEF coordinates, range and bearing can be exported. In addition to the relative position, the instantaneous differential velocity vector can also be calculated. For applications, that require heading, GrafMov's KAR algorithm can make use of the separation between the antennas for decreasing the initialization times. The pitch angle can be computed from the relative vector output.

5.1.6 Inertial Explorer

The Inertial Explorer is a post-processing software suite, that integrates data from an IMU with GNSS information processed via GrafNav, which is included in this package. The Inertial Explorer is designed to utilize strapdown accelerometer and angular rate information to produce high-rate coordinate and attitude information from a wide variety of IMU's, from high-accuracy navigation grade to inexpensive MEMS (Micro Electro- Mechanical Systems) sensor types.

5.2 Evaluation settings

For the computation of the attitude parameters a local level frame is needed. This frame will be spanned by the GNSS antenna array, where two antenna pairs provide a baseline. The software package GrafMov allows the processing of the kinematic baselines. Beside the coordinates also the heading of the baselines can be computed, because of the fixed installation of the GNSS antennas.

The software package GrafNav provides the computation of the kinematic trajectory for each receiver by relative positioning. For a fast quality interpretation a plot of the evaluated trajectory can be generated, where each trajectory point is assigned with a color code representing the computation quality. In Table 5.1 the meaning of the quality code is specified.

Color	Interpretation	Accuracy[m]
green	Relative positioning with integer ambiguities	0.00 - 0.15
cyan	Relative positioning with converged float or noisy fixed integer ambiguities	0.05 - 0.40
blue	Relative positioning with converged float ambiguities	0.20 - 1.00
purple	Relative positioning with converged float ambiguities	0.50 - 2.00
magenta	DGPS solution	1.00 - 5.00
red	DGPS solution / Single point solution	2.00 - 10.00

Table 5.1: Quality interpretation of the computed position solutions

The colors green, cyan, blue and purple represent the mathematical model of relative positioning. The best quality is reflected by green, the worst by purple, where the solution of the ambiguity can not be fixed.

The mathematical model of differential positioning is used for computing the trajectory, if the ambiguity could not be sufficiently solved. As a consequence the position solution is worse and corresponds to the color magenta and red, see Table 5.1. The difference between magenta and red is the accuracy of the position.

For the data interpretation of each measurement campaign some settings for post processing have to be set in GrafNav and GrafMov. The settings are adjusted to get the best performance with respect to the position determination.

5.2.1 Kinematic and static mode

The kinematic or static processing mode is used to get the best performance regarding visible satellites versus multipath. An easier understanding of the kinematic and static working process should be given by evaluating a static measurement with both processing modes. The solutions - static and kinematic - are shown in Figure 5.1 and 5.2.
The static processing mode performs an average at the end of the interpretation for each defined measurement interval. This means that position solutions within internal defined limits are averaged to one coordinate triple (cf. Figure 5.1).

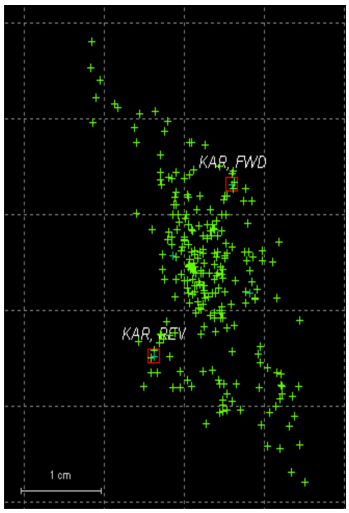

Figure 5.1: Solution of the static processing mode

On the other hand the kinematic processing mode computes each measurement epoch. As a result the static measurements do not seem to be static any longer, by evaluating them with the kinematic processing mode (cf. Figure 5.2). The measurements show a high position accuracy but a low precision.

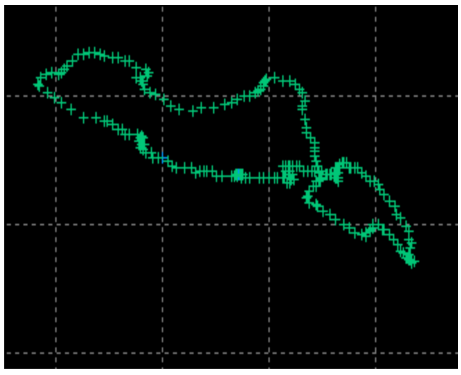

Figure 5.2: Solution of the kinematic processing mode

It must be mentioned that both solutions show position scatterings in the same interval. The position solutions of the static processing mode are accurate and precise, whereas the solutions of the kinematic processing mode are also accurate but not precise. During the drive, measurements are evaluated in kinematic mode whereas at states of rest the data is processed in static mode.

5.2.2 Elevation angle

Beside the static and kinematic mode also the evaluation angle of the satellites influences the position solutions. The elevation angle is the angle between the horizontal plane of the user and the line of sight to the satellite, measured in the vertical plane (cf. Figure 5.3).

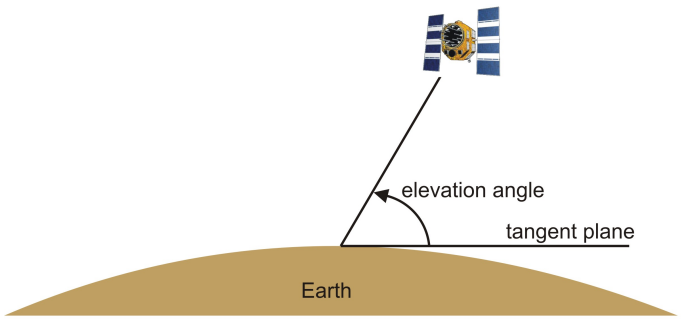

Figure 5.3: Elevation angle between the user and the satellite position

A low elevation angle of a satellite means that the signal propagates near the earth surface where the atmospheric influences are high. Because of this the signal gets a high signal to noise ratio which results in a negative effect on the positioning. Therefore only satellites above an elevation angle of 10°-15° are considered for the position determination. The selected elevation angle depends mainly on the satellite geometry during the measurements.

5.2.3 Processing mode

For kinematic applications the data processing in both directions, forward and reverse along the trajectory, is most effective. After the computation, the forward and reverse solution are combined. For static processing, the use of either forward or reverse is favorable. Figure 5.4 shows an extraction of the user interface.

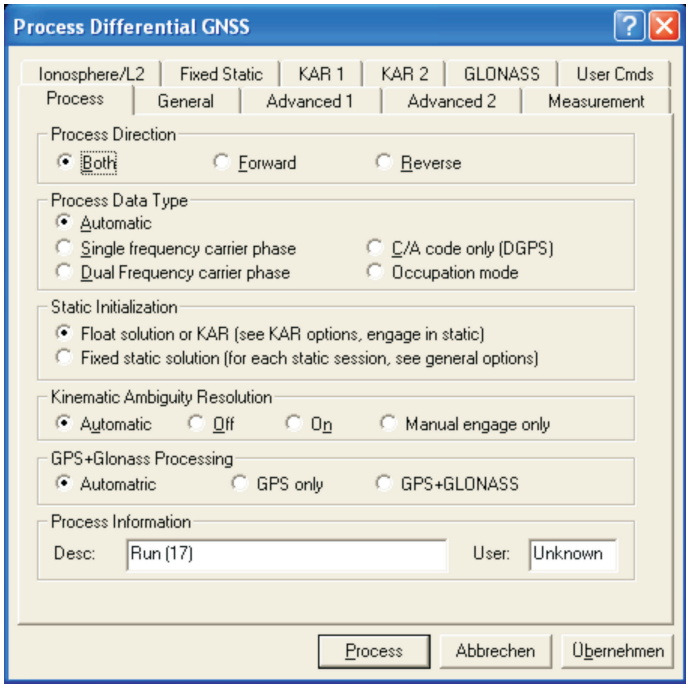

Figure 5.4: Graphical interface of the GrafNav software program for the definition of the processing settings

The option *Process Data Type* is set to *automatic* (cf. Figure 5.4). This setting tries to detect dual frequency, single frequency or code only receiver data. If the master and the remote receiver are logging different types, then the type which is recorded by the both receivers is selected. It must be mentioned that single frequency data is generally more accurate than C/A code only. It is possible to fix the carrier phase ambiguities but the process is less reliable than the dual frequency mode, because ionospheric corrections can't be made. For the ionospheric correction dual frequency data is necessary. The elimination of the ionospheric error greatly improves the accuracy on baselines longer than 10 km. Secondly, employing dual frequency improves the reliability of integer ambiguity search techniques. If only C/A code data is available the data will be processed in an advanced

differential correction mode. Only C/A-code processing is only performed on data with little or no carrier phase information.

For the *static initialization* process at the beginning of the data processing two options are available (cf. Figure 5.4). The *Float solution or KAR* is used to get the best position solutions during test drives. A float solution does not solve integer ambiguities and can take much longer to converge to centimeter accuracies. Since integers are not forced, the float solution tends to be less accurate than fixed or KAR solutions. For longer baselines the integers are often not solvable anyway. In such cases, the float solution is often the best alternative. The Kinematic Ambiguity Resolution searches the ambiguities after a serious loss of lock and is useful for precise kinematic processing as it achieves centimeter accuracies. This is the so called On The Fly (OTF) method. This technique requires five or more satellites in view and is supported considerably by L2 phase measurements. KAR is generally engaged at the start or after periods of extremely poor geometry or loss of lock. The other opportunity is the *fixed static solution*. This method is used when sufficient cycle slip free data is available. The algorithm starts with the float solution, and uses this as a seed. It searches then for the nearest integer combinations. Fixed solutions are not reliable on baselines longer than 15 km for single frequency and 30 km for dual frequency data. For data sets with multiple static sessions, fixed solutions are solved for all static epochs.

5.2.4 Kinematic Ambiguity Resolution (KAR)

Kinematic Ambiguity Resolution allows the user to compute an integer fixed solution while the remote antenna is in motion. Applications of KAR include kinematic initialization and initialization after a loss of lock. KAR solutions which use dual frequency data are considerably more reliable than those using only single frequency data. Both single and dual frequency solutions require at least five satellites. If KAR fails after a given length of time, it starts searching over again. As long as KAR successfully resolves, GrafNav restores the ambiguities from the moment it engages. Following centimeter accuracies are only unavailable for the actual period of signal obstruction. If there are good quality phase measurements,low multipath and no loss of lock then KAR resolves.

The *Minimum Time* values represent the minimum amount of time before KAR is invoked (cf. Figure 5.5). A fast KAR solution involves lower data, which can be an advantage for

kinematic applications. In both cases, the values entered are added to the value in the *min/10 km* input box, which is applied for every 10 km of baseline distance. The *Minimum Time* defaults under the KAR tab represent enough data to reliably resolve satellite ambiguities under reasonable GPS conditions. The time value for *Dual frequency* can be lower then 1 minute if measurements were performed in non urban areas. In environments with signal obstructions, KAR might not resolve.

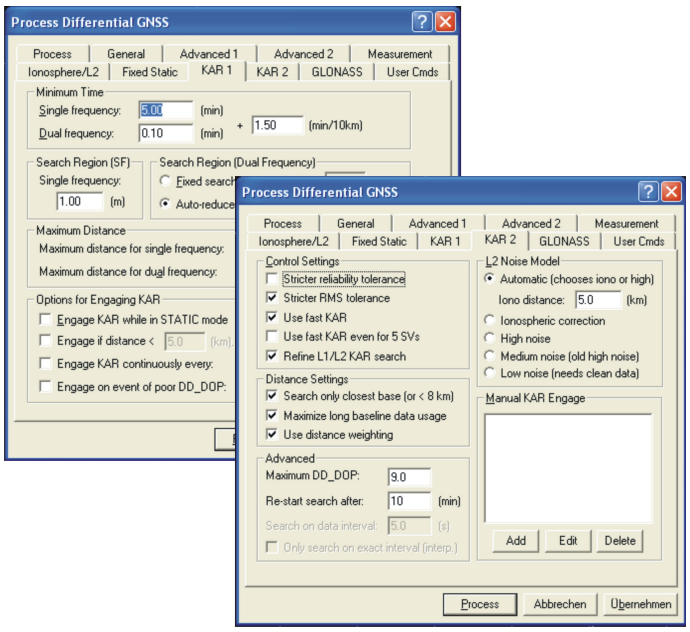

Figure 5.5: Graphical interface of the software program GrafNav for the definition of the KAR settings

The option *Stricter RMS tolerance* reduces the tolerance for the RMS (Root Mean Square) error value of the best intersection (cf. Figure 5.5). The tolerance, normally 0.065 cycles, is downsized to 0.05 cycles. This option reduces incorrect KAR intersections and is usually more effective than the stricter reliability tolerance option.

Fast kinematic ambiguity determination (cf. Figure 5.5) can be a benefit for car trajectory determination. This option is only available for dual frequency processing because *Fast KAR* with single frequency data is unreliable. The *Use Fast KAR* option makes several internal changes to accommodate this, including the reduction of the minimum KAR time to zero, which tells GrafNav to resolve the ambiguities as quickly as possible. The maximum time before KAR restarts is 1.5 minutes, which forces KAR to be recomputed more often. This option also increases the amount of data that KAR uses in it's computations,

reducing the amount of time it takes to resolve. Fast KAR is only reliable under following conditions:

- relatively short master-remote separations (less than 7 km)
- seven or more satellites in view above a 10° elevation mask
- low multipath environment
- carrier phase measurements with low noise

5.2.5 Azimuth determination options

The azimuth determination can be performed with the software tool GravMov. This requires the *Moving Baseline Options* feature which is exclusive available for GravMov. The *Moving Baseline Processing* feature determines whether or not data should be processed as a moving baseline project. If this option is disabled, the computation acts like the GrafNav package, and assumes that the base station is static. The option *Azimuth Determination* handles the processing of measured data and the determination of the baseline information. The available options are listed in Table 5.2.

Option	Interpretation
Off, no azimuth determination	By using this option first the quality of the solution can be analyzed. If the quality is good, then the second or third option will work.
On, use distance constraint in KAR and engage KAR if out of tolerance	Single frequency users, who know the fixed distance between the L1 phase centers of their moving antenna, should use this option because it speeds up the KAR resolution time. Otherwise, use the third option.
On, but compute only	Use this option if you need straightforward azimuth, if the quality of the data is not suitable for KAR usage or if the distance is not known or unstable.
On, but only use distance constraint to engage KAR if out of tolerance	Dual frequency users should use this option if they know the fixed distance between the L1 phase centers of the two moving antennas.

Table 5.2: Possible settings for the azimuth determination in the software program GrafMov

For the evaluation of the test drives within this master thesis, the fourth option is used. The reasons therefore are the known distances between the antennas, computed by calibration, and the opportunity of the receivers to measure both frequency bands. The *Standard deviation/tolerance* value is used to engage KAR, if the distance between the two antennas becomes too large or too small. All kinematic measurements presented in the following chapters are evaluated with the explained software settings.

6 Update rate

For kinematic applications an adequate measurement interval is important. A kinematic test with different update rates should be performed to test the influences of signal shadings which cause data gaps and involve new ambiguity resolutions. Further the test enables the determination of the distance between two following measurement points. This fact is important, because a new kinematic ambiguity resolution needs some measurement epochs, which can be measured by covering a short distance with a high update rate or by covering a long distance with a low update rate. As a result of the tests, the gaps between the measured GNSS points can be evaluated and in a further step the influences of signal shadings due to trees, houses and other obstructions can be analyzed. This measurements are an important foundation for future test drives for the attitude determination. Furthermore the behavior of the new Javad receiver could be tested during the kinematic motion. The whole kinematic update rate tests have been performed with two receivers. The first one was the Javad receiver, the second one was the DLV3 from NovAtel. The two antennas were mounted on a magnet roof rack, which enabled the use of two antennas in a distance of 22 cm on the roof of a car. During the whole test drive a reference station was set up next to the test route, so that the relative positioning method could be executed.

6.1 Test route

The kinematic test drive has been performed in the vicinity of Wildon in the south of Styria. The distance between Matzelsdorf and Grötsch has been covered by a speed of nearly 30 km/h. The rest of the route was covered by a speed of approximately 60 km/h. The route is principally chosen because of low traffic and good satellite visibility.

However some signal shadings can't be avoided (cf. Figure: 6.1).

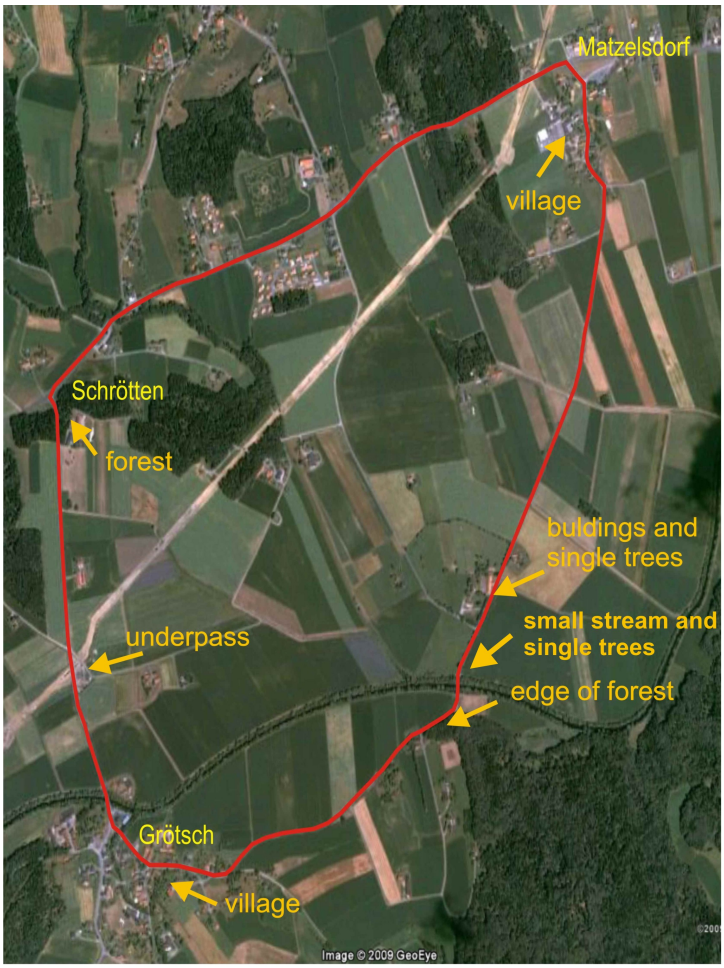

Figure 6.1: Trajectory for the update rate test

The main obstructions which appear on the route are because of:

- buildings and single trees (a),
- small stream and single trees (b),
- edge of a forest (c),
- village (d, g),
- underpass for railway (e),
- forest (f).

The parameters a, b, c, d, e, f and g are introduced for an easier interpretation of the correlation between shading effects in the different solutions in the following.

6.2 Comparison of different update rate solutions

The trajectory was covered three times. For each lap a different update rate is chosen to select the optimum update rate during kinematic motions. Update rates of 1 Hz, 10 Hz and 20 Hz are investigated. The measured data are evaluated with the software tool GrafNav. The appropriate settings of the program for kinematic conditions are explained in chapter 5. In the following only the 1 Hz and 20 Hz solutions are considered, because the differences between the 10 Hz and the 20 Hz solutions are very small.

An important parameter for the interpretation of the measurements is the PDOP (Position Dilution of Precision) parameter. The PDOP value gives information on the accuracy of the position determination, with respect to the geometric distribution of the satellites. An accurate position solution should be mirrored by a low PDOP value (Hoffmann-Wellenhof et al. (2001)). The PDOP values during the test drives are shown in Figure 6.2. The upper plot shows the 1 Hz trajectory and the lower plot shows the 20 Hz trajectory.

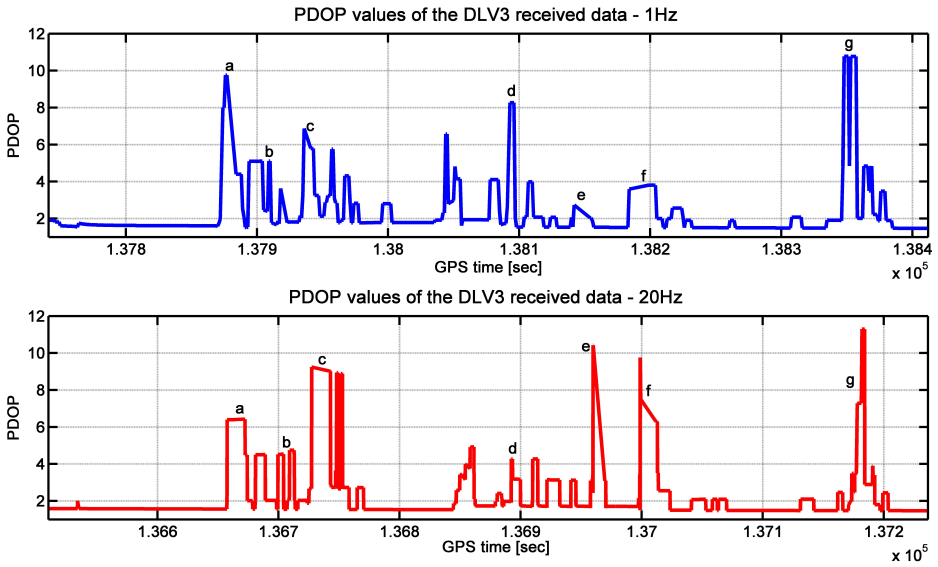

Figure 6.2: Comparison of the PDOP values of the 1 Hz and 20 Hz measurements

The PDOP values of both test drives show a similar behavior. The position determination gets worse near large obstructions. The reason for this is the loss of the satellite signals (cf. Figure 6.3) or the higher multipath effects due to the shadowing objects.

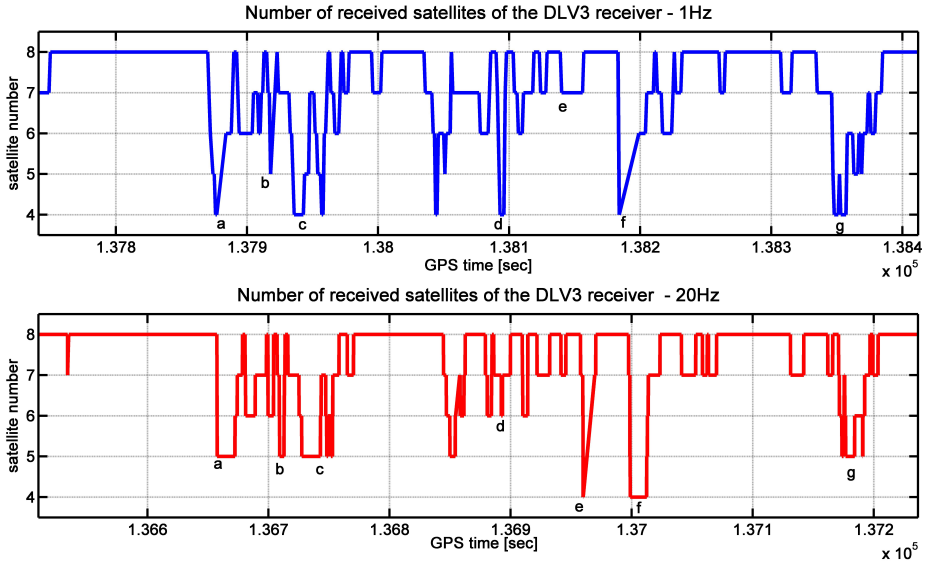

Figure 6.3: Satellite number during the test drive of the 1 Hz and 20 Hz measurements

The parameters a, b, c, d, e, f and g mark the shadowing effects along the trajectory. The parameters are described in the previous section 6.1. The influence of the first three main shadowing effects a, b and c seem to influence the PDOP parameters in a negative way. Both the 20 Hz and the 1 Hz solutions show poor positioning accuracy due to the natural obstructions of mainly houses, and trees. The village 'Grötsch' (d) causes a high PDOP value at the 1 Hz measurements, whereas the 20 Hz measurements show only minor influences in the village. The reason for this could be the different satellite geometry during the two test drives, combined with obstructions, which accordingly influence the PDOP values in a different way. In contrast the 20 Hz data are more influenced by the obstructions of the railway underpass (e) and the forest (f). The signal is completely lost there during the drive. Due to the higher update rate of 20 Hz, a signal loss induces a larger data gaps, as it would arise during the 1 Hz drive. Therefore, the PDOP value is getting worse due to the larger data interval, where no satellites can be tracked. Furthermore the PDOP value is again influenced by the different satellite geometry during both test drives, as mentioned before.

The number of measured satellites (cf. Figure: 6.3) fluctuates mostly between eight and six satellites, which offers a good foundation for the position determination. The 1 Hz measurements show a more rapid drop to four visible satellites when passing the possible shading obstacles a, b, c, d, e, f and g. The measurements with the 20 Hz update rate show a more stable number of satellites. The number only drops twice for a short time period to a number of four satellites. At most obstacles along the trajectory, the satellite number drops to a minimum of five satellites. Most of the time the satellite number varies between seven and eight satellites. The different influences of visible satellites during both test drives have it's cause in the changing satellite geometry.

Another parameter for comparing different solutions is the quality of ambiguity solutions. The ambiguity parameter distinguishes between an integer value, which is resolved or fixed, and a real value ambiguity which is also called float ambiguity. In this case the software program GrafNav distinguishes between tree different ambiguity states (cf. Table 6.1).

0	float ambiguity solution
1	fixed ambiguity solution, with one baseline
2	fixed ambiguity solution, with two or more baselines

Table 6.1: Ambiguity solutions of the software program GrafNav

The aim of the ambiguity resolution is the determination of the fixed ambiguities, since float ambiguity solutions are scattering in meter range in the coordinate components north, east and up. In comparison, the fixed solutions allow the position determination in a centimeter level. The use of double-differences is important for carrier phase processing. Single-difference measurements require the consideration of an additional unknown parameter for the receiver clock. Therefore a separation of the integer ambiguities from the clock offset is prevent. In contrary the double-differences enable the elimination of the clock terms and allows the isolation of the ambiguities. The ambiguities have to be resolved to their correct integer ambiguity, because one cycle error on the L1 carrier rises to 19 cm position error. An important aspect for ambiguity resolution is the consideration of short baselines (<20 km) between rover and reference station. Therefore the double-difference model can be simplified by neglecting the influences of ionosphere and troposphere. Another important aspect for the ambiguity determination is the satellite geometry (Hoffmann-Wellenhof et al. (2001)). The ambiguity quality of the two test drives are shown in Figure 6.4. Again in the upper plot the 1 Hz trajectory is shown, while the lower plot represents the 20 Hz trajectory.

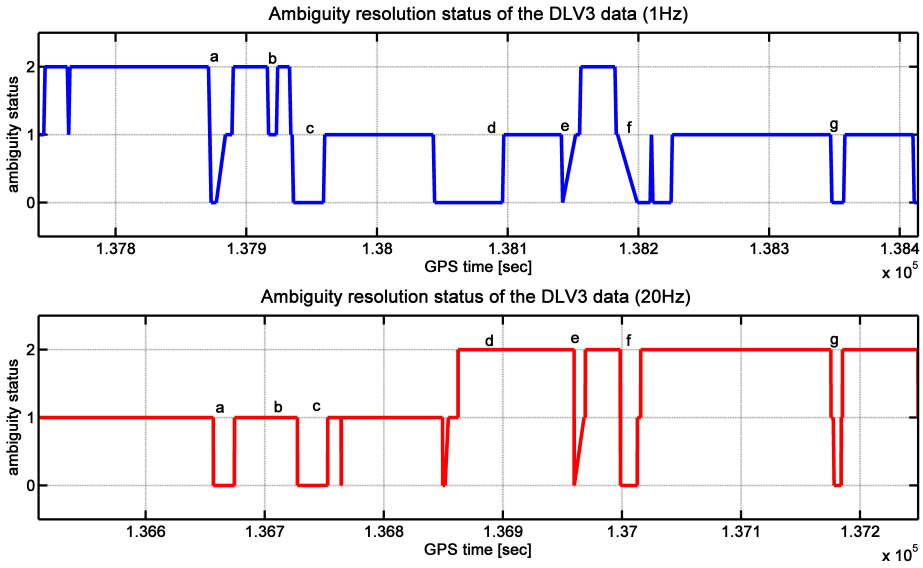

Figure 6.4: Ambiguity solutions of the 1 Hz and 20 Hz measurements

The ambiguity solutions of the 20 Hz data show fewer float solutions than the 1 Hz measurements. At the start epoch, the 10 Hz measurements show a better ambiguity resolution. The shadowing due to some houses and trees (a, b and c) act as a disturbing factor of the ambiguity solutions. At almost every epoch where obstacles exist, a jump to float ambiguity solutions can be observed. The reason for this is the sudden loss of the satellite signals. The 1 Hz trajectory shows a better ambiguity solution during the first part of the trajectory. After the forest edge c the ambiguity solution shows a change from two to one, which means that only one baseline is usable for the ambiguity determination. On the other hand the ambiguity solution of the 20 Hz measurements gets better and shows almost a good ambiguity solution of two, with short deteriorations when passing the obstacles. The railway underpass and the forest, for example, cause a jump in the ambiguity quality in both trajectories.

The quality parameter provides information about the GNSS solution type and the positioning stability. The high jumps are due to the loss of lock of the signal. Another influence of the quality parameter is the satellite geometry, besides the ambiguity resolution. The quality parameters are briefly described in chapter 5. The parameters of the test drives are presented in Figure 6.5.

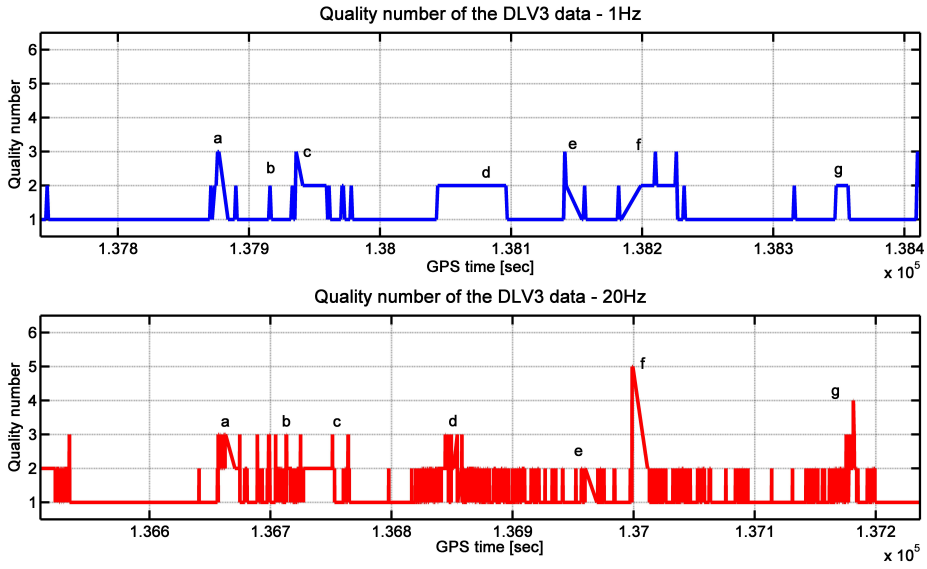

Figure 6.5: Quality parameters of the 1 Hz and 20 Hz evaluation solutions

The quality values at the start of the 20 Hz solution are not as good as of those of the 1 Hz data. The reason for this is the shorter initialization phase of the receiver at the beginning of the measurements. A longer measurement epoch in static mode before the start of the kinematic part improves the position solution, especially at the beginning of the drives. The quality parameter at the first shadowing effect *a* impairs both quality parameters to a DGPS solution. The signal disturbance at *b* and *c* influence the 1 Hz data more than the 20 Hz measurements. The underpass and the forest show a higher quality value in both measurement data sets, which implies a position determination with large errors. The village *g* causes no big influences during the 1 Hz measurements, whereas the 20 Hz data show a jump in the quality plot.
In conclusion it must be mentioned, that the 20 Hz data seem to be more sensitive to shadowing effects, but are more reconstructive after such anomalies.

A plot of the computed position data of both test drives can be seen in Figure 6.6.

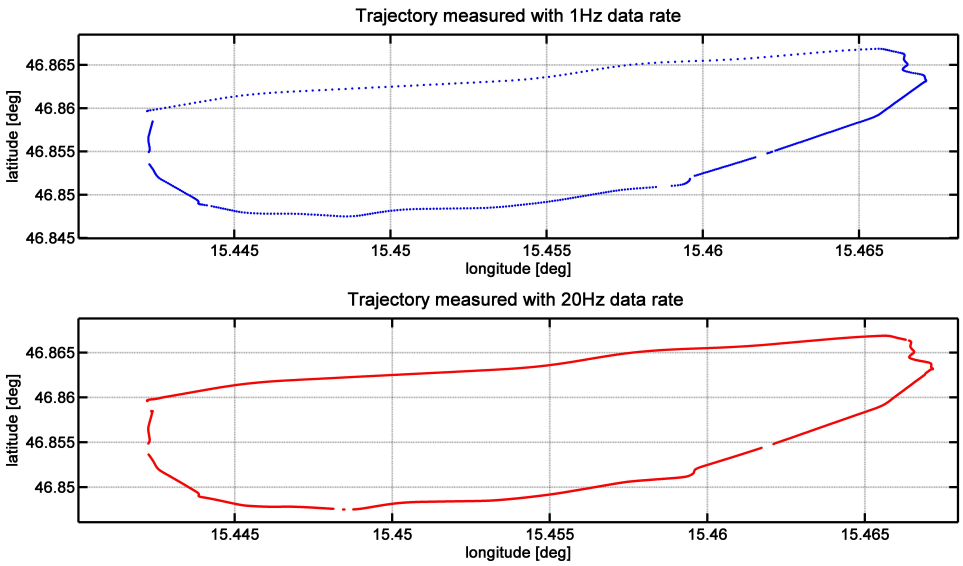

Figure 6.6: 1 Hz and 20 Hz trajectory of the update rate test

The different data gaps between the trajectory solutions in the south results from the fact of different satellite geometry.

A problem of the 1 Hz measurements is the low density of measurement points. The distance of consecutive measurement points is about 17 m at a velocity of 60 km/h, whereas a distance of about 0.8 m can be covered with 60 km/h using 20 Hz. The relationship between velocity, distance and update rate is shown in Table 6.2.

velocity	1 Hz	10 Hz	20 Hz
60 km/h	16.66 m	1.66 m	0.83 m
30 km/h	8.33 m	0.83 m	0.41 m

Table 6.2: Gaps between two consecutive measuring points along the trajectory

An update rate of 20 Hz, together with a driving velocity of 30 km/h, enables a high point density. A high point density supports/improves the ambiguity resolution as well as the quality factor of the position determination. Furthermore the data volume of 20 Hz measurements still enables a reasonable data processing. Therefore all future tests were done by using a 20 Hz update rate.

7 Attitude solutions

This chapter deals with two measured trajectories, which are processed and evaluated regarding the attitude determination performance. The attitude determination is based on three vectors which are defined by the multi antenna array. The evaluation is done by comparing the GNSS attitude solutions with the IMU attitude solutions.

7.1 Trajectories

The attitude computation is realized for two driven trajectories, which show different surrounding conditions. The first measurements took place at the OEAMTC driver safety training center in Lebring, in the south of Styria. The area at the OEAMTC center can be perfectly used for GNSS measurements due to the fact that shading and multipath effects are expected to be low, because of the lack of obstructions. Negative influences on the received satellite signal can be expected by the high-voltage line, which crosses the center. The circular circuit provides a good track for the attitude determination plots. The starting point which is identical to the end point of the trajectory is marked by a red point (see Figure 7.1). At this point it must be mentioned that the satellite image in Figure 7.1 shows the area before the construction of the OEAMTC center. The yellow points represent the determined positions by GNSS.

The second trajectory was measured within a bigger area in the north of Graz. The trajectory starts and ends in front of the AVL test circuit in Gratkorn, marked by the red point in Figure 7.2. The conditions for GNSS measurements are less favorable, because of the surrounding hills and the city zone of Graz, which cause strong shading an multipath effects.

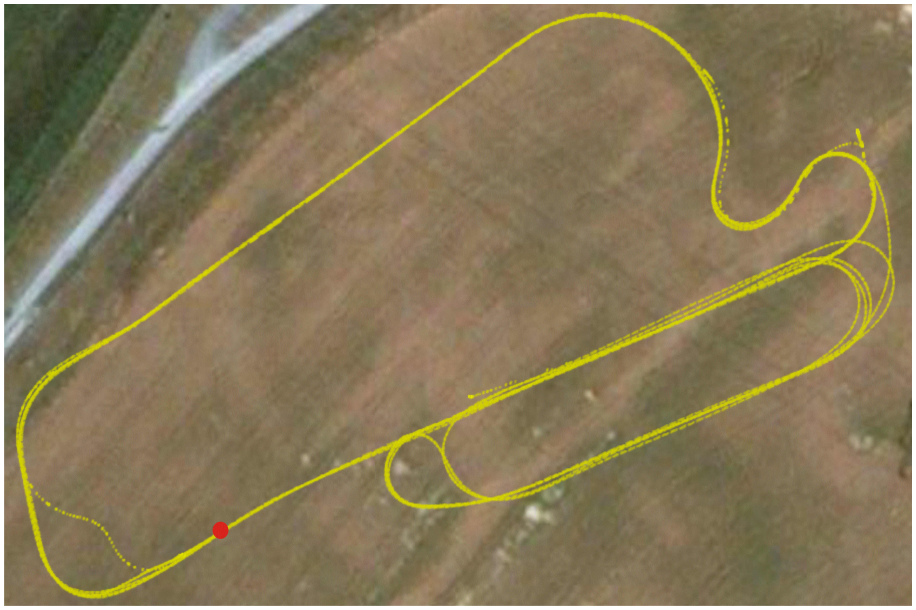

Figure 7.1: OEAMTC trajectory

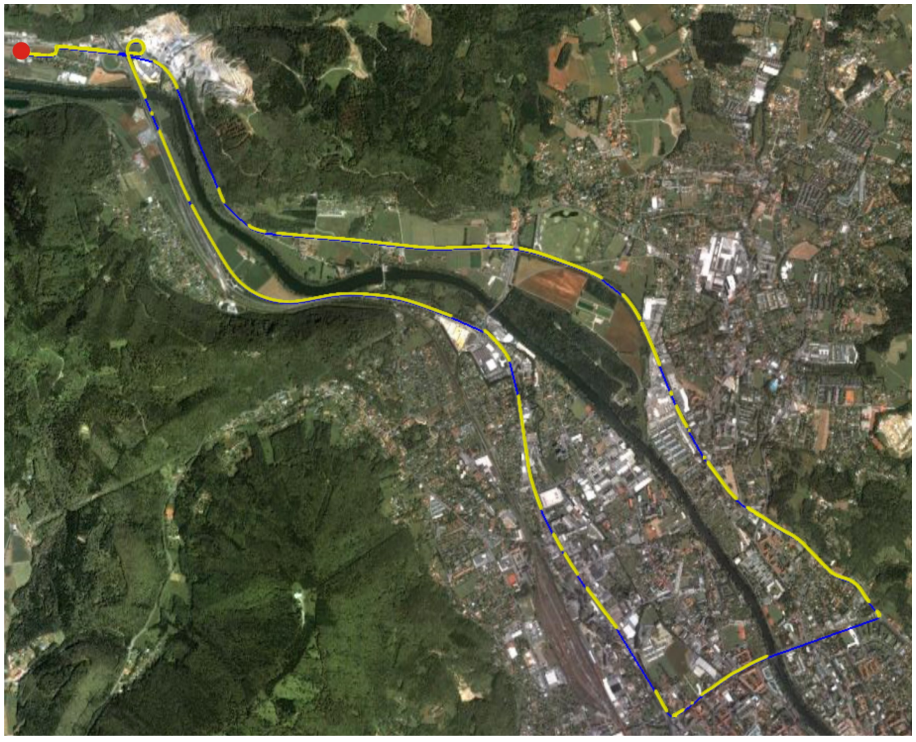

Figure 7.2: AVL trajectory

The yellow points in Figure 7.2 visualize the computed positions. A continuous signal reception, and therefore a continuous trajectory is not longer possible. This is shown by

the interruption of the yellow line in Figure 7.2. The area bordering the trajectory is densely populated which causes most of the signal shading. Both trajectories are used for the attitude determination with three antennas.

To enable the relative positioning method, a reference station near each trajectory is used. The reference station used at the OEAMTC trajectory was installed near the OEAMTC center. The reference of the second trajectory was set up on the roof of the geodesy building, Steyrergasse 30.

7.2 Attitude determination by three receivers

The attitude computation needs at least three receivers. This means, that no redundancy of measurements is available. The setup of the test measurements consists of one Javad receiver, which is connected with the IMU, one DLV3 receiver and two FlexPak receivers, all from NovAtel. Each receiver records the GNSS measurements with 20 Hz update rate. Figure 7.3 represents the used measurement configuration.

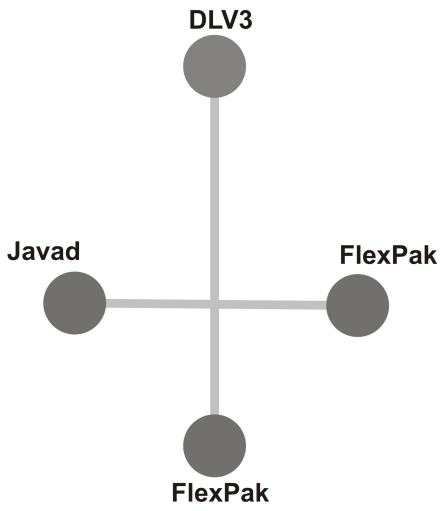

Figure 7.3: Measurement configuration during the test drives

The longer baseline in driving direction is determined by the two receivers, the DLV3 and one of the FlexPak receivers. The orthogonal shorter baseline is defined by the Javad and the second FlexPak receiver.

Because of software problems with the FlexPak receiver of the longer baseline, the recorded data could not be stored. Therefore the measured data of only three receivers are available for attitude determination. In principle the theory states that, the longer the baseline length, the better the computation stability. With the problem of the failing receiver the longer baseline cannot be realized. Therefore the attitude computation is based on the baseline between the Javad and the DLV3 receiver ($v\bar{e}c_1$) and the second baseline between the Javad and the FlexPak receiver ($v\bar{e}c_2$) (cf. Figure 7.4).

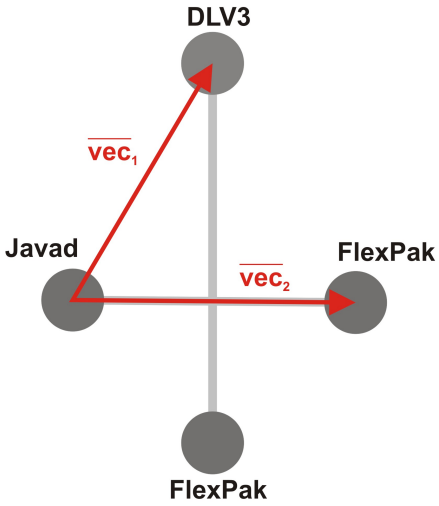

Figure 7.4: Actual setup for computing the attitude

The following subsection describes the mathematical concept for attitude computation using three antennas.

7.2.1 Mathematical concept

The main task of attitude determination is the definition of the body frame, the local-level frame and the computation of the transformation matrix R_l^b between both frames. The determination of uncorrelated attitude angles is based on the fact, that the three vectors, which are used for the attitude computation, are orthogonal to each other (see Figure 7.5).

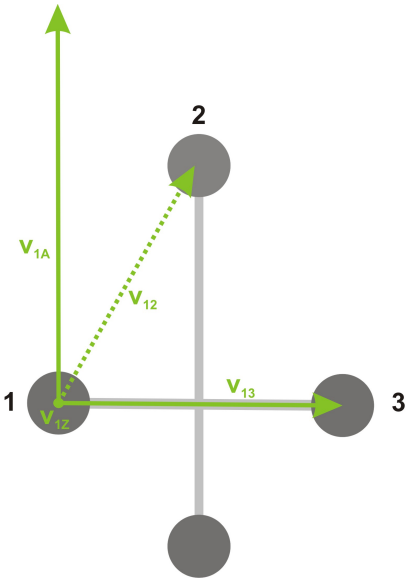

Figure 7.5: Computation of the orthogonal vectors

The problem of the antenna positions is, that the vector, which is formed by the Javad and DLV3 antennas (v_{12}), and the vector which is build up by the Javad and the FlexPak antennas (v_{13}), are not orthogonal (see Figure 7.5). Orthogonal vectors are needed for the comparison with the attitude solutions of the IMU data, which is based on orthogonal vectors in driving direction, in up-direction and across-track direction. Therefore the vectors for the attitude computation from the GPS data should be parallel to the IMU measurement axes. Because of orientation deviations between the axes of the IMU and the computed axis of the GPS measurements are the axes of both systems due to the mounting is not exactly parallel. Therefore some deviations in the attitude solution of both systems are expected. From the calibration and the IMU calibration protocol it is possible to determine the exact deviations between the GNSS antennas and the sensors of the IMU. For the determination of the deviations, the attitude computation algorithm is used. The defined vectors along the x-, y- and z-axis of the IMU build up the B matrix. The L matrix can be defined by the vectors orthogonal and in driving direction. The third vector can be computed by the cross product. It must be noted that the vectors of the L should in principle be parallel to the vectors of the B matrix. Only alignment errors between the antenna array and the IMU sensor axes should be observed. For the computation of the misalignment, the unit vectors for each vector in both matrices have to be computed and are defined in the same coordinate system. The rotation matrix and further the rotation angles roll, pitch and yaw have to be computed and represent the misalignment (cf Table 7.1).

roll [deg]	pitch [deg]	yaw [deg]
0.078	0.138	0.199

Table 7.1: Misalignment angles between the IMU sensor axes and the GPS multi antenna array.

The maximum misalignment of the axes is 0.199° in yaw. The angles are very small but will also influence the comparison between the IMU data and the GNSS data.

The orthogonal vector to the driving direction is defined by v_{13}. The vector in up direction v_{1Z} can be defined by computing the cross product between $v_{13} \times v_{12}$. By building the cross product again, between the vectors v_{1Z} and v_{13} the vector v_{1A} which points along the driving direction of the car, can be determined

$$v_{1Z} = v_{13} \times v_{12} = \begin{bmatrix} v_{13y} \cdot v_{12z} - v_{13z} \cdot v_{12y} \\ v_{13z} \cdot v_{12x} - v_{13x} \cdot v_{12z} \\ v_{13x} \cdot v_{12y} - v_{13y} \cdot v_{12x} \end{bmatrix}, \tag{7.1}$$

$$v_{1A} = v_{1Z} \times v_{13}. \tag{7.2}$$

The norm of the cross product determines the surface area of the parallelogram, which is defined by the vectors, which are used for the cross product. The length of the vector v_{13} is therefore longer than the other vectors v_{13} and v_{12} which is limited by the roof construction. To limit the vectors length v_{1A} to the average baseline length of the roof construction, a orthogonal projection of the point 2 onto the vector v_{1A} has been performed (cf. Figure 7.6). The projected point onto the v_{1A} axis is called A point. The determination of the point A allows the reduction of the vector v_{1A} to the length s_{1A}. The distance s_{1A} can be computed by a triangle resolution in the GK plane.

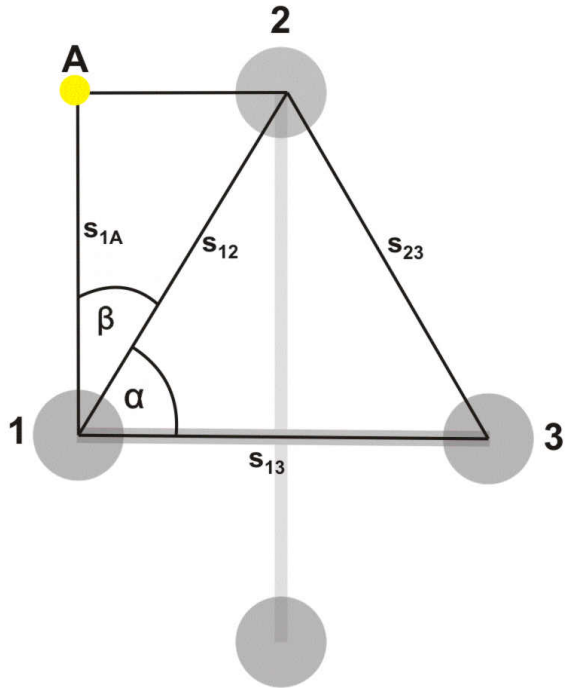

Figure 7.6: Definition of the auxiliary point A

In a first step the angles α, and β can be computed by

$$v_{ij} = \begin{bmatrix} x_j - x_i \\ y_j - y_i \\ z_j - z_i \end{bmatrix} \quad \text{,where i, j = 1,2,3} \tag{7.3}$$

$$s_{ij} = \| v_{ij} \|, \tag{7.4}$$

$$s = \frac{s_{13} + s_{12} + s_{23}}{2}, \tag{7.5}$$

$$\frac{\alpha}{2} = \arctan\left(\sqrt{\frac{(s - s_{13})(s - s_{12})}{s(s - s_{23})}}\right), \tag{7.6}$$

$$\beta = 90^\circ - \alpha. \tag{7.7}$$

The distances between the points 1, 2 and 3 are expressed by the coefficients s_{ij} where the term ij corresponds to the points i and j. The distance between point 1 and point A can be computed by

$$s_{1A} = \cos\beta \cdot s_{12}. \tag{7.8}$$

The experienced distortions of the vector length s_{1A} by the following transformation from the GK plane to the WGS84 system can be neglected, because the influences are very small.

The computation of the auxiliary point A in the body frame and the WGS84 is based on the cross product computations of the vectors v_{1Z} and v_{1A}, and the limitation of the vector v_{1A} to the length of s_{1A}

$$A(x, y, z) = \frac{v_{1A}}{\parallel v_{1A} \parallel} \cdot s_{1A}. \tag{7.9}$$

Body frame definition

The definition of the body frame is based on the calculated data from the calibration procedure (see chapter 4). The transformation from the GK system to the WGS84 system allows the determination of the distances between the antennas in the global frame, which are essential for the body frame definition. The body frame is defined as a left handed system, see Figure 7.7.

The position of the Javad receiver is defined to be in the origin of the body frame. The distance between the Javad and the FlexPak antennas defines the y-component of the body frame and this corresponds further to the first vector (v), which is used for the attitude

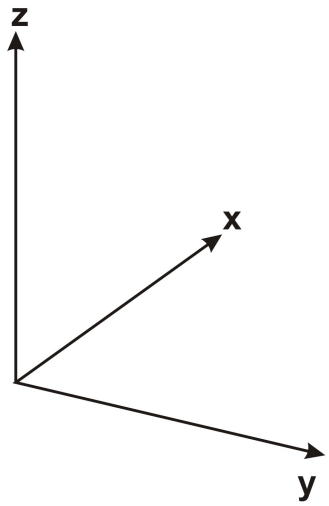

Figure 7.7: Left handed body frame

computation of v_{13}. The auxiliary point A can be defined by building the cross product twice to get the vector v_{1A}. Further the vector is limited to the length of s_{1A}. The vector between the point 1 and A defines the second vector (u) for the attitude computation algorithm. The third vector v_{13} can be defined by building the cross product between the vector v_{1Z} and v_{1A}. The body frame is defined by the points 1, 2 and A. In Figure 7.8 the body frame constellation and the corresponding point coordinates are visualized.

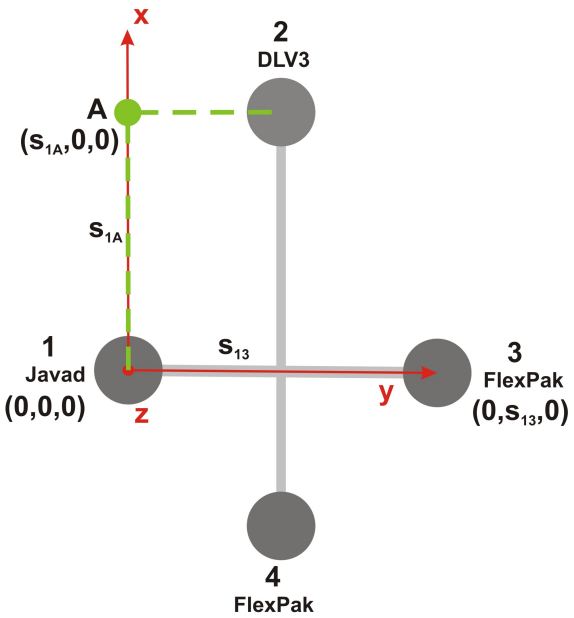

Figure 7.8: Definition of the body frame

The definition of the body frame is kept constant for all epochs. All in all the attitude computation requires three identical vectors in the body frame and the local-level frame.

Definition of the local-level frame

The point A has to be computed in the WGS84 system for each measured epoch by using the distance s_{1A}, which is known from the body frame. The direction of the vector v_{1A} can be determined by calculating the cross product twice. The vector between two antennas can be derived from the coordinate differences

$$v_{13} = \begin{bmatrix} x_3 - x_1 \\ y_3 - y_1 \\ z_3 - z_1 \end{bmatrix} . \tag{7.10}$$

The first cross product of the vectors $v_{13} \times v_{12}$ results in the v_{1Z} vector.

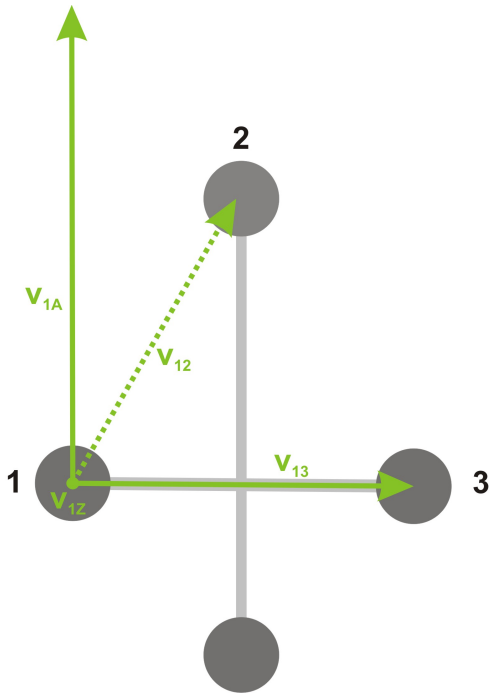

Figure 7.9: Local level frame of the roof construction

The vector in driving direction can be computed by building the cross product again, with the v_{1Z} vector and the v_{13} vector ($v_{1Z} \times v_{13}$).

The coordinates of the point A can then be computed by

$$A(x, y, z) = \frac{v_{1A}}{\parallel v_{1A} \parallel} \cdot s_{1A}. \tag{7.11}$$

The measured global WGS84 coordinates of the three receivers are used to define the local-level frame. Again, the same problem of non-orthogonal vectors appear. The Javad receiver, like in the body frame, is used as origin of the local-level frame. Another requirement is, that the vectors of the local-level frame must have the same orientation as the body frame, which corresponds to a left handed system (cf. Figure 7.9). The vector orthogonal to the driving direction can be defined in a direct way by computing the difference vector of the Javad antenna position and the FlexPak position (v_{13}). For the vector in driving direction the knowledge of the auxiliary point A in the body frame computation is reused.

Attitude computation

The local-level frame and the body frame consist of the three vectors v_{1A}, v_{13} and the v_{1Z} vector. The computation steps for the transformation from the WGS84 to the local-level frame, and the definition of the L and B matrices are described in chapter 3. The attitude computation results in the computation of the rotation matrix R_l^b.

In the following chapters the solutions of the three antenna attitude computations are presented and accordingly interpreted.

7.2.2 Attitude determination of the OEAMTC trajectory

The achievable accuracy of attitude determination mainly depends on the GNSS measurements and thus on the accuracy of the position determination. The GNSS position solutions are the source for the attitude determination. A higher positioning accuracy results in a higher precision of the attitude calculation. This was shown by applying a variance covariance propagation (cf. chapter 3). The trajectory at the OEAMTC center is expected to have more accurate GNSS position solutions, because of the good measurement conditions (cf. section 7.1). The major parameters for an accurate position determination are:

- number of visible satellites
- PDOP values (satellite geometry)
- ambiguity solution.

The positioning accuracy can be evaluated by the quality factors which are defined by the software program GrafNav (see Table 5.1).

Number of visible satellites

The minimum number of measured satellites needed for kinematic applications is four (cf. section 2.4). This means, that there is no redundancy and thus the position determination is not very reliable. For an overdetermined position solution and thus a more reliable one, a satellite number greater than four is favorable. The number of visible satellites during the test drive can be seen in Figure 7.10.

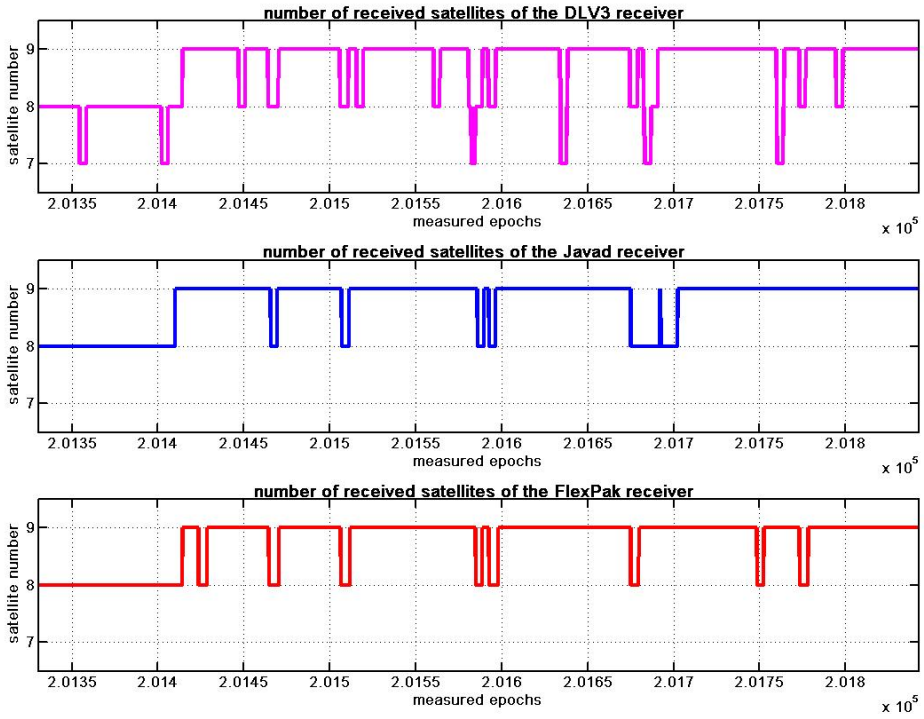

Figure 7.10: Number of visible satellites during the test drive at the OEAMTC area

The satellite number plot shows a total number between eight and nine satellites. Most of the time nine satellites are in view, which represents a good initial situation for the position determination with the software module GrafNav (cf. chapter 5). Only short periods with eight visible satellites are recognizable. The DLV3 receiver seems to have more problems for the kinematic case, because the total number of satellites drops sometimes suddenly to seven. However, also a satellite number of seven satellites allows a good position computation. The fluctuation of the one satellite is due to a low elevation angle and thus a lower signal to noise ratio in the signal.

PDOP value

The PDOP (Position Dilution Of Precision) values allow an interpretation of the accuracy of the position solutions. The lower the PDOP the better the position accuracy. The DOP values generally represent the quality of intersection for positioning and are due to the satellite geometry. A low PDOP value indicates good intersection conditions and thus a higher position accuracy. The PDOP values during the drive show low values for the Javad and the FlexPak receivers hence an accurate positioning can be performed (cf. Figure 7.11).

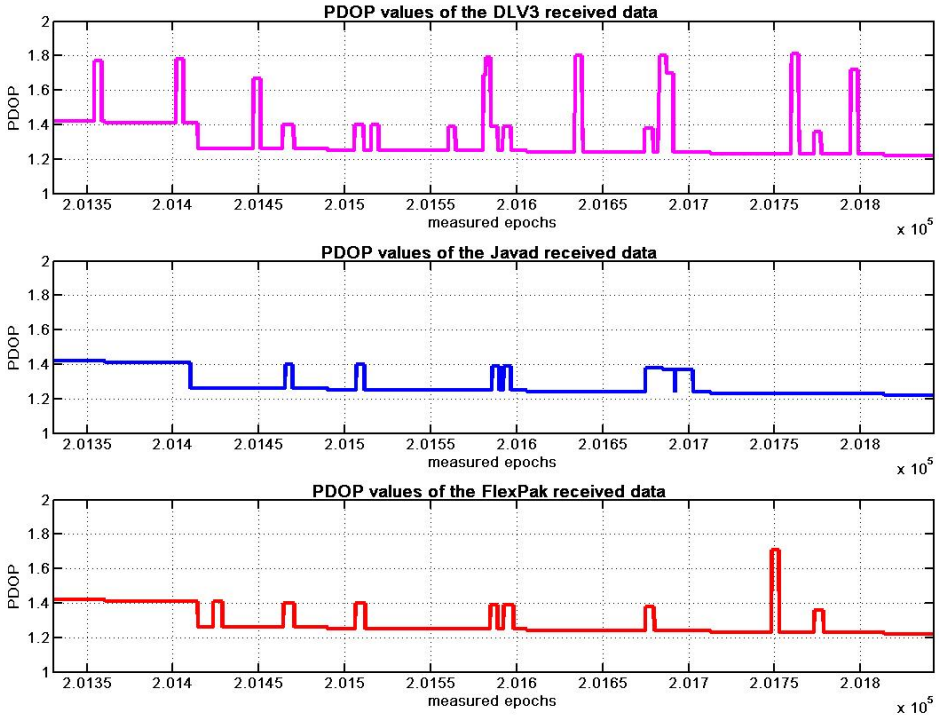

Figure 7.11: PDOP values during the test drive at the OEAMTC area

The DLV3 receiver shows higher PDOP values. This is mainly due to the sudden loss of a satellite signal. Therefore a lower positioning accuracy of this receiver can be expected.

Ambiguity solution

Another important factor is the quality of the ambiguities. To support an optimal KAR (Kinematic Ambiguity resolution), settings have to be changed in the software module GrafNav (see section 5.2). In principle three different ambiguity solutions can be distinguished, see Table 7.2.

ambiguity status	identification	definition
float	0	defined integer ambiguities are here computed as float values
fix1	1	one fixed ambiguity is used for position determination
fix2	2	more fixed ambiguities are used to determine a solution

Table 7.2: Possible ambiguity states, which are supported by the GrafNav software

Fixed integer ambiguities generally allow a more accurate position determination. The ambiguity solutions of the received data are mostly equal to one (cf. Figure 7.12).

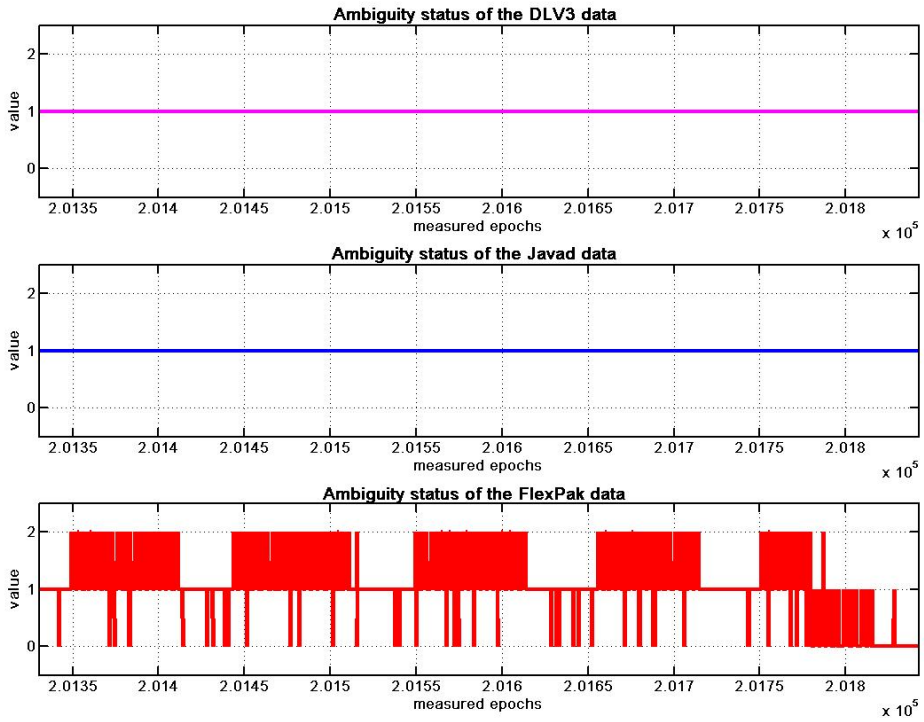

Figure 7.12: Status of the ambiguity solutions during the test drive at the OEAMTC area

Only the FlexPak receiver shows all three ambiguity states. However, most of the time the states show fluctuations between the different fixed ambiguity states. A reason for this could be the short loss of the satellite signals during the drive, which causes a new ambiguity solution processing.

Quality factor

The last parameter which influence the accuracy of the position determination, is the quality factor which describes the mode of position determination and the expected position accuracy (cf. Table 4.2). This parameter is defined by the software GrafNav. The quality parameters of the OEAMTC drive are shown in Figure 7.13.

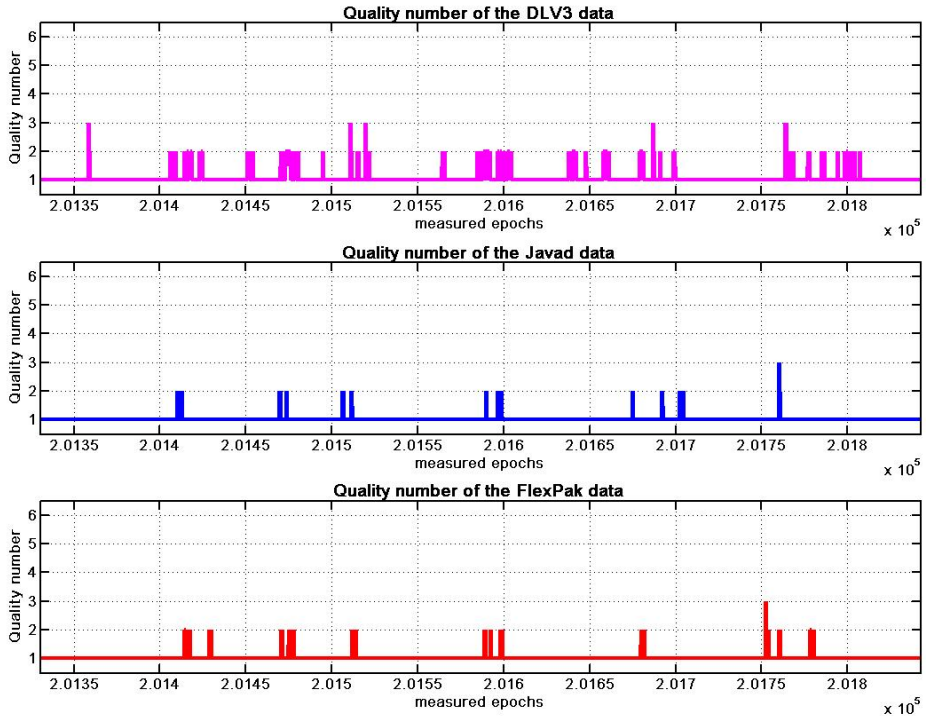

Figure 7.13: Quality factors during the test drive at the OEAMTC area

The quality parameters principally correspond to one, which means the measured data are evaluated by relative positioning with integer ambiguities, so that a position accuracy of less than 0.15 m can be expected. Some quality factors of two can be recognized in all three data records. This means that an accuracy between 0.05 m and 0.40 m is possible. The worst position instability varies between 0.20 m - 1.0 m which corresponds to a quality factor of three.

To sum up, the position accuracy parameters, like the visible satellite number, the PDOP value, the ambiguity solution status and the quality factor, which are important for a well determined trajectory, show only few anomalies. All quality informations about the positioning accuracy show that a well determined trajectory with few anomalies is available. Therefore a stable basis for the attitude determination was established, because the algorithm of the attitude computation mainly based on the computed positioning solutions.

Attitude parameters

The variance propagation solutions (see chapter 3) show that the reachable attitude accuracy is influenced by the positioning accuracy and the length of the baseline. An accurate position determination enables an accurate attitude determination. The computation steps for the attitude parameters roll, pitch and yaw are documented in the subsection 3.2.
The calculated coordinates are already filtered by a Kalman filter. The Kalman filter is a intern process of the GrafNav program for computing the GPS positions. For the interpretation of the computed attitude parameters, the values of the filtered position solutions from the GrafNav software are compared with the raw attitude parameters of the IMU, which are determined by coarse alignment.

The yaw angles during the test drive show large changes, because of the circular motions, where the angles vary between ±180°. Furthermore, the series of the yaw values are expected to be repeated, because of the driven circles (cf. Figure 7.14). The yaw angle describes the changes of the driving direction (cf. Figure 3.1).

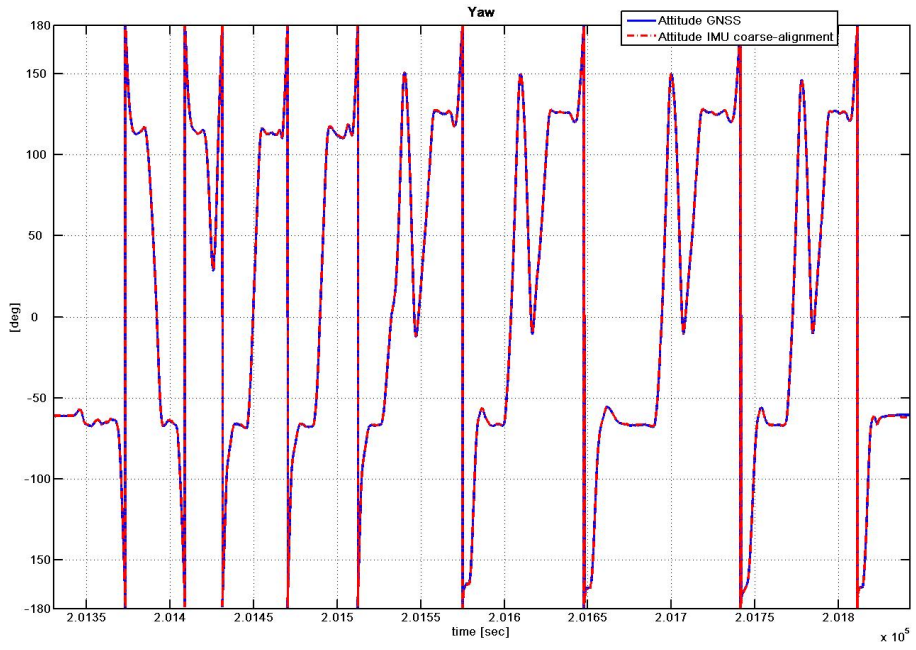

Figure 7.14: Comparison of the yaw solutions between GPS and the IMU during the test drive at the OEAMTC area

It must be recognized, that the yaw angles of both solutions of GNSS and IMU measurements fit very well. The differences between the two attitude solutions are very small and are shown in Figure 7.15.

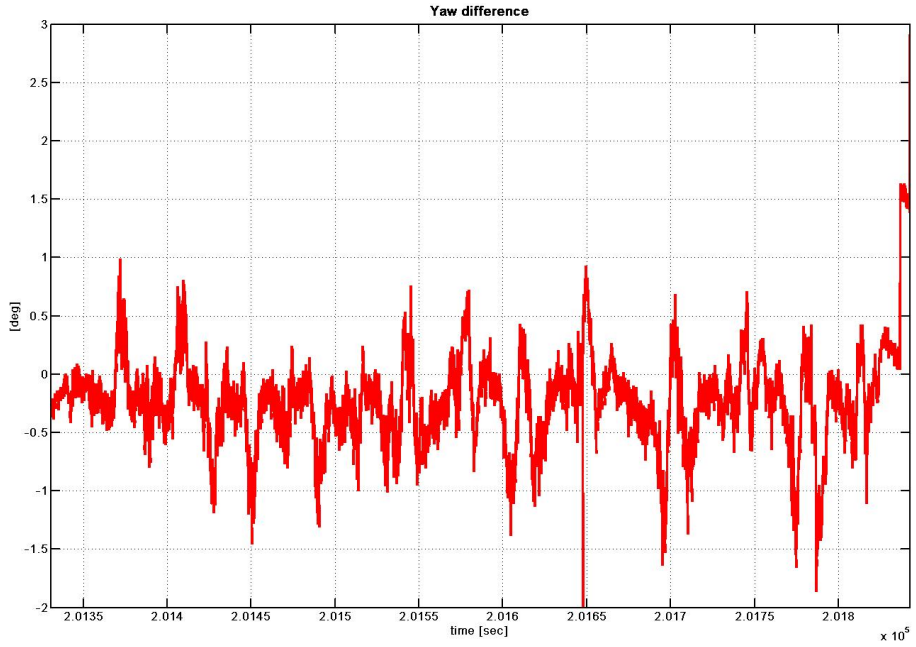

Figure 7.15: Differences between the yaw solutions of the GPS data and the IMU data (OEAMTC)

The mean value of the differences between the yaw angle from the GNSS computations and the yaw angle derived from the IMU data is -0.34°. The differences primarily vary between +1° and -1.5° and do not show any trend. In principal the gyro behavior is influenced by a drift. During the test drive at the OEAMTC area no significant drift of the sensors can be recognized. Furthermore a gyro bias leads to an unbounded error growth (cf. Legat et al. (2007)). Because no drift is apparent in the differences, the gyro bias and the typical gyro drifts are a minimum. The largest difference values appear during the jumps between +180° and -180°, because of numerical instability within the computation process.

The second attitude parameter roll describes the rotation of the car along the longitudinal axis (cf. Figure 7.16). The angle is expected to be very small, and can be described as tilt of the car.

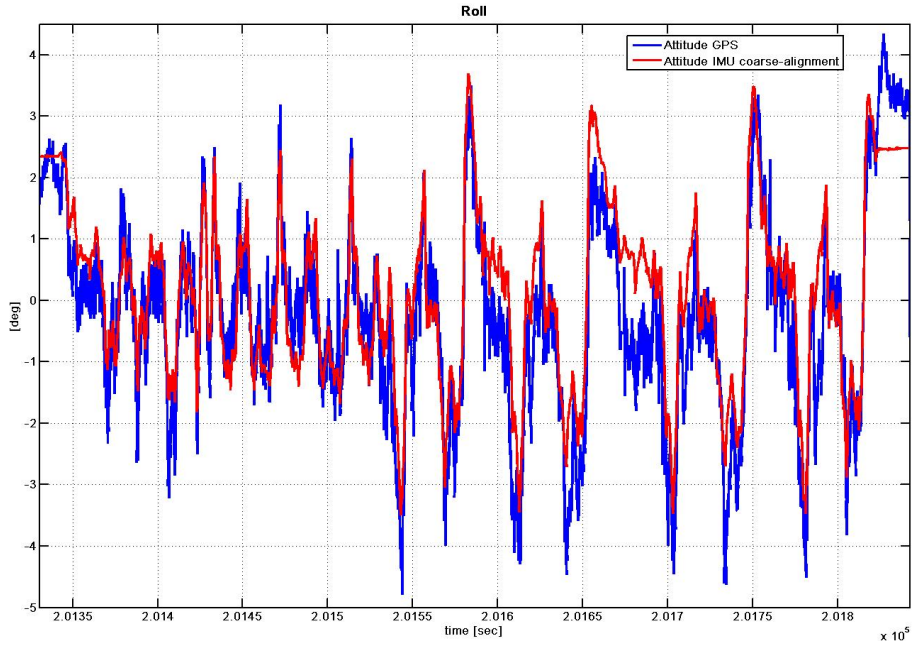

Figure 7.16: Comparison of the roll angles during the test drive at the OEAMTC area

The roll angle shows more rapid oscillations during the drive, as it can be recognized by the yaw angle. The roll as well as the pitch angle are more affected by the bumpiness of the street. Nevertheless a similar behavior between the GNSS and the IMU roll angles are discernible. The angle mostly varies around $\pm 4°$. The solutions of the roll angles allow an interpretation about the radius of the driven cycle. A smaller radius is reflected by smaller roll angles, which can be seen in the first part of the driven trajectory (cf. Figure 7.16). The second part shows larger roll values, which can be caused by a larger driving radius and a higher speed. The differences between both roll solutions are shown in Figure 7.17.

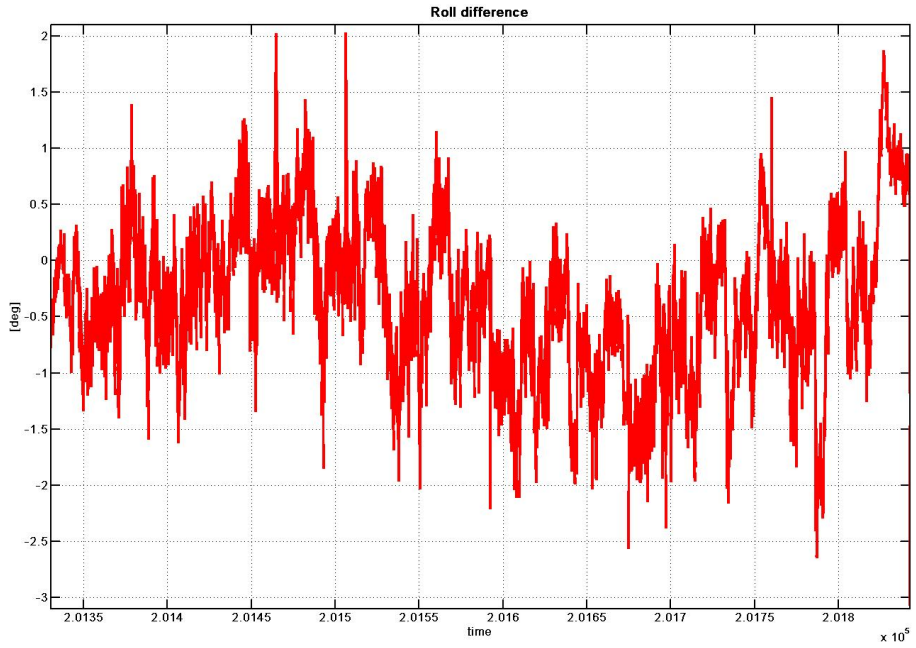

Figure 7.17: Differences between the roll solutions of the GPS data and the IMU data (OEAMTC)

The differences vary mainly between +1° and -2°. The mean value of the differences is -0.37°. In principle the computed roll solutions of the GPS data seem to be more scattered than the IMU data. Although the differences seem to be influenced by a period, no periodic behavior could be detected. The influence can be lead back to the behavior of the trajectory, by driving different tracks with different radii or different speed.

The last attitude parameter is the pitch angle. The pitch angle describes the slope of the street during the car drive. Again, only small angles are expected, because the track at the OEAMTC center is nearly flat, with the exception of a small hillock.

The pitch values during the measurement drive are displayed in Figure 7.18.

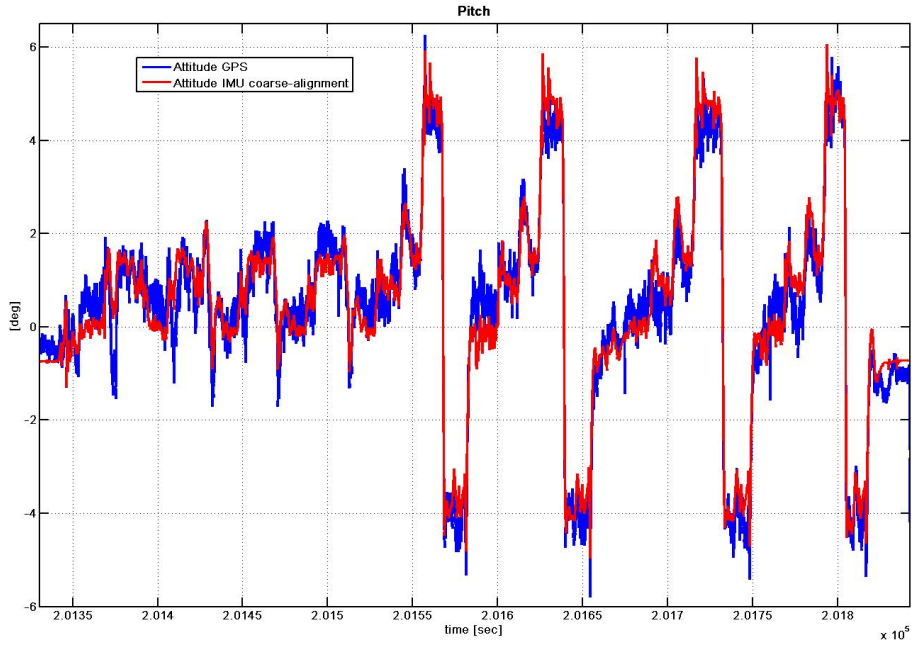

Figure 7.18: Comparison of the pitch angles during the test drive at the OEAMTC area

Beside the yaw angle also the pitch angle allows to distinguish different laps, which were driven during the test drive. The first laps are situated in the flat area. At the end of the test drive the last four laps were driven above the hillhock, which can be clearly recognized by looking at the computed pitch angles. The angle increases to nearly $\pm 6°$ in the last laps, which coincides with the downward motions over the hillock.

The pitch difference between the GNSS data and the IMU data show small fluctuations of approximately ±1.5° (cf. Figure 7.19).

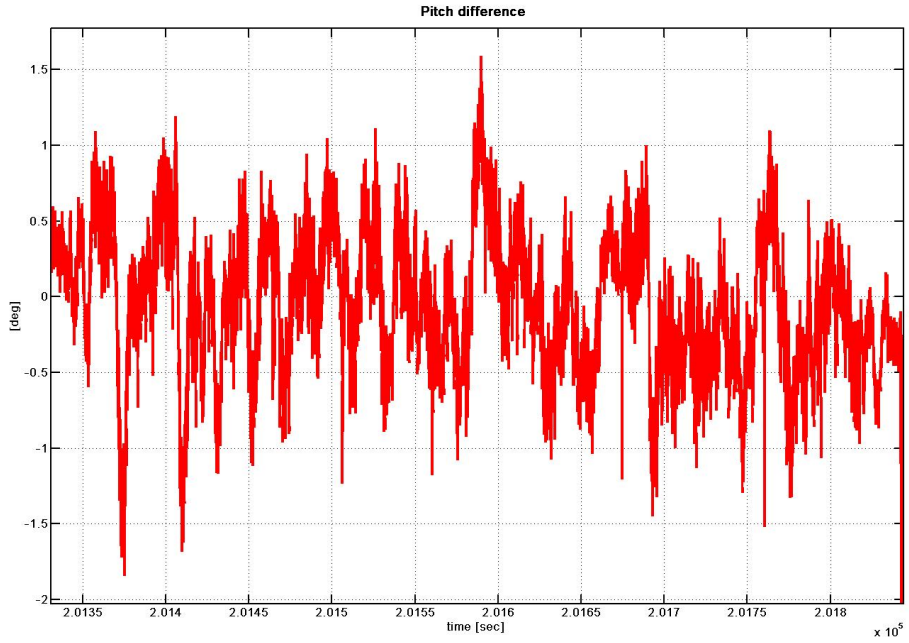

Figure 7.19: Differences between the pitch solutions of the GPS data and the IMU data (OEAMTC)

The differences of the pitch angle do not show any trend. The influences of the gyro drift could not be large because of the small difference values. The short observation period of eight minutes shows no large influences by a gyro drift. This fits with the classification of the used IMU, which is from the type of navigation grade.

Concluding, the GPS attitude solutions during the test drive the OEAMTC area show minimal differences compared to the IMU attitude parameters of ±2° or better. Table 7.3 presents the mean values and the standard deviations of the different attitude parameters. The results are very good and look very promising for the future use.

attitude angle	mean value [deg]	standard deviation [deg]
roll	-0.37	0.69
pitch	-0.06	0.46
yaw	-0.22	0.39

Table 7.3: Mean values and standard deviations of the attitude parameters during the test drive at the OEAMTC area

7.2.3 Attitude determination of the AVL trajectory

The AVL trajectory starts in the north of Graz and leads partly through the northern part of the town. As a consequence the satellite signal is expected to be degraded due to shading and multipath effects. Thus the position accuracy will become lower than in the first test. This effect will also influence the computation of the attitude parameters in a negative way. A part of the trajectory is displayed by a green rectangle, which marks better measurement periods. The first part of the trajectory represents a kinematic measurement mode, whereas after the GPS second 207150 the static part begins. In the following the data set is first evaluated regarding the position accuracy and afterwards the performance of the attitude is investigated.

Number of visible satellites

The number of received satellites has to be at least four. A lower satellite number does not enable kinematic positioning. A higher number of visible satellites provides redundancy for the position computation and thus a more accurate position determination. The number of visible satellites during the test drive is shown in Figure 7.20.

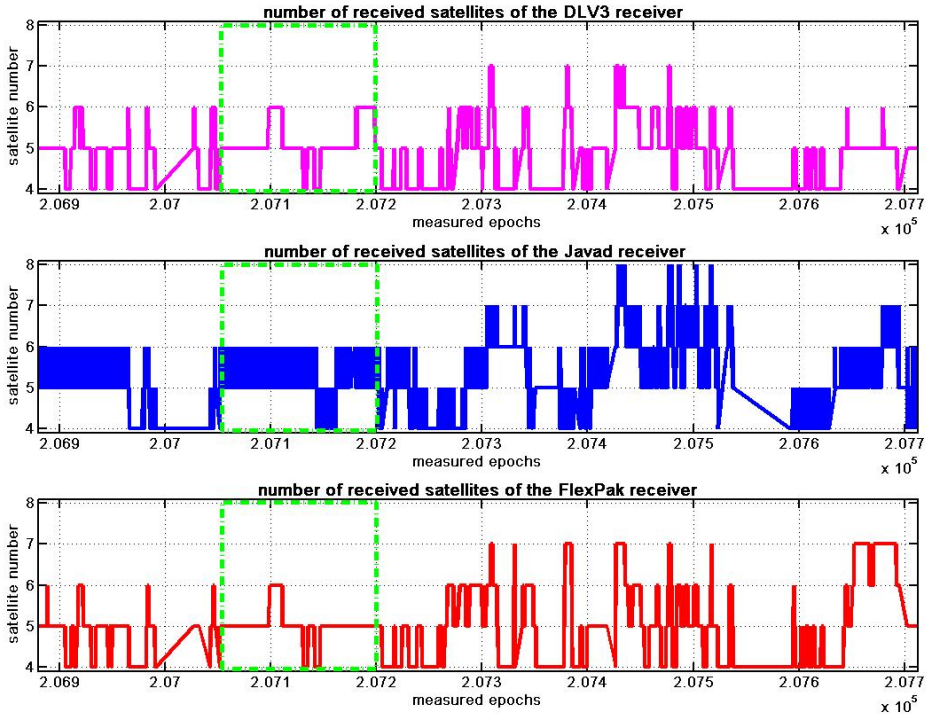

Figure 7.20: Satellite numbers during the test drive in the northern part of Graz

During the test drive the satellite number changes rapidly, which means that fluctuations between four and eight satellites occur. The fluctuations are mainly due to signal obstructions caused by buildings. The green rectangle emphasizes the period of better position solutions. The satellite number during this measurement interval is nearly constant at five satellites with variations to four or six satellites.

PDOP value

The PDOP value gives information about the geometric positioning accuracy. The lower the PDOP value, the higher the position accuracy. Like the satellite number also the PDOP values show strong variations over the whole interval (cf. Figure 7.21).

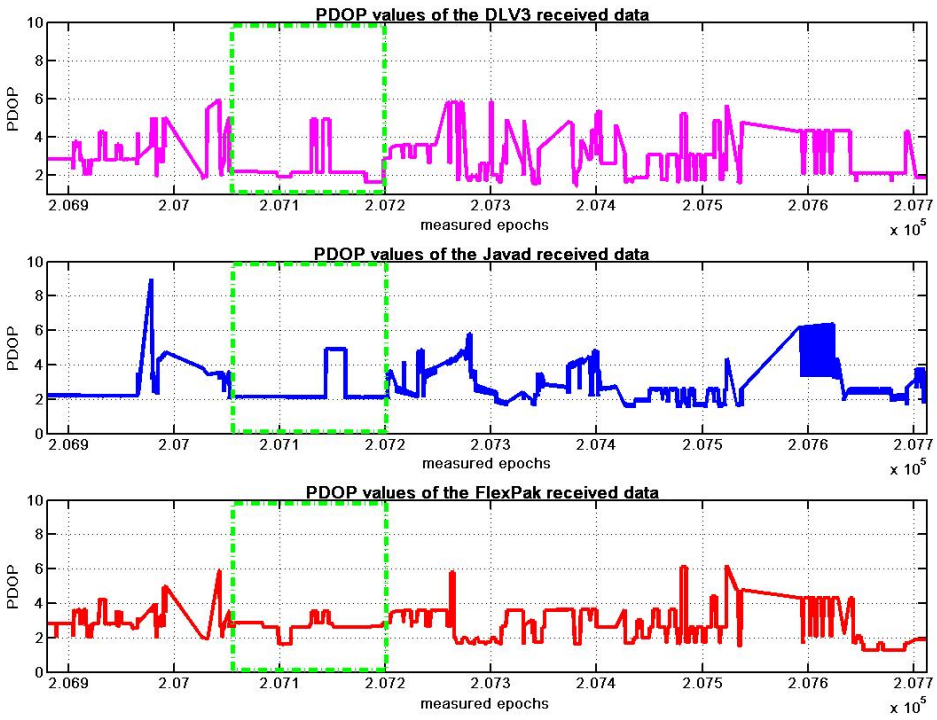

Figure 7.21: PDOP values during the test drive in the northern part of Graz

The higher PDOP values cause a lower positioning accuracy. A fast oscillation between the PDOP values, will also influence the attitude computation. The green rectangle again

marks the time interval of better measurement conditions. Short jumps to higher PDOP values occur in the measurements of the Javad and the DLV3 receiver, but with respect to the whole measurement period, the selected time interval shows a good PDOP.

Ambiguity solution

Another parameter, which indicates a good positioning accuracy, is the ambiguity status. The ambiguity status varies in this case between zero and two. The meaning of the different states are listed in Table 7.4.

ambiguity status	identification	definition
float	0	defined integer ambiguities are here computed as float values
fix1	1	one fixed ambiguity is used for position determination
fix2	2	more fixed ambiguities are used to determine a solution

Table 7.4: Possible ambiguity solutions, which are supported by the program GrafNav

The ambiguity status during this test drive show a variation between zero and one (cf. Figure 7.22). Most of the time only float solutions are available. Only at some intervals the GrafNav was able to solve integer ambiguities. This coincides with the number of visible satellites and the sudden loss of signals.

The ambiguity states of this trajectory lead to expectation, that the positioning accuracy will not be as accurate as it was during the first test drive. The ambiguity status corresponds mainly to a value of one during the selected interval, which is marked by the green rectangle. This means, that only one fixed ambiguity and therefore no ambiguity redundancy is used for the the position determination. Only a few jumps to a fixed ambiguity solution occur within the measured data of the Javad and the FlexPak receiver.

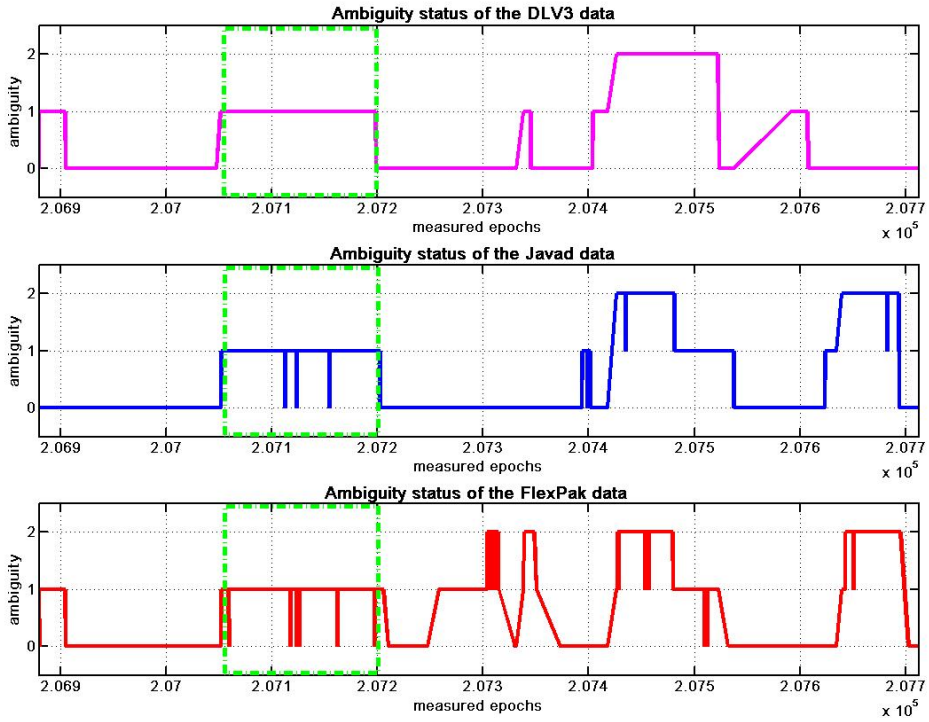

Figure 7.22: Ambiguity status during the test drive in the northern part of Graz

Quality factor

The quality factors during this test drive also show epochs with a quality factor of two (cf. Figure 7.23). A low quality factor describes a high accuracy in the computed coordinates. A low positioning accuracy is expressed by a higher quality factor. The positioning accuracy during the test drive varies between 0 m and 10 m.

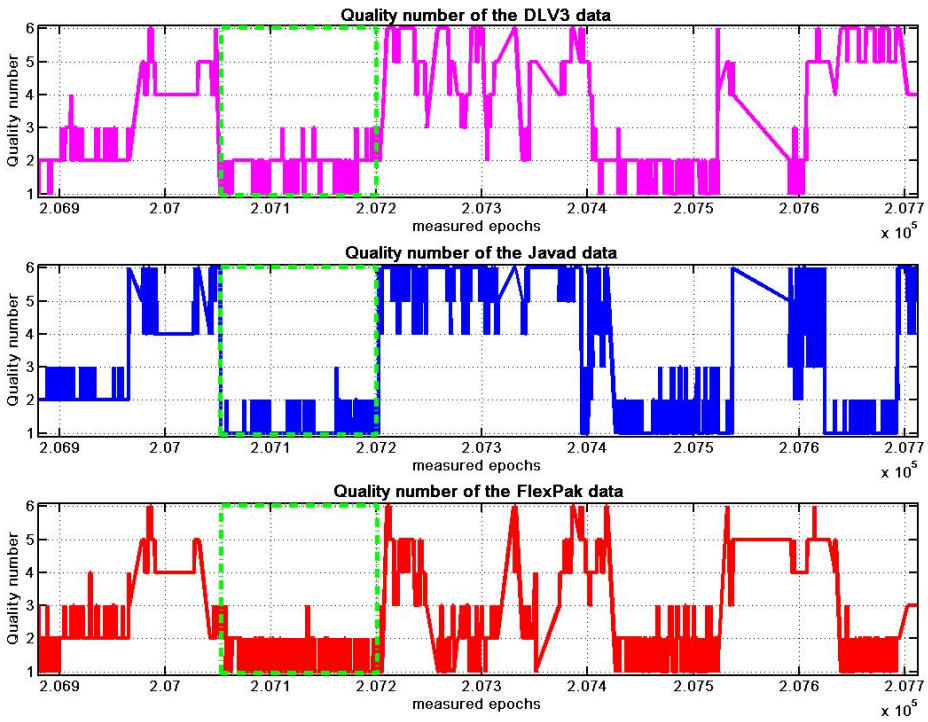

Figure 7.23: Quality factors during the test drive in the northern part of Graz

The poor positioning accuracy will thus influence the attitude computation. The accuracy of the position data is below 1 m within the selected interval - again marked by the green rectangle. All parameters which influence the position accuracy show large variations. Those variations reflect the environment of the test drive - many buildings and trees causing the signal to be lost.

Attitude parameters

The attitude computation is based, like the OEAMTC trajectory, on the computation steps which are explained at subsection 3.2. The yaw angle describes - by definition - the change in the driving direction. The computed yaw angles out of the GPS positions, as well as the attitude angles derived from the IMU data are displayed in Figure 7.24.

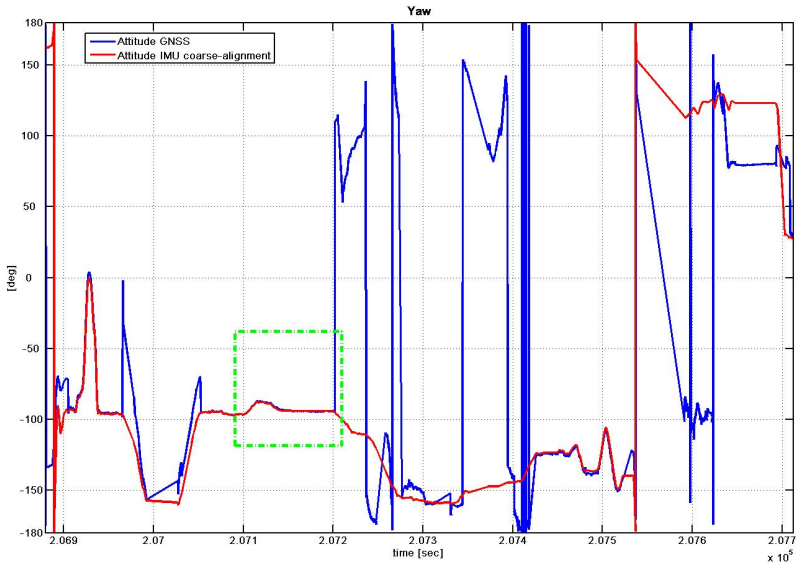

Figure 7.24: Comparison of the yaw angles during the test drive in the northern part of Graz

In contrast to the OEAMTC trajectory, where both sets of attitude parameter fit each other very well, the yaw angles of the GPS data and the IMU data show large differences during the second test drive in the northern part of Graz. The computed yaw angles from the GNSS data show large irregularities. Only at time intervals with a good positioning accuracy the attitude parameters have small deviations from the IMU based angles. The green rectangle emphasizes the selected time interval, which is chosen to mark a good position determination and thus a higher accuracy can be expected. During this time interval the yaw angles fit each other very well and show only small differences (cf. Figure 7.25).

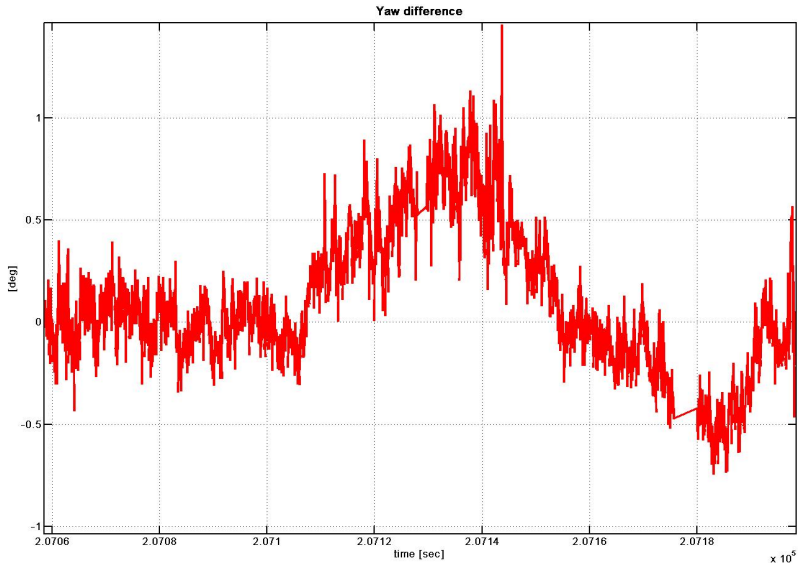

Figure 7.25: Differences between the yaw solutions of the GPS data and the IMU data (Graz)

The differences of the yaw angles vary between -0.75° and 1.5°. The range of these values correspond to the range of the OEAMTC yaw solutions. The differences show a strong scatter, which is mainly caused by the GPS attitude solutions. After the GPS second 207150 the static measurement mode starts. The large fluctuations during the static mode have its cause in the irregularities of the GPS attitude determination and in the position solution. Taking into account all these factors, it can be mentioned, that a good position solution during the test drive allows a good attitude determination. In contrast, a position solution with large errors which causes large errors in the attitude.

The roll angle of the car defines the rotation along the driving direction. Therefore this angle in case of a car is expected to be very small. In Figure 7.26 the roll angles based on the GNSS measurements and the IMU measurements are visualized.

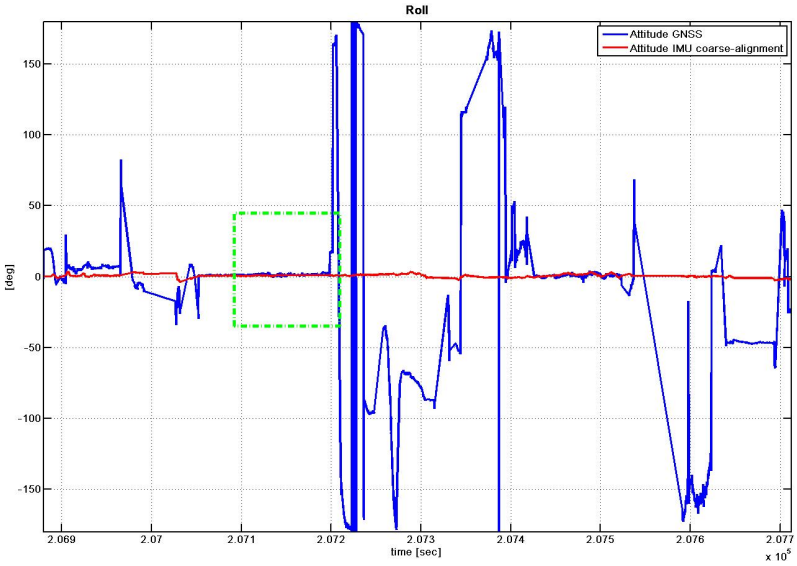

Figure 7.26: Comparison of the roll angles during the test drive in the northern part of Graz

The roll angles of the GNSS data show large irregularities with respect to the IMU data, but like the yaw angles, also the roll angles show some epochs, where the differences are small. The green rectangle marks the time interval with better positioning solutions (cf. Figure 7.26). During this time interval a good position accuracy is available and therefore attitude angles with small differences to the IMU angles can be derived (cf. Figure 7.27).

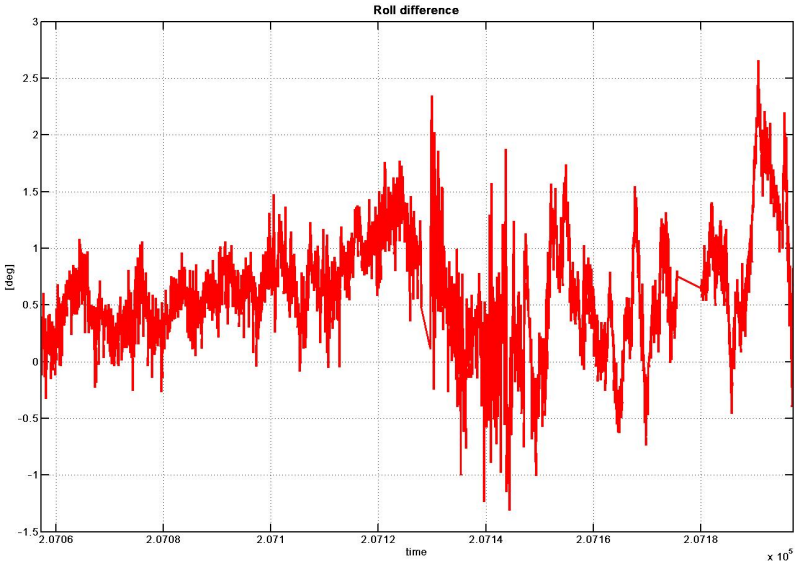

Figure 7.27: Differences between the roll solutions of the GPS data and the IMU data (Graz)

The differences again show no trend or drift effect of the gyro data. The largest influences occur through the fluctuations of the GPS data. Again large oscillations appear during the static measurements which start at the GPS second 207150. They are mainly caused by the position errors of the GPS measurements. The last attitude parameter - pitch - shows a similar behavior like the other two parameters. The pitch angle describes the gradient or the slope of the street and hence also of the car. The pitch angles are shown in Figure 7.28.

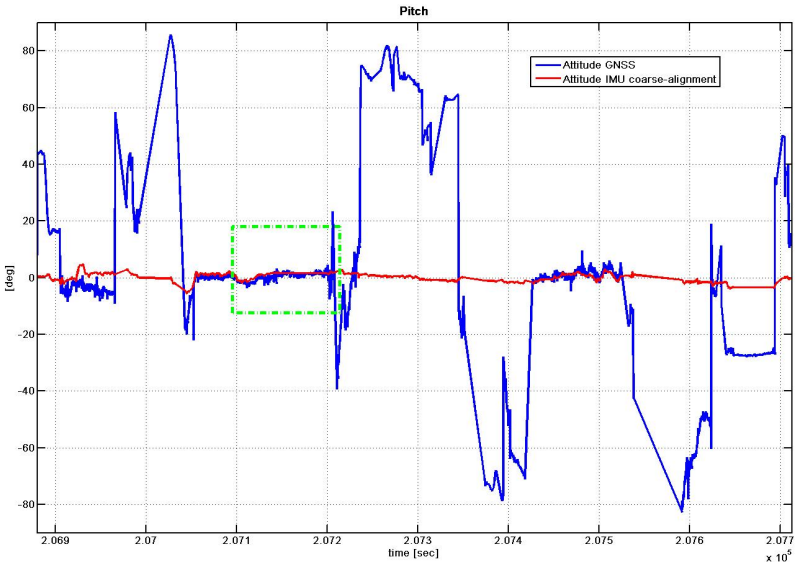

Figure 7.28: Comparison of the pitch angles during the test drive in the northern part of Graz

The green rectangular marks the better positioning interval during test measurements. The differences at this interval vary between -2° and +1° (cf. Figure 7.29).

The pitch differences show minimal larger values compared to the differences of the OEAMTC trajectory. Again no trend in the differences is recognizable. The larger difference values are mainly caused by the GPS solutions. The static epoch, which starts at the epoch 207150, shows also strong fluctuations, while the IMU data are almost static.

A large positioning error does not enable a reliable and accurate attitude computation. The mean values and the standard deviations of the three attitude parameters during the better observation period are listed in Table 7.5.

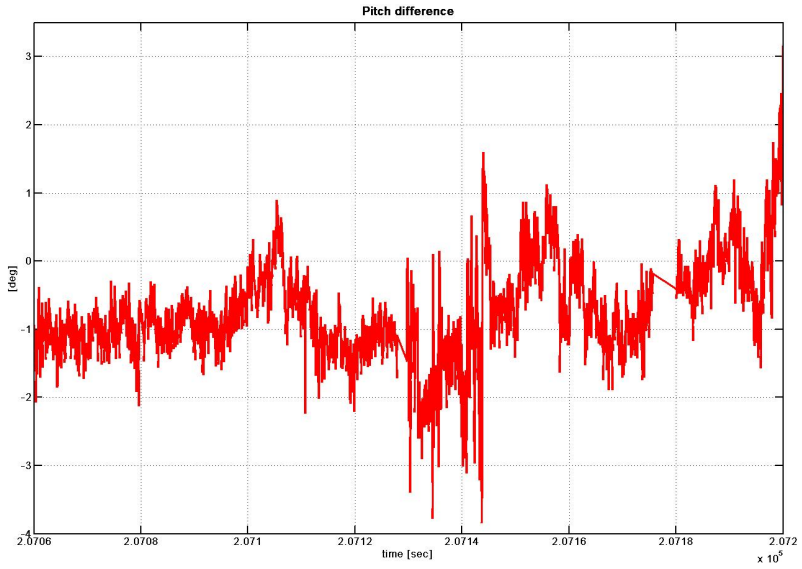

Figure 7.29: Differences between the pitch solutions of the GPS data and the IMU data (Graz)

attitude angle	mean value [deg]	standard deviation [deg]
roll	0.59	0.511
pitch	-0.79	0.68
yaw	0.03	0.34

Table 7.5: Mean values and standard deviations of the attitude parameters during the test drive in the north of Graz

The attitude parameters derived from GPS data correspond very well to the attitude parameters derived from IMU data, as long as the positioning accuracies are below approximately 0.2 m. Thus a good position accuracy is needed. This is only possible if a good satellite geometry (number of visible satellites, good PDOP values) is available. Furthermore, signal shadings and multipath effects have to be avoided. The tests showed that in rural areas the results are good but in populated areas the accuracy gets worse.

8 Conclusion and outlook

In the following a short conclusion of this master thesis and the achieved results for the attitude determination should be summarized. Finally an outlook on investigations regarding a more accurate attitude determination, is given.

8.1 Conclusion

The aim of this master thesis was the attitude determination with a GNSS multi antenna array. In a first step, a variance propagation shows that GNSS positioning errors and changes of the baseline lengths lead to a linear change of the standard deviation parameters in roll, pitch and yaw. The relative positioning method, which is preferred, enables a positioning accuracy of better than 5 cm. This leads to a standard deviation of roll of about $\pm 3.4°$. The standard deviations of pitch and yaw show a similar behavior and correspond to approximately $\pm 2.5°$. The characteristics of the standard deviations allow the conclusion, that the longer the baseline between the antennas, the better the standard deviation of the attitude parameters. The baseline length during the tests was about 1.5 m. This means, that for such a baseline length and a positioning error of 10 cm, the standard deviation of the attitude parameters is about $\pm 5.4°$.
In a further step, different update rates were investigated during various test drives. Three laps measured with 1 Hz, 10 Hz and 20 Hz were recorded. The influences of signal shadings and multipath effects are estimated for each update rate measurement. Further the density of the measured points during the kinematic motion are considered. It turns out that data gaps of about 80 cm for an update rate of 20 Hz and a driving velocity of 60 km/h have to be expected. Therefore the update rate for future test drives are set to 20 Hz, which allows a high point density and a fast ambiguity solution after signal obstructions. The test drives have been evaluated by using the software GrafNav. Different evaluation processes have been tested to enable a high kinematic positioning solution of the GNSS data. Special emphasize is put on the relative positioning method and the kinematic ambiguity solution, which facilitates a high positioning accuracy.

The attitude determination is based on the computed positions of the multi antenna array and needs therefore a high positioning accuracy. The attitude determination algorithm using three antennas is applied on two test drives. The first test drive was performed at the OEAMTC center in Lebring. It offers a good environment for GNSS measurements, which means less shading and multipath effects are present. Therefore an accurate position determination is possible. The attitude determination for this case shows only a few outliers. The computed attitude parameters are compared with the attitude values derived from the IMU data. The differences in the attitude parameters are between $\pm 1°$. The second trajectory is located in the urban area of Graz. Thus the satellite signal is often obstructed and multipath effects are present. Thus a relative positioning solution is not continually available. Sometimes, at bad positioning conditions, the positioning error increases up to ± 50 cm and more. This fact also influences the attitude computation. The attitude values show large jumps, caused by large positioning errors. The computed attitude parameters fit the attitude values of the IMU data, only during some short periods.

8.2 Outlook

The attitude adjustment algorithm can be tested, if measurements of four or even more GNSS receivers are available. Therefore a new test drive with more then three antennas will be performed in the near future, to facilitate a high redundancy of the observation data. Systems which are using eight antennas already exist.
Furthermore a better positioning accuracy can also help to improve the attitude determination. Therefore a trajectory with less shading and multipath effects has to be chosen. Multipath effects due to reflecting surfaces near the antennas, lead to a wrong pseudorange. Therefore, to avoid multipath effects, a surrounding with less density of buildings should be chosen for the following test drives. Additionally signal obstructions lead to cycle slips, followed by a new solution of the ambiguities, which lowers the positioning accuracy for that period. To handle this problem, several static measurement phases during the test drive will support a faster ambiguity solution, for which more than two epochs are needed, and thus will enable a higher positioning accuracy for the following kinematic motions.
An easier ambiguity solution can also be achieved by using the new satellite positioning system Galileo or the new L5 GPS signals as soon as they are available. Applying wide laning, leads to a combined signal with larger wave length, which simplifies the ambiguity determination. Furthermore Galileo will provide a higher satellite availability. Therefore

a higher positioning accuracy and thus a more accurate attitude computation can be expected in the future.
It must be mentioned that also the roof of the car causes multipath effects and distorts the measured pseudoranges. Therefore tests will be inevitable to estimate the multipath effects, which arise by signal reflections on the roof of the car.

The lower deviations of the computed yaw angles from the IMU data are due to the fact, that the GNSS antennas are fixed in an almost horizontal plane. Thus further investigations regarding the position of the antennas have to be done. Perhaps an additional antenna above the current antenna plane might give better results.

Concluding this thesis it can be stated, that the results of the attitude determination using GNSS measurements look promising. Possible improvements of the attitude determination can be achieved by obeying the above mentioned facts.

List of Figures

List of Tables

Bibliography

[1] A. Bruton. Improving the Accuracy and Resolution of SINS/DGPS Airborne Gravimetry. *UCGE Report*, (20145), 2000.

[2] B. Hofmann-Wellenhof, H. Lichtenegger, E. Wasle. *Global Navigation Systems - GPS, GLONASS and more*. Springer, Wien New York, 2008.

[3] B. Hofmann-Wellenhof, H. Lichtenegger, J. Collins. *Global Positioning System - Theory and Practice*. Springer, Wien, New York, 2001.

[4] B. Hofmann-Wellenhof, K. Legat, M. Wieser. *Navigation-Principles of Positioning and Guidance*. Springer, Wien, New York, 2003.

[5] De Jong C.,G. Lachapelle,S. Skone,I. Elema. *Hydrography*. VSSD, 1998.

[6] G. Abwerzger. Qualitaetskontrolle von Attitude-Messungen der BeeLine Empfaenger. Technical report, Oesterreichische Akademie der Wissenschaften, Institut Weltraumforschung, Abteilung fuer Satellitengeodaesie, 2000.

[7] Gang Lu. *Development of a GPS Multi-Antenna System for Attitude Determination*. PhD thesis, University of Calgary, Department of Geomatics Engineering, 1995.

[8] Gang LU, M.E. Casnnon, G. Lachapelle, P. Kielland. Attitude Determination in a Survey Launch Using Multi-Antenna GPS Technologies. *Proceedings of National Technical Meeting, The Institute of Navigation, Alexandria, VA, 251-260.*, 1993.

[9] Gang Lu, M.E.Casnnon, G.Lachapelle, P.Kielland, B.Loncarevic. Shipborne GPS Attitude Determiantion During MMST-93. *Journal of Oceanic Engineering*, 21(1), 1996.

[10] Graas F. van, MS. Braasch . Real-time attitude and heading using GPS. *GPS World, 3, 32-39.*, 1992.

[11] J. Farrell,M. Barth. *The Global Positioning System and Inertial Navigation*. McGraw-Hill, 1998.

[12] L. Marco. GALILEO Program Status Update to ION GNSS 2009. Website, 2009. Available online at *http* : *//www.ion.org/*; visited on 23 October 2009.

[13] M. Bauer, L. Wanninger. *Vermessung und Ortung mit Satelliten*. Wichmann, 2003.

[14] N. Kühtreiber. Terrestrial Moving-Base Gravimetry Using a GNSS/SINS Platform-GRAVIS, 2007. Proposal.

[15] POSITIM. GNSS Frequencies and Signal Structure. Website, 2009. Available online at *http* : *//www.positim.com/gnsssignals.html*; visited on 22 October 2009.

[16] U.S. Coast Guard Navigation Center-NAVCEN. Interface Control Document (ICD 200c). Website, 2009. Available online at *http* : *//www.navcen.uscg.gov/pubs/gps/icd*200/*default.htm*; visited on 23 October 2009.

[17] Waypoint. *A NovAtel Precise Positioning Product: GrafNav, GrafNet, GrafMov, GarNav Lite and GrafNav Batch NovAtel for Windows 98, 2000 and XP - User Manual*, 2006.